National Library of Canada

Acquisitions and Bibliographic Services Branch

395 Wellington Street
Ottawa, Ontario
K1A 0N4

Bibliothèque nationale du Canada

Direction des acquisitions et des services bibliographiques

395, rue Wellington
Ottawa (Ontario)
K1A 0N4

Your file Votre référence

Our file Notre référence

NOTICE

The quality of this microform is heavily dependent upon the quality of the original thesis submitted for microfilming. Every effort has been made to ensure the highest quality of reproduction possible.

If pages are missing, contact the university which granted the degree.

Some pages may have indistinct print especially if the original pages were typed with a poor typewriter ribbon or if the university sent us an inferior photocopy.

AVIS

La qualité de cette microforme dépend grandement de la qualité de la thèse soumise au microfilmage. Nous avons tout fait pour assurer une qualité supérieure de reproduction.

S'il manque des pages, veuillez communiquer avec l'université qui a conféré le grade.

La qualité d'impression de certaines pages peut laisser à désirer, surtout si les pages originales ont été dactylographiées à l'aide d'un ruban usé ou si l'université nous a fait parvenir une photocopie de qualité inférieure.

Canada

IONS & NEUTRALS IN THE GAS PHASE–

STRUCTURE, STABILITY

AND FRAGMENTATION MECHANISMS

By

David Harnish

A Thesis Presented to
the University of Ottawa
in Fulfillment of
the Thesis Requirement
for the Degree of
Master in Science in
the Department of Chemistry
University of Ottawa

ISBN 0-315-85839-7

Canada

UNIVERSITÉ D'OTTAWA
UNIVERSITY OF OTTAWA

Dedicated to

my Mother and Father

with Love

ABSTRACT

OVERVIEW

The elucidation of fragmentation mechanisms is an essential prerequisite to the understanding of any mass spectrum. Many tools exist with which mechanistic studies may be performed and which identify and characterize reacting, intermediate and product ions. With the advent of two new techniques, collisionally induced dissociative ionization and neutralization reionization mass spectrometry, it is now possible to investigate the structure and stability of neutrals as well as ions.

FRAGMENTATION MECHANISMS OF ALKYL PHENYL ETHERS

The metastable fragmentation mechanisms of alkyl phenyl ethers and methyl pentyl ethers have been thoroughly investigated. It has been shown that the formation of an ion/radical complex is the key step in the metastable loss of olefin from alkyl phenyl ethers and loss of methanol from methyl pentyl ethers. The alkyl moiety in an ion/radical complex between a primary alkyl cation and a phenoxy radical undergoes a rate determining isomerization to a secondary or tertiary alkyl cation at an energy above the dissociation threshold for the resulting complex. A $\beta(H^+)$ is then immediately transferred from the alkyl cation to the phenoxy radical followed by dissociation to products. The pentyl moiety in an ion/radical complex between a primary pentyl cation and a methoxy radical undergoes an isomerization to a more stable secondary or tertiary pentyl cation at an energy below the dissociation threshold for the resulting complex. Limited H-scrambling may then occur in the pentyl moiety prior to the rate determining transfer of a $\beta(H^{\cdot})$ to the methoxy radical and dissociation to products.

ASSIGNING STRUCTURES TO ISOMERIC $[C_5,H_{10}]^{+\cdot}$ IONS

The ten $[C_5,H_{10}]^{+\cdot}$ isomers may be distinguished based on their heats of formation, low ionizing electron energy mass spectra and charge stripping mass spectra. The fragmentation mechanisms for H_2O loss from 1-pentanol and HCl loss from 1-chloropentane were determined with the aid of deuterium labelling and identification of the product $[C_5,H_{10}]^{+\cdot}$ ions. 1,4-Elimination of H_2O from 1-pentanol occurred via a six membered transition state followed by a 1,2 H-shift in the resulting distonic ion and ring closure to produce ionized ethylcyclopropane. 1,3-Elimination of HCl from 1-chloropentane occurred via a five membered transition state followed by ring closure of the resulting distonic ion to produce ionized ethylcyclopropane. In the metastable timeframe 1,3-elimination of HCl is followed by a 1,2 H-shift in the intermediate distonic ion to produce ionized pent-2-ene.

COLLISION INDUCED IONIZATION EFFICIENCIES OF FAST NEUTRALS

The O_2 collisional ionization efficiencies of CO and CH_2=CH_2 depend on both the translational and internal energies of the neutral. The ionization efficiencies increased with increasing translational energy from 2000-5200 V as expected for ionization by the electron detachment mechanism. The ionization efficiencies decreased with increasing internal energy. This result is discussed in terms of ionization of the target (O_2) and bond dissociation reactions.

THE GENERATION OF STABLE BH_3 AND $BH_4^{\cdot}$ IN THE GAS PHASE

The stability of BH_3, $BH_4^{\cdot}$ and their deuterated counterparts BD_3 and $BD_4^{\cdot}$ were studied by neutralization reionization mass spectrometry. It was shown that all these species have significant stability and existed in the mass spectrometer for at least $5x10^{-7}$ seconds.

TABLE OF CONTENTS

FIGURES

TABLES

"Where shall I begin, please
your Majesty?" he asked.
"Begin at the beginning,"
the King said, very gravely,
"and go on till you come to
the end: then stop."

LEWIS CAROLL
Alice's Adventures in Wonderland

THEORY

The basic principle of mass spectrometry involves the creation of a (fast) beam of ions and the separation of these ions by their mass to charge ratio and/or kinetic energy. The various ways in which this is achieved will be detailed in the following sections.

Section 1.1 Vacuum Generators Analytical ZAB-2F

Figure 1.1 represents the Vacuum Generators Analytical ZAB-2F mass spectrometer (referred to from now on simply as the ZAB). The ZAB may be divided into several sections: ion source, first field free region (1FFR), first magnetic analyzer, second field free region (2FFR), electrostatic analyzer, third field free region (3FFR), second magnetic analyzer, and the detectors.

Figure 1.1 Schematic Diagram of the Vacuum Generators ZAB-2F Mass Spectrometer

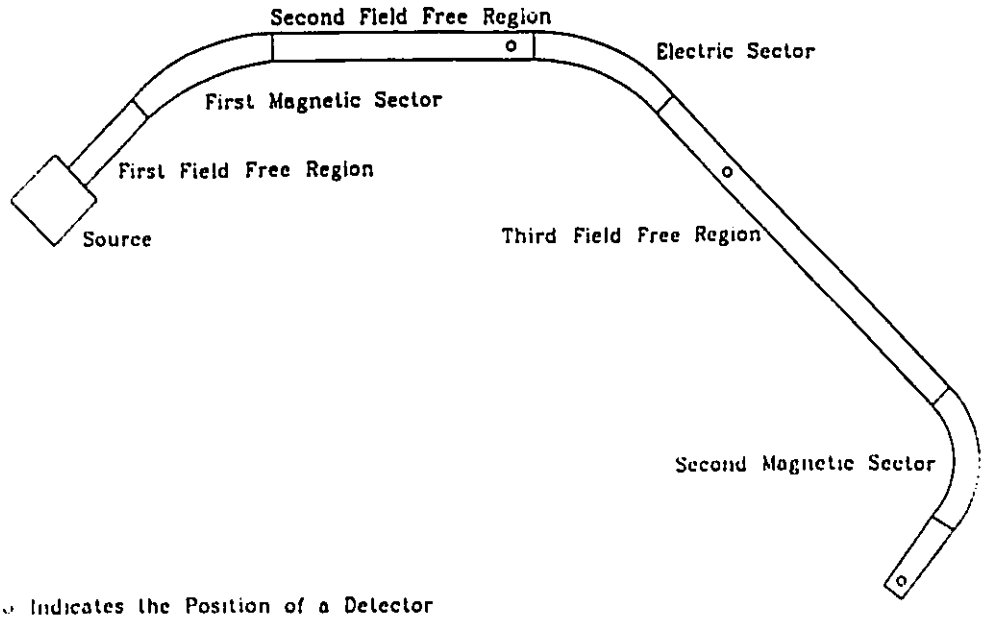

o Indicates the Position of a Detector

Section 1.1.1 Ion Source

The ion source (Figure 1.2) is the region of the mass spectrometer in which the sample is ionized. Samples are introduced via one of four methods.

(1) Liquids may be introduced through a neoprene septum into a heated reservoir. The vapourized sample then diffuses through a capillary tube into the source housing.

(2) Gases and compounds which are volatile at room temperature may be introduced by an unheated inlet system in which the sample "leaks" through a valve and then passes along a glass capillary into the ion source.

(3) Solid samples may be introduced via a direct probe inlet. The probe tip passes through a vacuum lock into the source. The probe may be heated in order to obtain the necessary sample pressure.

(4) Gases may be directly introduced through gas lines.

Figure 1.2 Representation of the VG ZAB-2F Ion Source

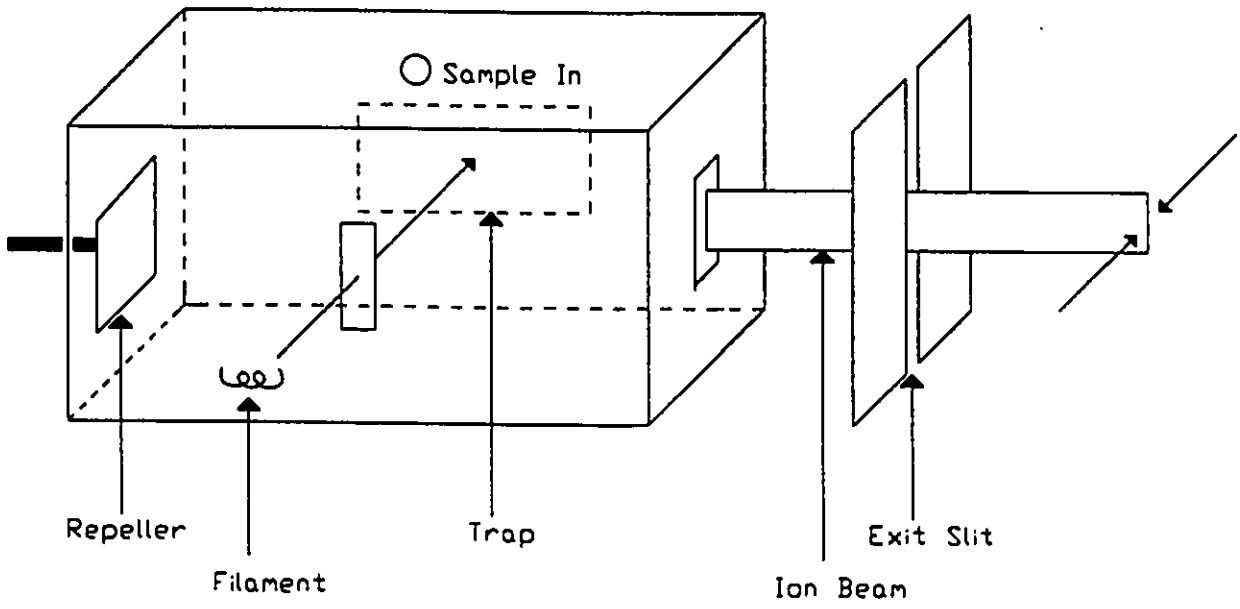

Once in the source the sample is subjected to a beam of electrons. The electrons are produced by electrically heating a tungsten filament in vacuo ($<10^{-8}$ torr). The electrons are accelerated across a variable voltage, V, to the trap (anode). Typically V = 70 volts. Therefore, an energy of 70 eV is imparted to the electrons. A value of 70 eV is used since near this value an electron energy invariant ion flux is obtained.[1]

Since the electron beam has an energy of 70 eV and most organic molecules have an ionization potential of ca 10 eV,[2] there is more than sufficient energy available to ionize the samples. A wide range of energies will be transferred to the sample by the electron beam. Thus, some molecular ions will be generated with sufficient internal energy to cause them to fragment while others will have insufficient energy to fragment.

The electrons continue across the ion source until they collide with the trap which is connected to an ammeter which measures the electron current.

The source block is maintained at a high voltage, V_{acc} (typically 8000 volts). A repeller electrode with a small positive potential, above 8000V, repels the ions through an exit slit. Since the source block is maintained at V_{acc}, the ions will gain, between the source and two grounded plates, a translational kinetic energy equivalent to 8000 V. i.e.

(1.1) $zV_{acc} = \frac{1}{2}mv^2$.

m = mass of ion
v = velocity of ion
z = charge on ion

The ion beam is collimated by paired focusing plates, capable of carrying positive or negative charges, before passing through the source slit, into the first field free region.

Section 1.1.2 The First Field Free Region - 1FFR

The ion beam will continue in a straight line through the 1FFR before entering the (first) magnetic analyzer. Near the beginning of the 1FFR, the ion beam will pass through a variable slit (Y1). This slit and all other variable slits (Y1-Y5) are, when narrowed, capable of increasing the mass and energy resolution (see Section 1.1.9).

Section 1.1.3 The First Magnetic Analyzer.

In the magnetic analyzer, the ion beam passes through a magnetic field produced by an electromagnet. The ions will experience a centrifugal force

(1.2) $Bzv = mv^2/r.$

B = strength of magnetic field
r = radius of circular path travelled by the ion due to the magnetic field

From equations (1.1) and (1.2) one obtains

(1.3) $m/z = B^2r^2/2V_{acc}.$

Since r and V_{acc} are constants, by varying the magnetic field one may successively transmit ions of different mass to charge ratio through the magnetic analyzer to the second field free region.

Section 1.1.4 The Second Field Free Region - 2FFR

The ion beam will continue to travel through the 2FFR and pass through yet two more variable slits (Y2 and Y3) prior to entering the electrostatic sector. There are two collision cells (see Sections 2.1.3, 2.1.4, 2.1.5 and 2.1.6) located in the second field free region as shown in Figure 1.3. Gas can be leaked into the cells while the pressure around the cells is maintained at low pressures due to the two pumps located adjacent to the cells. There is also a beam deflector electrode located between the two cells. The purpose of this electrode is to deflect all ions from the flight path so that only fast neutrals which have been produced in the second field free region prior to the electrode will continue through to the second collision cell (see Section 2.1.5 and 2.1.6). The deflector electrode is surrounded by a grounded shield to localize its electric field.

Figure 1.3 Schematic Diagram of the Second Field Free Region of the VG ZAB-2F

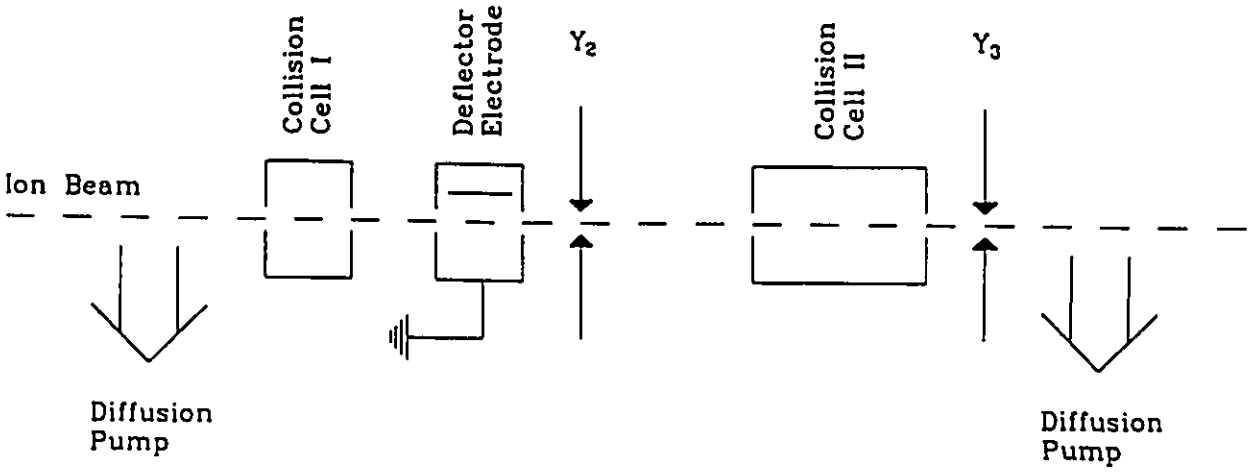

Section 1.1.5 The Electrostatic Analyzer

The electrostatic analyzer consists of two parallel curved metal plates of radius R. An electric potential is maintained across the plates creating an electric field. The ions will pass through the electrostatic analyzer if the electrical force is equal to the centrifugal force

(1.4) $zE = mv^2/R.$

E = electric field strength
R = radius of curved plates

Thus, the electrostatic analyzer is an energy selecting device. From equations (1.1) and (1.4) one obtains

(1.5) $E = 2V_{acc}/R.$

Therefore, when E is maintained at $2V_{acc}/R$ all ions which are generated in the source will be transmitted through the electrostatic analyzer into the third field free region.

Section 1.1.6 The Third Field Free Region and the Second Magnetic Analyzer

The ions will once again pass through a field free region. There are two more variable slits immediately following the electrostatic analyzer (Y4 and Y5). The ion beam then enters the second magnetic analyzer where the ions may once again be analyzed according to their mass to charge ratio.

Section 1.1.7 The Detectors

Detectors are located at three points along the instrument. The first is located after Y3 and before the elecrostatic analyzer. The second is located after Y5 and before the second magnetic analyzer. The third is located after the second magnetic analyzer. The first two detectors are off-axis electron multipliers (See Figure 1.4), the third detector is an on-axis electron multiplier. For the first two detectors, the ion beam is deflected onto a negatively charged conversion dynode which emits electrons. The electrons are accelerated to a 16 stage multiplier. Gain of the order of 10^6 is achievable.[3]

Figure 1.4 Schematic Diagram of a Conversion Dynode, VG ZAB-2F

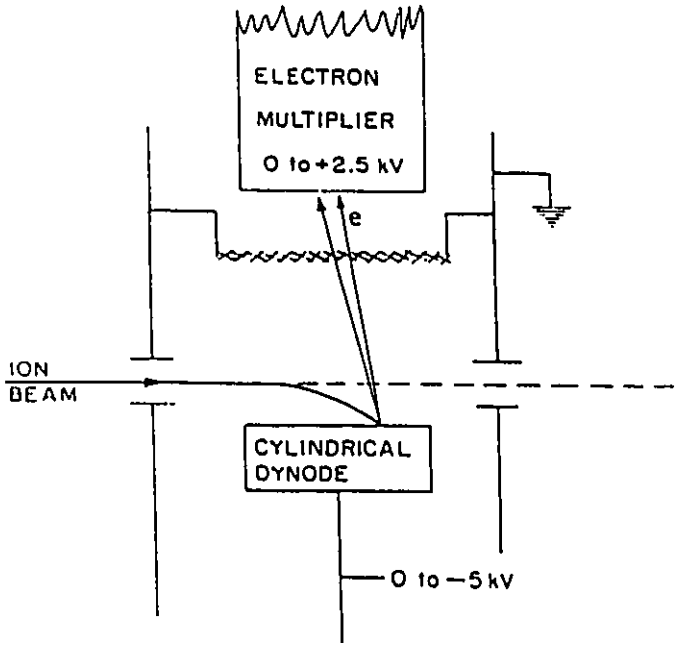

It is possible to replace the second multiplier by a Faraday Cup which lies directly in the flight path of the ion beam. The Faraday Cup is a thin, rectangular, metal box arranged such that the incoming ion beam hits the bottom of the box. Any electrons emitted by collision of the ions with the walls are kept in the box by a small magnetic field. In this way, the absolute ion current is measured (current is proportional to the number of ions and the number of charges per ion).

The response of an electron multiplier depends upon the mass, energy, charge and nature of the ions. In this laboratory it has been found, by comparing the relative intensities of the peaks in the normal mass spectrum of $CH_3C(O)CH_2CH_2CH_3$ recorded with the second multiplier to the relative intensities of the peaks recorded with the Faraday cup (which measures absolute ion abundances), that low mass ions (m/z 12-15) are discriminated against by no more than 15-20% with respect to ions of m/z 100. Moreover, it has been found that a recommended procedure to correct for mass discrimination[4]

(1.6) $$(I_1/I_2)_{true} = (I_1/I_2)_{measured}(m_1/m_2)^4$$

I = the ion current
m = the ion mass

does not hold true.

Section 1.1.8 Pumps

The ZAB is maintained at a pressure less than 10^{-8} torr with the aid of roughing and diffusion pumps. The oil (polyphenyl ether) diffusion pumps are located at seven points: one at the source, one in the 1FFR, two in the 2FFR, and three in the 3FFR.

Section 1.1.9 Resolution

The resolving power of a mass spectrometer is a measure of the ability to separate two ions of any defined mass difference. For two overlapping peaks, $M_1^{+\cdot}$ and $M_2^{+\cdot}$, the resolution is defined in terms of the mass difference between the two ions, $\Delta m = (m_2-m_1)$ such that the peaks are resolved when $(h/H)100 \leq 10\%$. H is the height of the peaks and h is the depth of the valley between them (see Figure 1.5). The resolution is then equal to $[m_1/\Delta m]$ when $(h/H)100 \leq 10\%$.

Figure 1.5 Two Overlapping Ion Peaks, M_1 and M_2, of Height, H and Overlap, h.

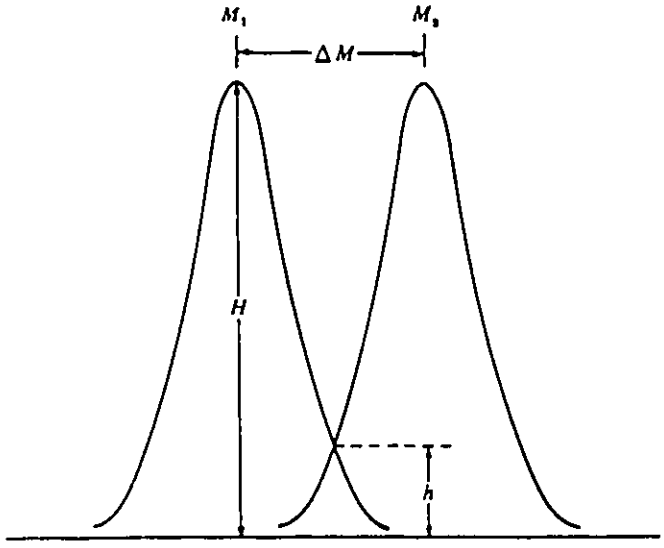

The resolution of the ZAB is approximately 1000 when all the variable slits (Y_1-Y_5) are fully open. Narrowing the slits increases the mass and energy resolution at the expense of signal intensity.

Section 1.2 Metastable Ions

Ions which do not have enough energy to fragment in the ion source but which fragment along the flight path of the mass spectrometer are known as metastable ions. Metastable ions were first recognized by Hipple and Condon.[5] The fragment ions which are generated may be detected if decomposition takes place in one of the three field free regions. These fragment ions give rise to metastable peaks. In order to transmit the fragment from a metastable ion through the magnetic analyzer or the electrostatic analyzer both the magnetic field and the electrostatic field must be adjusted by a factor of m_2/m_1 with respect to the values which would be required if the ion was generated in the source, as will be shown in the following two sections.

Section 1.2.1 Transmitting a Metastably Generated Fragment Ion Through a Magnetic Analyzer

Consider a metastable ion, $M_1^{+\cdot}$, which decomposes between the ion source and a magnetic sector as follows:

(1.7) $M_1^{+\cdot} \text{ -*-} \rightarrow M_2^{+} + M_3^{\cdot}$ (an asterix represents a metastable reaction)

From equation (1.1), and keeping in mind conservation of momentum, M_2^{+} will have a kinetic energy of

(1.8) $zV_{acc}' = \frac{1}{2}m_2v^2.$

$V_{acc}' = (m_2/m_1)V_{acc}$
m_1 = mass of M_1
m_2 = mass of M_2

Combined with equation (1.2) one obtains

(1.9) $(m_2^2/m_1)/z = B^2r^2/2V_{acc}.$

Metastably produced M_2 will have an apparent mass of m_2^2/m_1.

Section 1.2.2 Transmitting a Metastably Generated Fragment Ion Through an Electrostatic Analyzer

Fragment ions generated outside of the source will have a different kinetic energy than source generated ions and thus a different electric field strength is needed to transmit them through the electrostatic analyzer. Combining equations (1.4) and (1.8) yields

(1.10) $E = 2(m_2/m_1)V_{acc}/R.$

Therefore, the kinetic energy of metastably produced M_2 must be adjusted by a factor of m_2/m_1 with respect to source generated M_2 in order to be transmitted through the electrostatic analyzer.

Section 1.3 Kratos-AEI MS-902S

Figure 1.6 represents the Kratos-AEI MS-902S mass spectrometer (MS-9). The MS-9 is a two sector instrument with the electrostatic analyzer preceding the magnetic analyzer.

Figure 1.6 Box Diagram of the Kratos-AEI MS-902S Mass Spectrometer

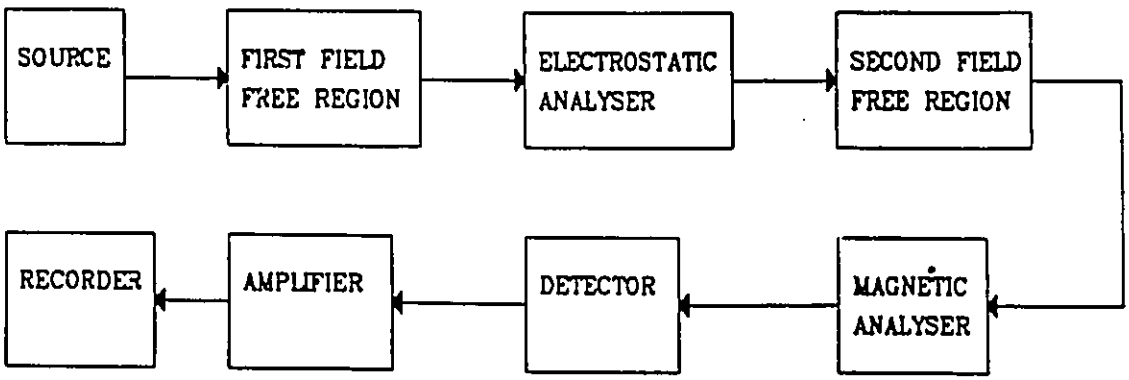

Sample inlet into the source may occur via a variable molecular leak or through a probe. The ion beam is then accelerated and the ions separated on the basis of energy and mass. There is a Daly detector located after the magnetic sector. There is a repeller voltage, V_r, applied to the detector such that when $V_r > V_{acc}$ all ions are turned back and strike a metal plate causing secondary electrons to be emitted (see Figure 1.7). The secondary electrons are detected by a scintillator-photomultiplier.

Figure 1.7 The Daly Detector

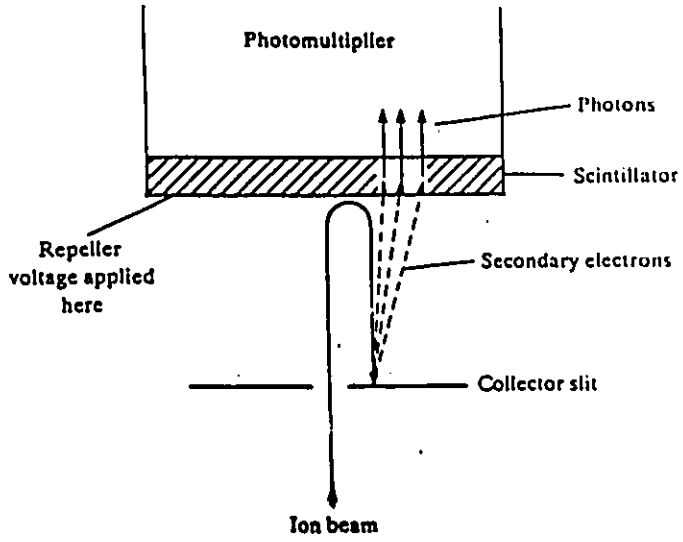

Section 1.4 Energy-Selected Electron Impact Ion Source and Quadrupole Mass Filter

Under normal conditions a filament emits electrons with a large energy spread which causes great uncertainty in the analysis of efficiency curves for ion production.[6] An ion source has been developed in which it is possible to obtain a well collimated beam of electrons with an energy half width in the range of millivolts.[7] See Figure 1.8

Figure 1.8 Energy Selected Electron Impact Ion Source and Quadrupole Mass Filter

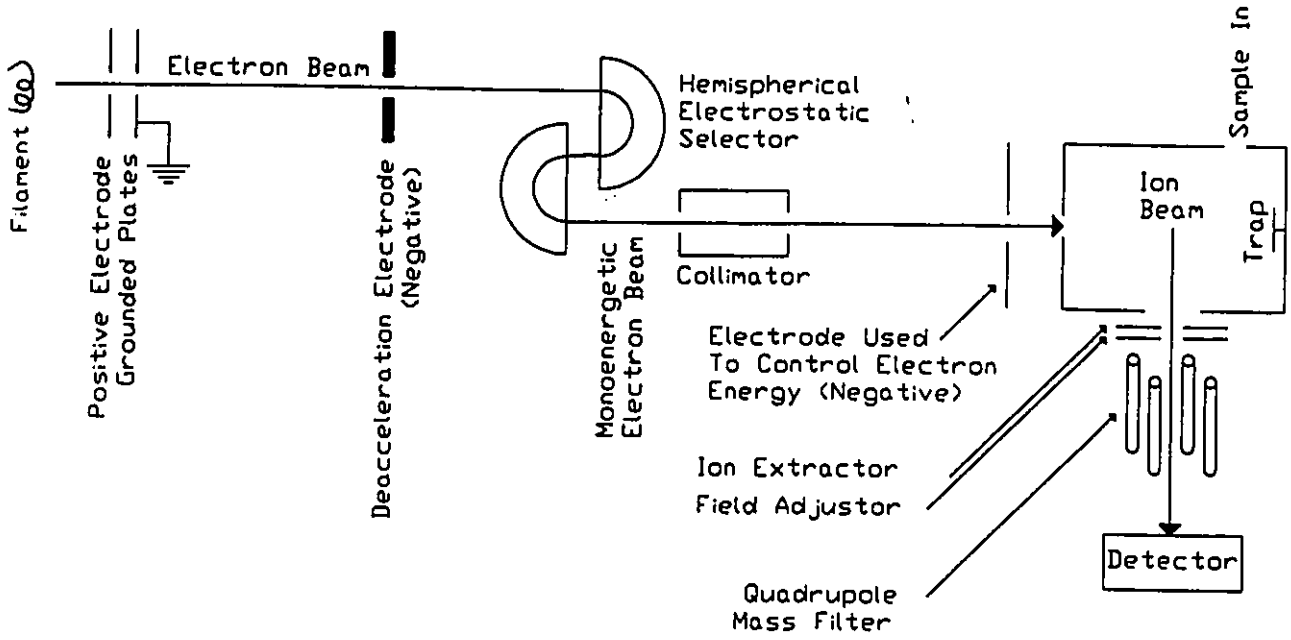

A beam of electrons, produced by an electron gun, is decelerated at a small aperture (0.36 mm diameter) leading to two mutually perpendicular hemispherical electrostatic selectors. The potential of the hemispheres may be adjusted to give the maximum yield of electrons. The electrons leaving the hemispheres have a roughly triangular profile and are focused to a cylindrical beam in a collimator. The collimation of the beam minimizes any effects due to wall bombardment.

The resulting electron beam energy can be varied from 5-30 eV by varying the charge on an electrode following the collimator with little effect on the energy spread. The electrons travel through an ionization chamber to the trap at which the electron current can be measured.

Ions are extracted from the chamber, with as little effect as possible to the cylindrical field in the reaction chamber, via the ion extractor and field adjustor electrodes. Little broadening of the electron energy half width was found when the ion extractor was maintained at ca -6 eV.

Finally the ion beam is focused through grounded plates into the entrance of a quadrupole mass filter where mass separation of the ions occurs.

A mini-computer is used to produce repetitive staircase voltage outputs which control the electron energy. The mini-computer is also used to store and analyze the ion current.

Section 1.5 Ion Fragmentation

The behaviour of ions formed by electron impact may be extremely complex. An outline of the factors which govern ion fragmentations in the mass spectrometer is given in the following sections.

Section 1.5.1 Energy Gained Upon Electron Impact Ionization

During the approach of an electron to a molecule there may be interaction leading to the electronic excitation of the molecule. An electron may be promoted to a higher orbital (equation 1.11), or ejected to give a positive ion (equation 1.12). The molecule responds to some effects of the electron beam and may be distorted. Therefore, the ionization may not be strictly vertical allowing more states to be accessed than by photoionization.[1] See Section 1.6.1 and Figure 1.13.

(1.11) $M + e \rightarrow M^{*} + e$

(1.12) $M + e \rightarrow M^{+\cdot} + 2e$

Ionization may occur to the ground electronic state or to an electronically excited state of the ion.

Once ionization has occurred, the excess internal energy may cross from one state to another state of equal or similar energy. Since polyatomic molecules have closely spaced rotational levels combined with vibrational levels, crossing between potential surfaces is easily achieved and equilibration of the excess energy occurs.

For those ions with sufficient energy to fragment, fragmentation will occur at different rates depending on the electronic state of and vibrational energy in each ion. Some ions will have insufficient energy to fragment. The proportion of these ions increases as the electron energy is lowered, reducing the amount of fragmentation. The distribution of energy following electron impact ionization is shown in Figure 1.9.

Figure 1.9 Distribution of Internal Energy Following Electron Impact Ionization

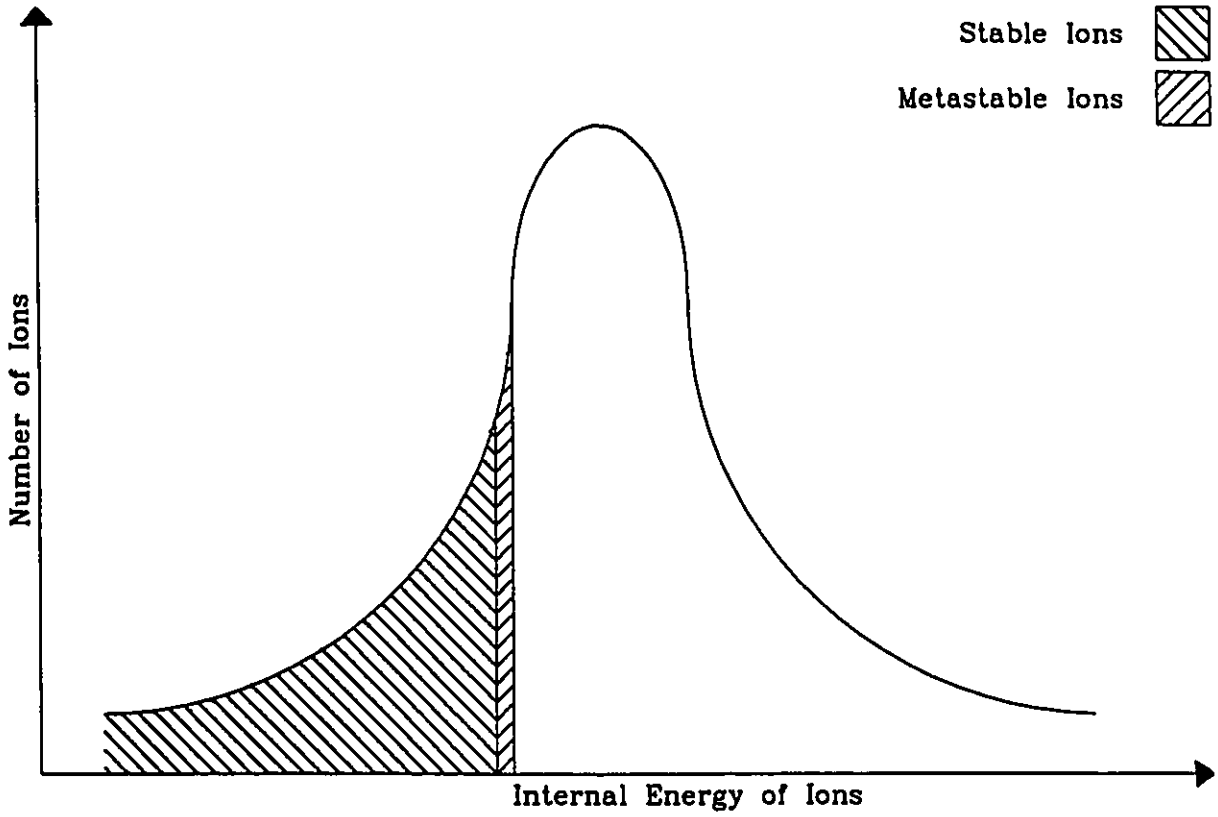

Section 1.5.2 Rate and Pathway of Ion Fragmentation

The quasi-equilibrium theory (QET) is a quantitative treatment of ion fragmentation which allows one to calculate the rate of decomposition of an ion, via bond cleavage, at any given excess internal energy.[8] The QET depends on three assumptions:

(i) Immediately after ionization/excitation (ca 10^{-16} seconds) the excited electronic states relax to vibrational/rotational levels of the ion's ground state.

(ii) The rate of dissociation is slow compared with the rate of redistribution of internal energy among all internal degrees of freedom.

(iii) Fragments are formed in competing and consecutive unimolecular decompositions.

The QET yields a rate expression of

(1.13) $k_E = (\sigma/h)[w^{\ddagger}(E-E_o)]/\rho E.$

k_E = rate at an excess of internal energy E
σ = symmetry factor
h = Planck's constant
$w^{\ddagger}(E-E_o)$ = number of vibrational and rotational states in the excited ion which have an energy in the range $E \rightarrow E_o$
E_o = minimum energy required for reaction (activation energy)
ρE = density of states for reactant ion from E to $E + \delta E$

In general, a low density of states (shallow potential well) will lead to a fast dissociation. A high density of states (deep potential well) will lead to a slow dissociation.

The value of the rate constant derived from the QET may be simplified to yield Equation 1.14.[9] This simplification is not accurate at low values of the internal energy, E.

(1.14) $k(E) = \nu[(E-E_o)/E]^{s-1}$

s = the total number of oscillators
ν = the frequency factor

This equation may be expressed in a logarithmic form

(1.15) $\ln k = \ln\nu - (s-1)(E/E_o)[1 + \frac{1}{2}(E/E_o) + \ldots].$

The rate of dissociation will depend on the internal energy of the molecule as shown in Figure 1.10. Near threshold, the rate of reaction rapidly increases with increasing internal energy. At high internal energies the curve tends to a limit at the frequency factor which is approximately equal to the time required for one vibration.[4]

Figure 1.10 Effect of Internal Energy on the Rate Constant for Unimolecular Dissociation

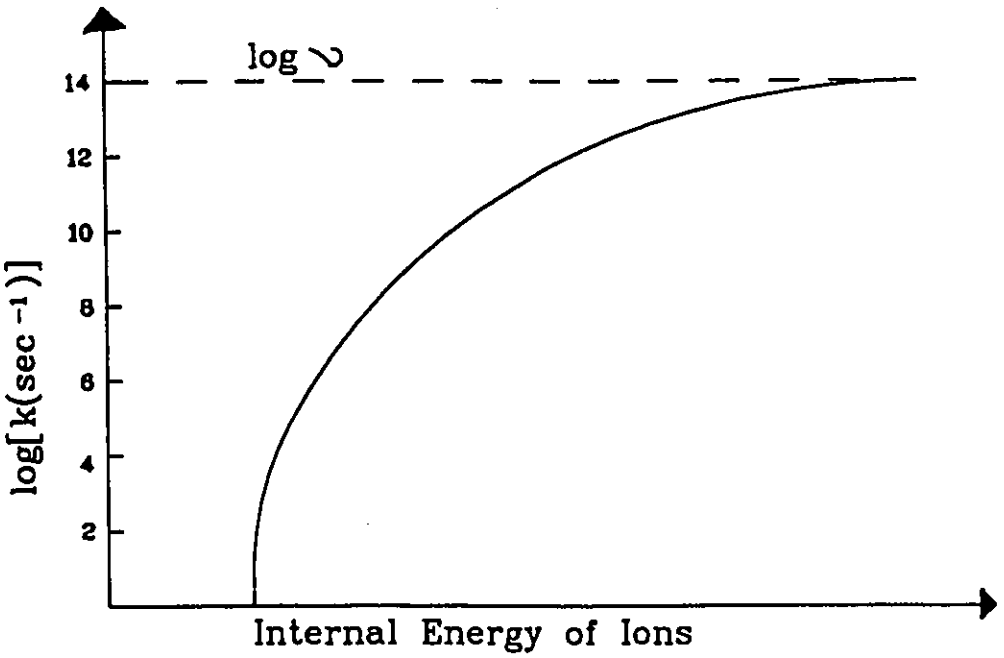

The frequency factor may be considered as a measure of the entropy factor for the fragmentation. For a simple bond cleavage it is approximately equal to the vibrational frequency of the bond which is broken (which can be measured from an infrared spectrum). For a rearrangement reaction, a particular arrangement of the atoms is probably required and so the frequency factor is generally lower than for a bond cleavage.[10] The number of oscillators is 3n-6, where n is the number of atoms in the ion. However, all oscillators are not equally effective and the number of oscillators is usually divided by three to give better values of the rate constant.

If the frequency factors are similar then the rates of fragmentation are approximately proportional to the activation energies. Also, where the activation energy for rearrangement followed by dissociation is lower than for a simple bond cleavage, the former process may become kinetically preferred as the internal energy is lowered (lowering the electron energy), even though the frequency factor is smaller.

A qualitative approach to ion fragmentation predicts that fragmentations involving a simple bond cleavage will have a larger rate than those involving rearrangement. Also, the most abundant fragment ions in the mass spectrum will be those which belong to the dissociations leading to the lowest energy products.

Section 1.5.3 Rearrangement of the Molecular Ions

Although the structure of the ion immediately after ionization is the same as the sample molecule, it is common for the ion to rapidly isomerize to a structure that may be quite different from the initial molecule.[11] The ion once rearranged may be stable or may have sufficient energy to fragment. For instance, it was shown by deuterium labelling and kinetic energy release (see Section 2.1.2a) measurements that the $[M-C_2H_4]^{+\cdot}$ distonic ion (an ion in which the radical and charge bearing sites are separated by at least two atoms) from o-hydroxybutyrophenone, 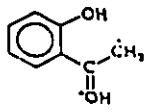 , rearranges to the keto form, 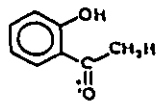 , prior to loss of $\cdot CH_3$.[12]

The most widely known mass spectrometric rearrangement is the McLafferty rearrangement[13] which involves the six-centred transfer of hydrogen in carbonyl compounds. The McLafferty rearrangement of ionized 1-pentanone is illustrated in Equation 1.16.

(1.16) 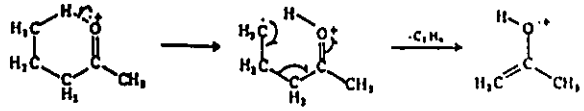

The stable structure from which a molecular ion fragments is known as the reacting configuration.[14] Consider two isomeric ions A_1^+ and B_1^+ which fragment to give products $A_2^+ + A_3$ and $B_2^+ + B_3$ respectively. The behaviour of A_1^+ and B_1^+ will depend on the barriers for rearrangement and decomposition (Figure 1.11).

Figure 1.11 Three Possible Potential Energy Diagrams Illustrating the Relationship Between Rearrangement and Dissociation for Two Isomeric Ions, $A_1^+ + B_1^+$

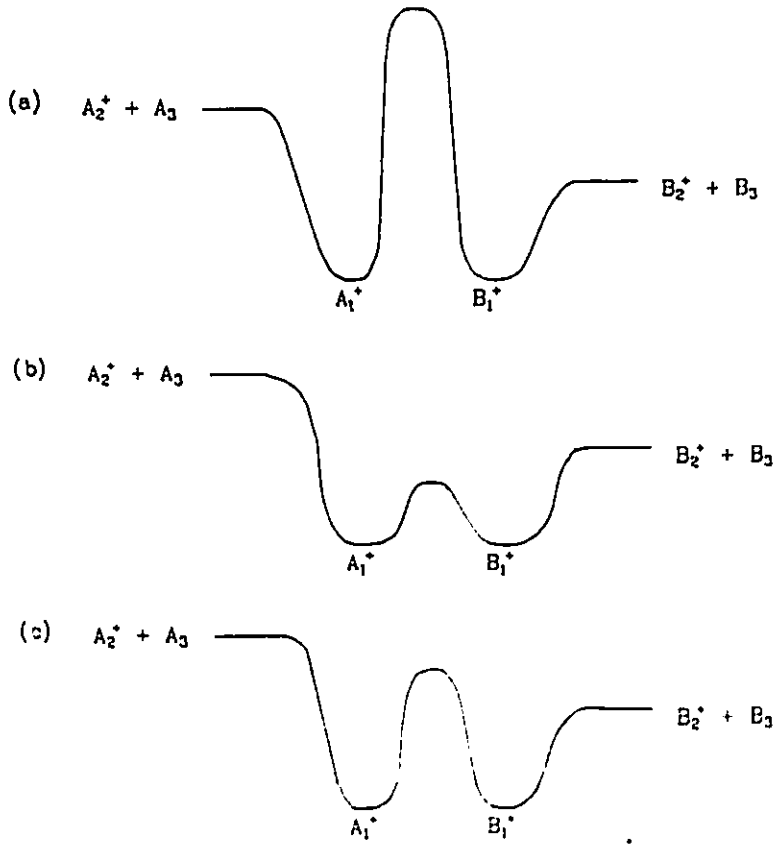

In case (a), the barrier for isomerization is larger than the barrier for dissociation. Therefore, A_1^+ and B_1^+ will not interconvert below the energy for decomposition. Even above this energy, it is unlikely that isomerization will occur since the rate for decomposition will be much faster ($W^+(E-E_o)$ will be larger for dissociation).

In case (b), the barrier for isomerization is smaller than either dissociation barrier. Therefore, there will be equilibrium between the two structures prior to dissociation.

In case (c), the isomerization barrier lies between the two dissociation barriers. Ion B_1^+ will dissociate with no rearrangement while it is likely A_1^+ will isomerize to B_1^+ prior to dissociation.

Section 1.5.4 Ion Lifetimes

A mass spectrum does not solely depend on the kinetics and thermodynamics of ion fragmentation but also on the time between formation and detection of ions. Ions which have a very small excess energy above the products or which undergo extensive rearrangement prior to fragmentation will decompose much more slowly than ions initially formed with a large excess of energy.[1] The time scale of events occurring in the ZAB is shown in Figure 1.12.[15]

Figure 1.12 Timescale of Events Occurring in the ZAB-2F Mass Spectrometer (Accelerating Voltage = 8 kV, Ion of m/z 100)

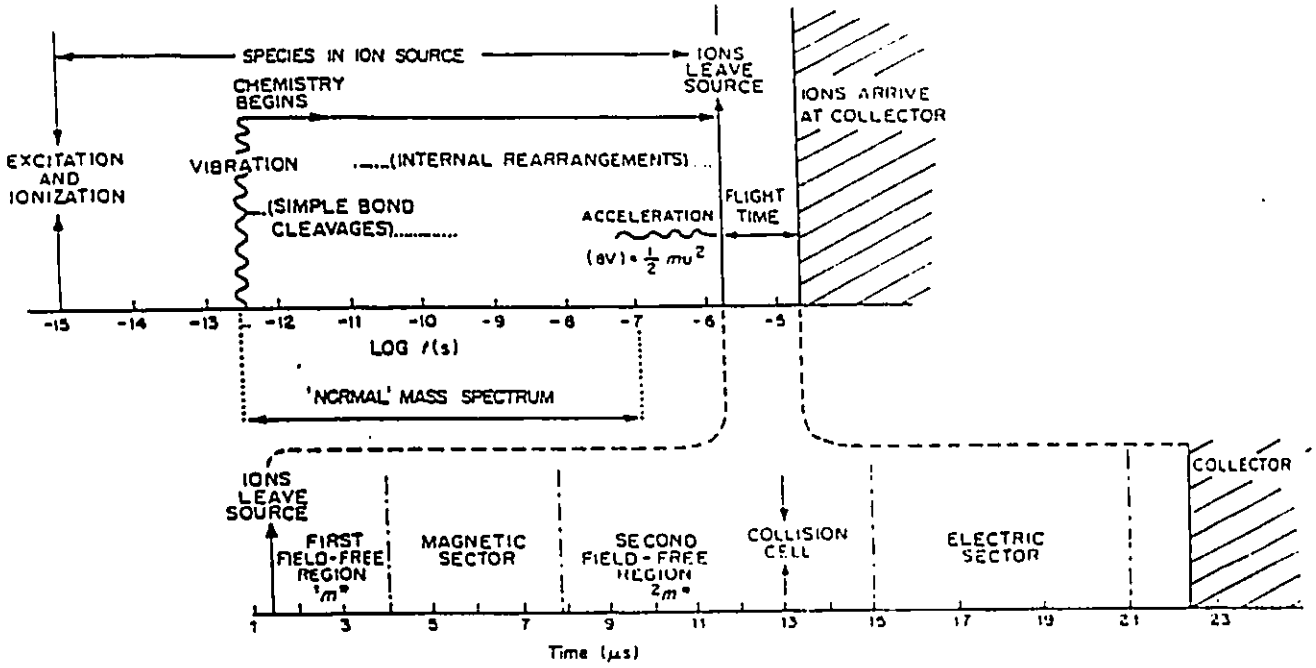

Section 1.6 Ion Thermochemistry

Mass spectrometry is one of the most versatile and useful techniques for obtaining thermochemical data on gaseous ions (and neutrals). There are essentially two types of measurements performed: The minimum energy required to ionize a molecule (ionization energy, IE) and the minimum energy required to cause the appearance of a fragment ion (appearance energy, AE).

Section 1.6.1 Ionization Energies

Equation 1.12 shows the removal of an electron from a molecule to form an ion. The time required for electron impact ionization (ca 10^{-16} sec) is much less than the time required for a single vibration (ca 10^{-14} sec).[4] Thus, little change will occur in the

position of the nuclei during the electronic transition (see Section 1.5.1). The ion will not be formed in its ground state but in the vibrational, rotational state of the ion most closely corresponding to the geometry of the molecule prior to ionization. This generality is what is known as the Franck-Condon principle.[16] (See Figure 1.13). The energy difference between this state and the molecules' ground state is known as the vertical IE (the name is self explanatory). A transition from the ground state of the molecule to the ground state of the ion gives a measure of the adiabatic IE. NO_2 provides an excellent example of the Franck-Condon principle. Neutral NO_2 has a bent ground state. The ionic ground state is linear. The adiabatic ionization IE as measured by resonance enhanced multiphoton ionization is 9.59 eV.[17] The vertical IE as measured by photoelectron spectroscopy is 11.22 eV.[18] If there is little or no geometry change between the ion and molecule then the vertical and adiabatic IE will be the same.

Figure 1.13 Franck-Condon Diagram Illustrating Vertical (V) and Adiabatic (A) Ionization Energies

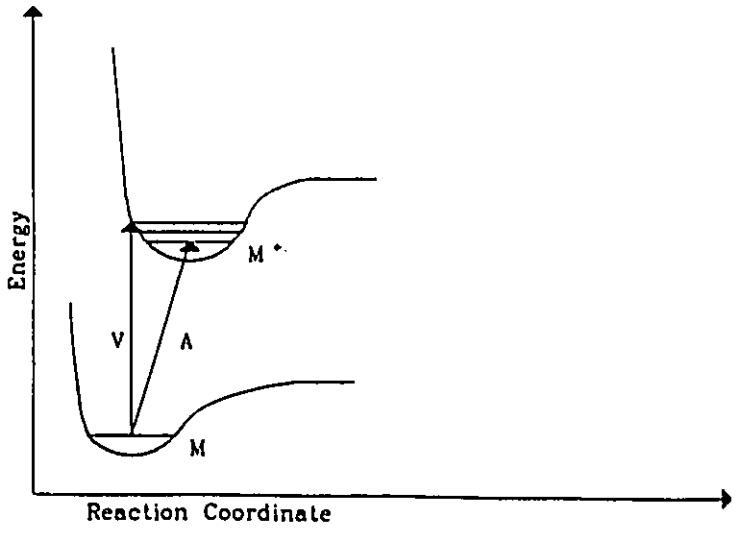

The heat of formation of the molecular ion may then be calculated from Equation 1.17.

(1.17) $\Delta H_f[M^{+\cdot}] = \Delta H_f[M] + IE_{adiabatic}$

The heats of formation of a wide variety of molecules have been tabulated.[2] Where the necessary thermochemical information for the neutral molecules is unavailable one may reliably estimate $\Delta H_f[M]$ using the group additivity tables of Benson.[19]

Section 1.6.2 Appearance Energies

Consider a reaction in which an ion, $M_1^{+\cdot}$, dissociates unimolecularly to form a fragment ion, M_2^+, and a neutral, $M_3\cdot$ (Equation 1.18).

(1.18) $M_1^{+\cdot} \rightarrow M_2^+ + M_3\cdot$

Measuring the appearance energy for the reaction shown in Equation 1.18 will give one the heat of formation of M_2^+ according to Equation 1.19 provided that (see Figure 1.14)

(1) The reverse energy barrier (E_{rev}) =0

(2) The kinetic shift (E_{kin}) = 0.

(1.19) $\Delta H_f[M_2^+] = \Delta H_f[M_1] + AE - \Delta H_f[M_3\cdot]$

As one can see from Figure 1.14 a reverse energy barrier will cause the calculated heat of formation of the fragment ion to be high. For most reactions involving simple bond cleavage the reverse energy barrier will be zero since ion-free radical recombination reactions normally proceed without activation energy.[9,16] However, rearrangement reactions in which stable neutral and ionic products are formed may often have a large reverse energy

barrier.[20] For example, $CH{\equiv}C\text{-}CH_2Br^{+\cdot}$ fragments to give as products cyclo-$C_3H_3^+$ + $Br^\cdot$ with a reverse energy barrier of 0.83 eV.[21] In other words, the $CH{\equiv}C\text{-}CH_2Br^{+\cdot}$ ion rearranges (prior to loss of $Br^\cdot$ to give the thermodynamically most stable ion, cyclo-$C_3H_3^+$) but with a transition state 0.83 eV higher in energy than the products.

Figure 1.14 Energy Diagram for the Unimolecular Dissociation of $M_1^{+\cdot}$ Illustrating the Effect of a Kinetic Shift and a Reverse Energy Barrier on the Measured Appearance Energy of M_2^+

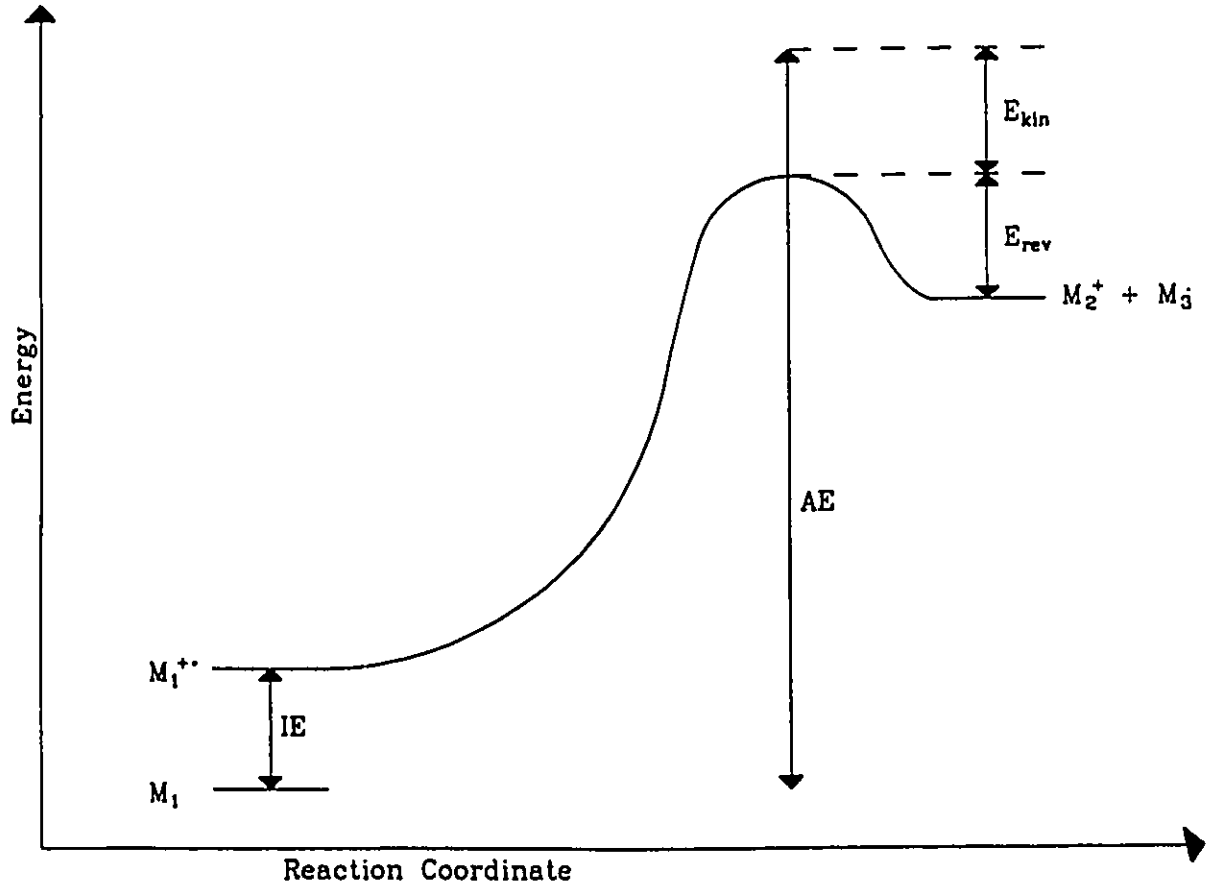

The kinetic shift, E_{kin}, is the energy above the transition state which is required so that fragmentation occurs during the timescale of the experiment. Therefore, the kinetic shift is determined by the relationship between the internal energy and the rate constant for fragmentation. For example, the E_{kin} of an ion formed in the ion source (time between ionization and fragmentation <0.1 μsec) will be larger than that of an ion formed in the 1FFR (time between ionization and fragmentation = 0.1-1.0 μsec). The AE of $C_6H_4^{+\cdot}$, m/z 76, for the reaction $C_6H_5CN + e \rightarrow C_6H_4^{+\cdot} + HCN + 2e$ falls by ~ 0.3 eV when the rate constant falls from 10^5-10^4 sec^{-1} (as the observation time prior to fragmentation increases).[22] For ion decompositions in which the rate of fragmentation rises only slowly with increasing internal energy there will be a large kinetic shift which should not be ignored.[15] For reactions which do <u>not</u> occur on the metastable time frame the rate constant rises rapidly with increase in internal energy and so the kinetic shift is generally less important.[23]

For the vast majority of fragmentations the two assumptions that there is no reverse energy barrier and that the kinetic shift may be ignored are valid.[15]

<u>Section 1.6.3</u> Ionization Efficiency Curves

An ionization efficiency curve is a measure of the molecular ion (or fragment ion) beam intensity as a function of electron energy. The cross-section for electron impact ionization near threshold (Equation 1.20) is determined mainly by the number of

degrees of freedom for removal of excess energy from a collision complex involving the neutral molecule and approaching electron (ie one less than the number of electrons leaving the complex).[24]

(1.20) $\sigma(E) = c(E-IE)^{n-1}$

$\sigma(E)$ = the cross-section at an electron energy, E
c = a constant

For single ionization (n=2) one should therefore get a linear threshold. However, since one gets ionization from various rotational levels of the molecule to various rotational/vibrational levels of the ion, and due to a lack of electron energy resolution, the ionization efficiency curve will appear not as a straight line but as a smooth curve.

The shape of the curve near threshold is very sensitive to the electron energy.[4] Therefore, two major problems in determining IE and AE from these curves are the energy spread of an electron beam produced from a heated filament and determining the exact energy of the electrons.

In cases where one may obtain a monoenergetic beam of electrons one generally obtains quite a sharp onset, with curvature extending over only 0.1 eV or less, at the electron voltage which corresponds to the IE or AE.[25] It is therefore quite sufficient simply to measure the initial onset and to calibrate the electron energy using a calibrant with a well established IE.

However, in cases where there is a significant spread in the energy of the electron beam it is still possible to get a satisfactory value. The value is obtained using the extrapolated voltage difference technique.[26] This technique was first used by

J.W. Warren in 1950.[27] The ionization efficiency curves of both a known and the unknown are recorded. The two curves are normalized such that they become equally steep. Then a plot of ΔV versus i is made where ΔV is the difference in electron voltages corresponding to various values of the ion current, i. This plot is extrapolated to i = 0. This value corresponds to the difference between the IE (AE) of the unknown and calibrant (see Section 2.2.3).

Figure 1.15 The Effect of Franck-Condon Factors on the Shape of an Electron Impact Ionization Efficiency Curve

The vertical lines represent the relative probabilites of a transition from the ground state molecule to various vibrational states of the ion. The vertical (v) and adiabatic (a) ionization energies are shown.

I no geometry change
II small geometry change
III large geometry change

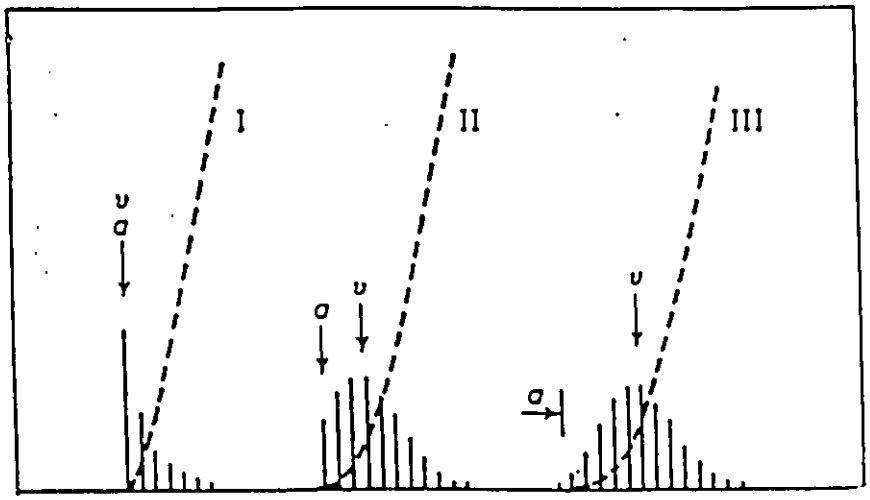

With the extrapolated difference technique it is important that the shape of the two curves are similar.[28] The shape of ionization efficiency curves are affected by several factors including the Franck-Condon Principle, Autoionization, and Hot bands.[28] The effect of the Franck-Condon factors can be seen in Fig. 1.15.[29] As the geometry change between the neutral molecule and its molecular ion increases, the ionization efficiency curve becomes more and more shallow. Hot bands (which arise from transitions from vibrationally excited states (v>0) of the molecule) will tend to put a tail on the low energy side of the "true" threshold curve. This effect will be enhanced if the molecule is heated since the increased thermal energy will increase the population of vibrationally excited states.

Section 1.6.4 Competing Reactions

The measurement of an AE may be affected if there are two or more competing fragmentation channels. Consider the following example.

(1.21) $M_1^{+\cdot} \xrightarrow{-k_1} M_2^{+} + M_3^{\cdot}$

(1.22) $\xrightarrow{-k_2} M_3^{+} + M_4^{\cdot}$

The rate constants as a function of internal energy for reactions (1.21) and (1.22) are shown in Figure 1.16. Near the threshold for reaction (1.21) the rate of reaction (1.22) is much greater than the rate of reaction (1.21). Thus, observation of reaction (1.21) will not occur until some energy above its

threshold where the rates for reactions (1.21) and (1.22) are comparable. Therefore, the measured value for the AE of $M_2^{+\cdot}$ will be too high.

Figure 1.16 Rate Constants as a Function of Internal Energy for Two Dissociation Pathways of $M_1^{+\cdot}$

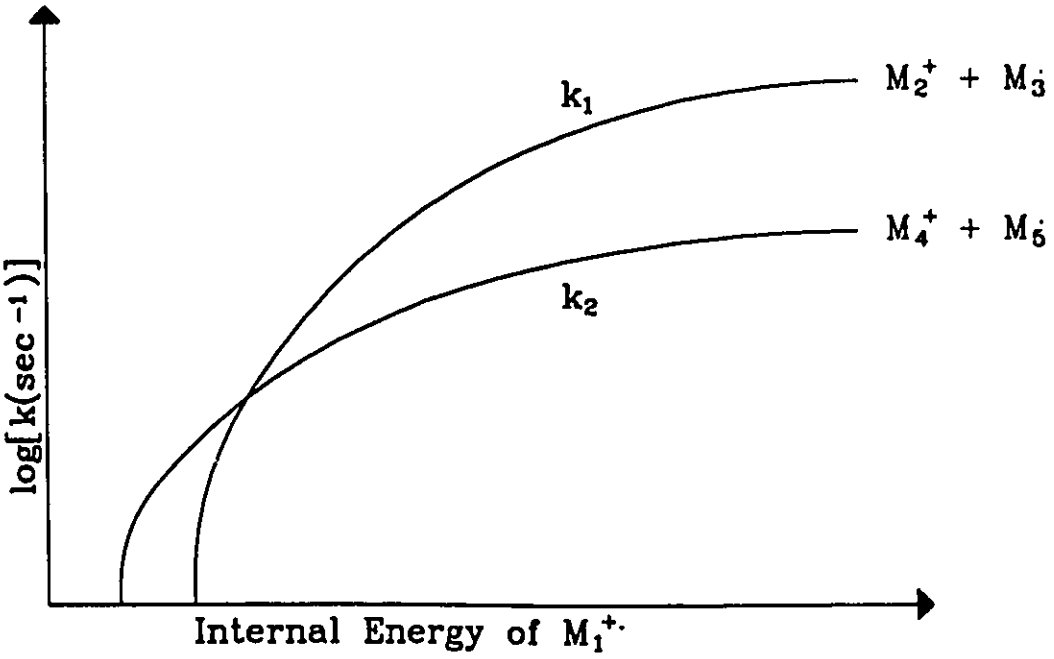

Section 1.6.5 Importance of Correct Product Identification

Another difficulty which may be encountered with AE measurements is identifying the products (ions and neutrals). One cannot simply assume that the products are due to simple bond cleavage since rearrangement is not uncommon. Therefore, structure

assignment from an independent experiment(s) is important before any ΔH_f may be confidently assigned to ions or neutrals. For instance, it was concluded[30] from a previous collisional activation study[31] and from AE measurements that the $[C_2H_5O]^+$ ions formed from the fragmentation of $C_2H_5OC_2H_5$ have the structure $CH_3CHOH]^+$ and that the neutral fragments are $H\cdot$ and C_2H_4 not $C_2H_5\cdot$

There is also the possibility of a mixture of products in which case the AE will generally correspond to the isomeric ion with the lowest ΔH_f.

If by fire
Of Sooty coal th'emperic alchymist
Can turn, or holds it possible to turn,
Metals of drossiest ore to perfect gold

MILTON
Paradise Lost

EXPERIMENTAL

The following sections will describe the various experiments that were performed on the ZAB, the MS-9, and the energy selected electron ion source and quadrupole mass filter along with relevant theory and some of their practical uses.

Section 2.1 Experiments Performed with the Vacuum Generators Analytical ZAB-2F Mass Spectrometer

Several different experimental techniques may be performed using the modified ZAB-2F which has been described in Section 1.1: normal mass spectrum, mass analyzed ion kinetic energy spectroscopy, collisional activation, charge stripping, collisionally induced dissociative ionization, neutralization reionization mass spectrometry, and negative ion mass spectrometry. These techniques are described in the sections below.

Section 2.1.1 Normal Mass Spectrum

The normal mass spectrum run on the ZAB involves scanning the magnetic field to transmit ions of different mass through the magnetic analyzer while maintaining the electric field at a constant value such that all source generated ions are transmitted through the electrostatic analyzer and may be detected at the second detector. What one observes is the abundance of ions which are generated in the ion source (no metastable peaks are observed). The most intense peak is known as the base peak.

Section 2.1.1a Interpreting A Normal Mass Spectrum

Interpretation of a normal mass spectrum is based upon rationalization of the observed peaks. The first step is usually deciding which peak is the molecular ion, $M^{+\cdot}$. One usually assumes that the highest observed mass of significant intensity is the molecular ion. The molecular ion is accompanied by isotope ions one or more mass units higher [$(M+1)^{+\cdot}$, $(M+2)^{+\cdot}$, etc.] which may be useful in assigning the presence of various atoms (such as S, Cl, Br) and/or the number of carbon atoms. If $M^{+\cdot}$ is at an odd mass number than it probably contains an odd number of nitrogen atoms. One may then calculate a molecular formula; applying simple rules of valency to determine the presence of rings and/or multiple bonds. The next step is to note the major fragment ions closest to $M^{+\cdot}$ (ignoring low mass ions because they can be produced from several different precursor ions and therefore give no direct structural information about the molecular ion) and attempt to elucidate the main fragmentation pathways. It may be useful to take a functional-group approach in which compounds containing a common functional group may be expected to follow similar fragmentation pathways. It is also often observed that certain functional groups give rise to characteristic peaks at particular m/z values. For example, an intense peak at m/z 91 ($C_7H_7^+$) often indicates the presence of a benzyl group. Therefore, it may be possible to assign a structure to an unknown compound based on its normal mass spectrum.

The electron impact normal mass spectra of many thousands of known compounds have been determined and published in volumes such as the EPA/NIH Mass Spectral Data Base.[32] It is therefore useful to compare a normal mass spectrum with the reference spectra with the aim of finding a match.

It is also possible to obtain the single focusing normal mass spectrum by recording the spectrum at the first detector. In this way, the ions are only mass analyzed, not energy analyzed, and so both source generated ions and fragment ions formed in the 1FFR (metastable peaks with an apparent mass to charge ratio of m_2^2/m_1) are observed. See Section 1.2.1.

Section 2.1.2 Mass Analyzed Ion Kinetic Energy Spectroscopy -MIKES

During a MIKES experiment, the first magnetic analyzer is set to transmit ions of one selected mass into the 2FFR. Some of these ions will decompose in the 2FFR to give fragment ions with kinetic energy $(m_2/m_1)zV_{acc}$. These fragment ions are observed by sweeping the electric field and then are detected at the second detector.

Section 2.1.2a Metastable Ions and Kinetic Energy Release - KER

When $M_1^{+\cdot}$ fragments, internal energy of $M_1^{+\cdot}$ is isotropically converted into translational degrees of freedom of the products. This broadens the energy spread of the fragment ion, M_2^+. Metastable ions which fragment with a large reverse energy barrier and/or kinetic shift produce products with significant amounts of internal energy; whereas metastable ions which fragment near their

thermochemical threshold produce products with little or no internal energy. The amount of excess energy of the products above their thermochemical minimum is indicated in the release of kinetic energy. If there is a large reverse energy barrier and/or kinetic shift then there will usually (but not always) be a large KER and a dish-shaped metastable peak (see Section 2.1.2b). If the reaction occurs near threshold then there will always be a small KER and a narrow Gaussian metastable peak (see Section 2.1.2b).

The release of kinetic energy is amplified due to the high translational energies of the ions and results in peak broadening with respect to source generated ions in the laboratory frame of reference. In order to convert the measured peak width, ΔV, into an actual kinetic energy release one must perform an analysis based on conservation of energy and momentum.[33] If T measures the internal energy of m_1^+ that is converted into translational energy in the fragmentation then the resulting expression is

(2.1) $$T = [m_1^2/16m_2m_3][\Delta V^2/V_{acc}].$$

In order to correct the metastable peak width for the energy spread of the main beam one must use a corrected value of ΔV.[34]

(2.2) $$\Delta V_{corr} = (\Delta V^2 - \Delta V_{mb}^2)^{1/2}$$

ΔV_{mb} = the width of the main beam

It is common to use the width at half height to calculate the kinetic energy release ($T_{0.5}$) even though this value has no special significance. It is however, a convenient value for comparisons. More significant values correspond to the average kinetic energy release <T> and to the most probable kinetic energy release T_{mp}.

In order to measure a $T_{0.5}$ value, good energy resolution is required. This resolution is accomplished by narrowing Y_1, Y_4 and Y_5 (see Section 1.1.9) until the width of the main beam at half-height is less than 3V. The effect of narrowing an energy resolving slit on metastable peak shape is shown in Figure 2.1.[35] It should be noted that the height of broad signals will decrease relative to the height of narrow signals with increasing resolution.[15]

Figure 2.1 The Effect of Increasing Energy Resolution on Metastable Peak Shapes

(a) Gaussian Shaped Metastable Peak
$[C_2H_4O_2]^{+\cdot} \rightarrow [C_2H_3O]^+ + [OH]^\cdot$

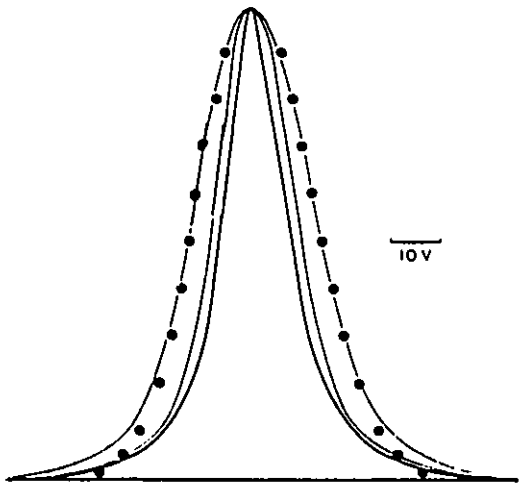

(b) Dished Metastable Peak
$[C_3H_7]^+ \rightarrow [C_3H_5]^+ + H_2$

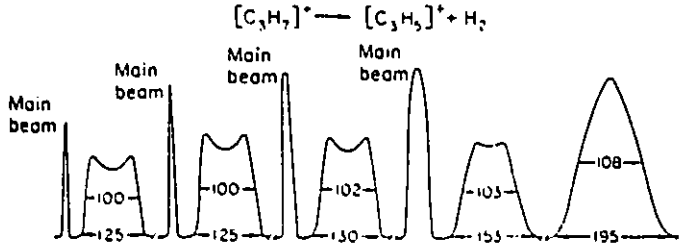

Section 2.1.2b Metastable Peak Shapes

There are three commonly observed types of metastable peak shape: Gaussian, dished, and composite (see Figure 2.2).

Figure 2.2 Metastable Peak Shapes

(a) Gaussian - Acrylic Acid [$C_3H_3O_2$], m/z 55 → m/z 27

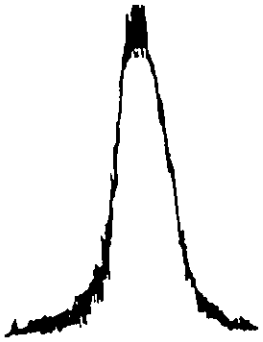

(b) Dished - o-Nitrotoluene [$C_7H_7NO_2$], m/z 137 → m/z 107

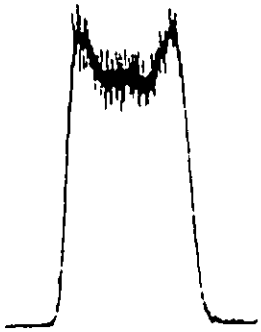

(c) Composite - p-Chloronitrobenzene [$C_6H_4ClNO_2$], m/z 157 → m/z 127

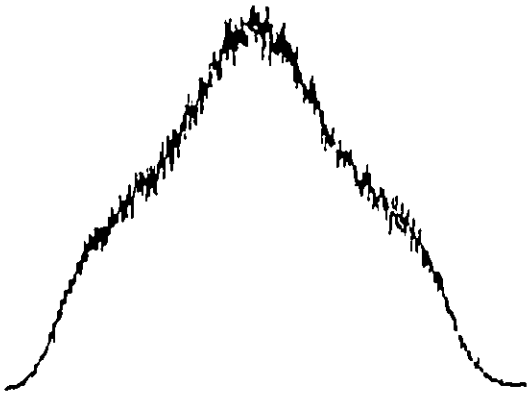

Gaussian shaped metastable peaks are typically associated with $T_{0.5}$ < 80 meV. The distribution of released energies, n(T), and the average released energy can be obtained by analytical methods.[36] The n(T) curves, plots of the probability of having a kinetic energy release of T, have maxima (T_{mp}) close to zero and Maxwell-Boltzmann type profiles (see Figure 2.3).

Figure 2.3 Metastable Peak Profiles and n(T) Curves for $CH_3^{\cdot}$ Loss from Two $[C_6,H_{10}]^{+\cdot}$ Isomers

(a) Metastable Peak Profiles (b) n(T) Curves

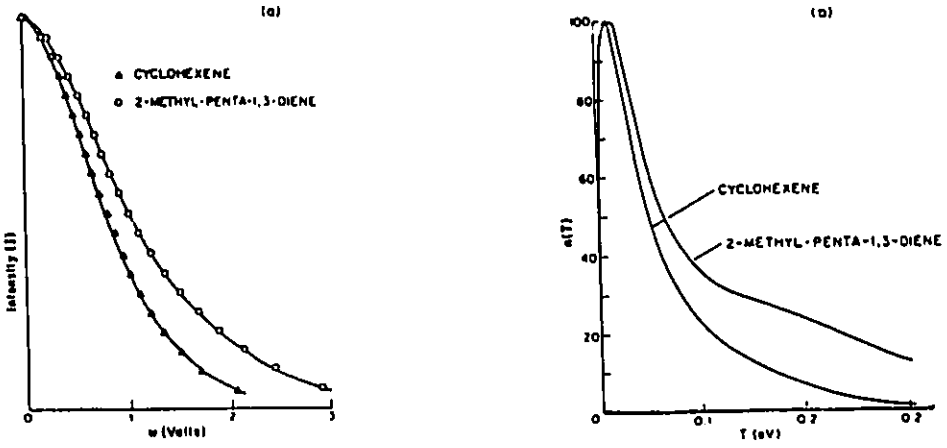

T_{av}[cyclohexene] = 0.07 eV
T_{av}[2-methylpenta-1,3-diene] = 0.13 eV

Flat-topped and dished metastable peaks arise when $T_{0.5}$ values are considerably larger than that of a typical Gaussian peak. The dish has no physicochemical origin but is produced by z-axial discrimination. Fragment ions which have received a large kinetic energy release in the plane of the long axis of the energy resolving slits are not transmitted because the slit is not long

enough. The longer the slit, the more shallow the dish will be. All flat topped or dished metastable peaks are produced from reactions involving a reverse energy barrier. The reverse is not necessarily true. No general method has been presented to calculate n(T) for these peaks. However, it has been discovered that T_h (width of the metastable peak across its maxima or "horns") approximates the minimum released kinetic energy, T_{min}.[37]

Composite peaks may show marked discontinuities in their profiles and can be seen to consist of a Gaussian peak atop a dished peak or a pair of superimposed dished peaks. However, a composite peak involving two Gaussian peaks may not be discernable to the naked eye. In these cases the n(T) curve will have a shoulder which illustrates the composite nature of the peak (see Figure 2.3).

Composite peaks may arise as follows:

(i) Two isomeric precursors decompose by loss of a common neutral

$$[ABCD]^{+\cdot} \rightarrow ABC^{+} + D^{\cdot}$$
$$[ACBD]^{+\cdot} \rightarrow ACB^{+} + D^{\cdot}$$

(ii) A single precursor ion fragments to give two isomeric daughter ions

$$[ABCD]^{+\cdot} \rightarrow ABC^{+} + D^{\cdot}$$
$$\rightarrow ACB^{+} + D^{\cdot}$$

(iii) When an ion loses two isobaric fragments such as CO and C_2H_4.

Apparent composite peaks may arise from experimental artifacts. ^{13}C contribution from a metastable process one mass unit less than the ion of interest may produce an apparently composite peak. For example[21]

$C_4H_8^{+\cdot}$ → $C_3H_4^{+\cdot}$ + CH_4 (dish shaped)

$^{13}CC_3H_7^+$ → $^{13}CC_2H_3^+$ + CH_4 (Gaussian)

If the fragmentation is particularly collision sensitive, then even at the lowest gas pressures achievable in the mass spectrometer, collision induced dissociation of the mass selected ions (see Section 2.1.3) may occur, resulting in an apparently composite peak.

Lowering the ionizing electron energy and observing the peak at longer lifetimes (ie. in different field free regions) should each change the shape of a composite peak since the relative abundance of the higher energy process will be reduced in both cases. Deuterium and ^{13}C labelling may also serve to separate the two fragmentation pathways.

Section 2.1.2c Ion Structure and Metastable Peaks

One can learn a great deal from metastable peak shapes, the relative abundance of metastable peaks and from $T_{0.5}$ values.

Metastable peaks arise from ions having a narrow range of internal energies (< 1eV) fragmenting over a small time interval (1-2μsec) in the range of ca 1-20μsec, depending on the mass spectrometer used.[38] Therefore, they contain more discernable information than a normal mass spectrum (arising from ions having a large range of internal energies).

Metastable peak characteristics apply only to the reacting configuration (stable structure which leads directly to the transition state) of the fragmenting ion. It was proposed that

when an ion of a given structure has two or more reasonably intense metastable peaks than their relative intensities will be constant, independent of the method of the ions' generation.[39] Therefore, the abundance ratio test[40] stated that "if dissociating ions of a given m/z ratio derived from a variety of precursors all display the same metastable peaks, having similar abundance ratios, then it can be assumed (but not proved) that the fragmenting ions have the same reacting configuration (or common compositions of different reacting configurations)."

The comparison of metastable peak shapes and kinetic energy release values for the fragmentation of isomeric ions may be used to characterize the structure of these ions: an idea first proposed by Jones et al. in 1970.[41] The $T_{0.5}$ values of a metastable peak which arises from a single reacting configuration should vary little with mode of preparation of the metastable ion (±5%).[38] There are three cases to consider (see Section 1.5.3).

(i) The isomeric ions do not interconvert prior to any of their metastable fragmentations. (Figure 1.10a)

In this case any common metastable peaks from the different isomeric precursors are unlikely to have an identical shape and/or $T_{0.5}$ value. Also, any competing reactions will most likely have different abundance ratios. For example, loss of $H^{\cdot}$ from two isomeric $[C_2H_4O]^{+\cdot}$ ions (acetaldehyde and ethylene oxide) produces metastable peaks having completely different peak shapes and $T_{0.5}$ values.[42]

(ii) The isomeric ions can freely interconvert at energies below the activation energy for any fragmentation. (Figure 1.10b)

In this case closely similar metastable ion phenomena are to be expected. There may be one reacting configuration or several which freely interconvert. Thus, it was found that the other two stable $[C_2H_4O]^{+\cdot}$ ions (vinyl alcohol and $[CH_3COH]^{+\cdot}$) both lose $H^{\cdot}$ to produce $[CH_3CO]^{+}$ via a common reacting configuration, $[CH_3COH]^{+\cdot}$, and so cannot be distinguished on the basis of this observation.[43]

(iii) One or more isomeric forms of the ion must surmount an energy barrier in order to attain an isomeric structure (reacting configuration) from which fragmentation can occur. (Figure 1.10c)

If the energy barrier exceeds the fragmentation threshold and a significant fraction of the ions isomerize on the metastable time frame ($k = 10^6$-10^5 seconds^{-1}) then the energy rich reacting configuration will rapidly fragment. Thus, the kinetic energy release should be larger than via fragmentation directly from the reacting configuration. For example, it was shown that $[CH_3CHOCH_3]^{+}$ undergoes a rate determining isomerization to $[CH_3CH_2OCH_2]^{+}$ prior to loss of H_2O, C_2H_4 and CH_2O.[44]

In summary, different $T_{0.5}$ values and/or peak shapes can arise from dissociation via different reacting configurations or from isomeric ions which fragment following a rate-determining rearrangement to a common reacting configuration.

Section 2.1.3 Collisionally Induced Dissociation - CID

Collisional activation (CA) occurs when ions which possess high translational energy collide with neutral atoms or molecules. During CA the ions acquire excess internal energy (a small fraction of their translational energy is converted into internal energy) which will lead to decomposition. This process (Equation 2.3) is known as collisionally induced dissociation (CID).

(2.3) $M_1^{+\cdot} + T \rightarrow [M_1^{+\cdot}]^* \rightarrow M_2^+ + M_3^\cdot$

The average amount of internal energy acquired per collision in an 8000 V ion of mass 100 is comparable to the average excess energy a molecular ion has after ionization by 70 eV electrons.[45] The large amount of energy imparted by collision makes subsequent fragmentation rapid and almost independent of the original internal energy of the precursor ion.[46] Therefore, ion abundances observed are reproducible and mostly independent of the mode of ionization. This is true provided that peaks arising from (slow) low energy pathways (metastable peaks) are excluded from the analysis.[46,47] Therefore, it is useful to record a MIKE spectrum of a precursor ion following collisional activation (CA mass spectrum). The abundance of peaks in the CA mass spectrum often correlates with the peaks in the normal mass spectrum thus providing information concerning pathways for the formation of ions in the ion source.[33]

Section 2.1.3a Collisional Activation (CA) Mass Spectrum

The ion of interest, $M^{+\cdot}$, is mass selected with the first magnetic analyzer. The collision gas (usually oxygen or helium) is

leaked into a collision cell (collision cell II) located in the second field free region. The pressure inside the cell can be maintained at a relatively high pressure while the regions around the cell are still at a very low pressure. The precursor ion will be induced to fragment and the fragment ions will have a kinetic energy of $(m_2/m_1)zV_{acc}$ where m_2 is the mass of the collision induced fragment ion, M_2'. These fragment ions may be separated by scanning the electrostatic analyzer.

The appearance of a CA mass spectrum will depend on several factors: choice of gas, gas pressure and ion translational energy.

Oxygen and helium have been used as the collision gas for CA experiments in this thesis. Helium has been used due to its high efficiency in causing CID. Helium, on average, converts more of the translational energy of the ion into internal energy than does oxygen and so causes a larger degree of fragmentation. Oxygen is more useful in looking at lower energy processes.

The pressure of gas in the cell is adjusted so that the intensity of the mass selected ion beam is reduced by 10%. This beam reduction corresponds to a measured pressure of about 5×10^{-7} torr (this pressure is measured at a nearby ionization gauge) and is roughly four orders of magnitude smaller than the true pressure in the collision cell. The 10% beam reduction ensures that the majority of fragments are due to single collision processes. The relative abundance of single and multiple collisions as a function of beam reduction is shown in Figure 2.4.

Figure 2.4 Total Collision Probability and the Fractions of Single and Multiple Collision Processes as a Function of Collision Gas Pressure (For an Ion of Collision Cross-Section 5×10^{-18} cm^2, Collision Path 1 cm)

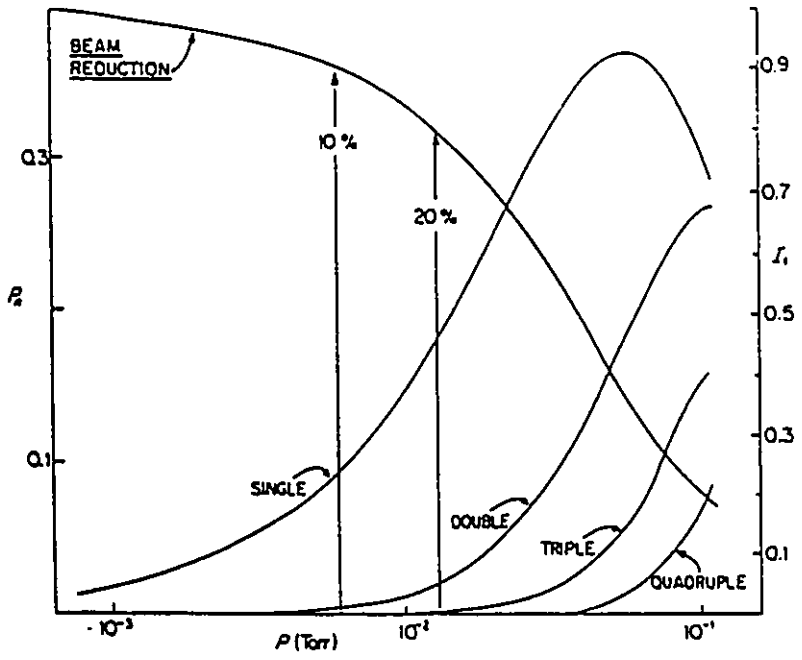

Multiple collision conditions may reduce structure-specific information.[15] As a simple example, the effect of increasing gas pressure on the CA mass spectrum of [allene]$^+$ ions is shown in Figure 2.5. As the percentage of multiple collisions increases so does the percentage of ions generated from high energy dissociation pathways. This point is illustrated by the decrease in the relative intensity of the structure characteristic m/z 14 peak with respect to the more energy demanding processes responsible for the peaks at m/z 12 and m/z 13.

Figure 2.5 The Effect of Collision Gas Pressure on the CA Mass Spectrum of [allene]$^{+\cdot}$ Ions, m/z 12-15
The Main Beam Transmission is Given as a Percentage and the Relative Signal Strengths are in Parentheses

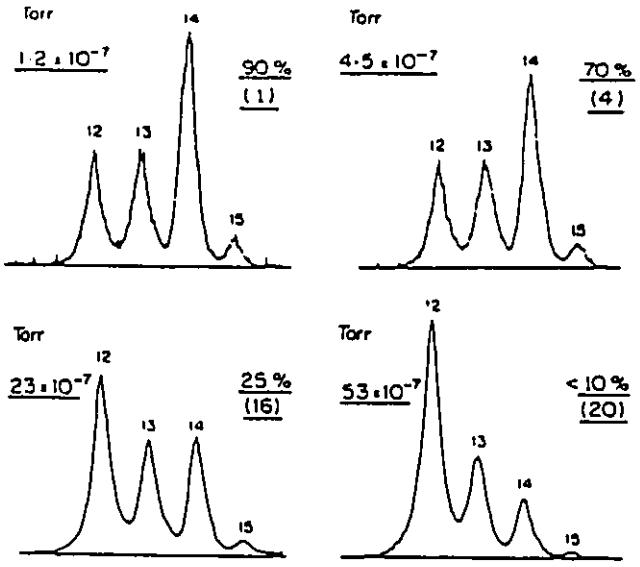

It was shown that the most probable energy gained on collision is proportional to the square of the translational energy of the ion.[48] This will increase the relative intensity of the lower energy fragmentation processes with respect to higher energy processes as the translational energy is reduced.

Section 2.1.3b Metastable Peak or Peak due to Collisional Activation?

Peaks in a CA mass spectrum will have a width related to the KER for their fragmentation, as do metastable peaks. Generally, the CA peak will be wider since there is a larger range of internal energies which can be given to the ion and the fragment still be observed (the collision takes place in the 2FFR allowing fast fragmentations to be observed, unlike metastable ion fragmentation

where fast fragmentations have already taken place in the ion source).

The cross-section for CID may be very high and so peaks which appear to be metastable (occur in a MIKE spectrum) may be in fact due to CID. One way to determine whether a peak is due to a CA process and not a unimolecular metastable process is to measure the peak width, under energy resolution conditions, in the absence of and in the presence of increasing amounts of collision gas. If the width is constant for all measurements then the peak is most likely due solely to a CA process (if there was also a metastable component then the width would change with an increasing amount of contribution from CID unless by (rare) chance the kinetic energy releases for both the CID and metastable processes were the same).

In a CA mass spectrum peaks which are due both to unimolecular fragmentation and collisionally induced dissociation may be separated by putting a positive or a negative voltage on the collision cell. Consider the fragmentation $M_1^{+\cdot} \rightarrow M_2^{+} + M_3^{\cdot}$ and assume that there is a positive voltage, V', on the collision cell. $M_1^{+\cdot}$ will either fragment (i) inside the collision cell (following CA) or (ii) outside the collision cell (metastable ion)

(i) $M_1^{+\cdot}$ fragments inside the collision cell.

Upon approaching the cell, the kinetic energy of $M_1^{+\cdot}$ will be reduced from its initial value of zV_{acc} to a new value, $z(V_{acc}-V')$. $M_1^{+\cdot}$ then fragments to give M_2^{+}. The kinetic energy of M_2^{+} will be $(m_2/m_1)z(V_{acc}-V')$. After exiting the cell, $M_2^{+\cdot}$ will gain zV' of kinetic energy. The total energy of M_2^{+} will be $(m_2/m_1)zV_{acc} + (1 - m_2/m_1)zV'$ when it leaves the 2FFR.

(ii) $M_1^{+\cdot}$ fragments outside the collision cell.

For metastable ion fragmentation which occurs before the cell, the kinetic energy of $M_2^{+\cdot}$ will be $(m_2/m_1)zV_{acc}$. On passing through the cell, the kinetic energy will be decreased and then increased by an equal amount, zV'. Thus, there is no observable change in the kinetic energy of M_2^{+}.

Applying a positive voltage to the cell increases the kinetic energy of CA fragments and leaves unchanged the kinetic energy of metastable ion fragments. Thus, by scanning the electric sector, CA components will appear at higher energy than unimolecular components. If a negative voltage is applied to the cell then CA components will appear at lower energy than unimolecular components.

Section 2.1.3c Ion Structure, Isomeric Ions and Collisional Activation

The ions which undergo collisional activation are those ions which have insufficient energy to fragment between the source and the collision cell. Therefore, they cover a broad range of energies from the IE (AE) of the ion up to and including energies appropriate to metastable fragmentation in the 2FFR (Fig 1.8).

If the precursor ion $[M_1^{+\cdot}]$ retains its initial structure (no rearrangement) over this whole range of internal energies then the CA mass spectrum will be structure specific for $M_1^{+\cdot}$ and should be similar to the normal mass spectrum.

Therefore, in cases where, at energies appropriate to metastable fragmentation, isomers freely interconvert and the

isomers cannot be distinguished based on their metastable peak characteristics, one may be able to distinguish the isomers due to their CA spectra since ions of lower internal energy are being sampled.

This point is illustrated by considering five $[C_3,H_8,N]^+$ ions: $[CH_3CH=NHCH_3]^+$, $[(CH_3)_2N=CH_2]^+$, $[CH_2=NHCH_2CH_3]^+$, $[(CH_3)_2C=NH_2]^+$, and $[CH_3CH_2CH=NH_2]^+$. Metastable peak characteristics indicated that the first two isomers rearranged to a common structure (or mixture of structures) prior to fragmentation while the last three isomers decomposed from distinct structures.[49] However, the CA mass spectra of the first two isomers were clearly different, illustrating that these two isomers exist as distinct stable species at energies below their common dissociation limit.[49]

Ions generated in the metastable time frame are generally produced with a very narrow range of internal energies only slightly over threshold. Therefore, a CA mass spectrum of an ion produced in the 1FFR will be specific to the structure for the ion generated since no rearrangements are expected to occur at such low internal energies. The ion of interest, $M_2^{+\cdot}$, must be produced by the fragmentation of a metastable ion, $M_1^{+\cdot}$. The first magnet is tuned to transmit an ion of apparent mass m_2^2/m_1 ($M_2^{+\cdot}$ ions which have been produced by the metastable fragmentation of $M_1^{+\cdot}$ in the 1FFR). A collision gas (O_2 or He) is leaked into collision cell II and the ions produced following CA are separated by scanning the electrostatic sector. The fragment ions, M_3^+, will have a kinetic energy = $m_3/(m_2/m_1)$.

Section 2.1.4 Charge Stripping - CS

In addition to CID, the presence of a collision gas may also produce singly charged ions which are sufficiently excited to lose an electron. This process (Equation 2.4) is known as charge stripping (CS).

(2.4) $M^{+\cdot} + T \rightarrow M^{++} + T + e$

$\rightarrow [(M-H)^{+}]^{*} \rightarrow (M-H)^{++} + T + e$

The charge stripping mass spectrum is a recording of the doubly charged ions which are formed following collision with a target gas. It is obtained by following the same procedure as for a CA mass spectrum. The only difference is that for a CS mass spectrum one scans the electric sector in the energy range corresponding to transmission of ions having half the translational energy of the mass selected ion since the ratio of the charges is one-half and the mass only changes slightly.

(2.5) $M_1^{z+} + T \rightarrow M_2^{(z+n)+} + T + ne$

For the reaction shown in Equation 2.5, the kinetic energy of $M_2^{(z+n)+}$ will be

(2.6) $\frac{1}{2}m_2v^2 = (m_1/m_2)zV.$

M_2 will pass through the electrostatic analyzer when

(2.7) $(z+n)E = m_2v^2/R.$

Combining these two equations yields

(2.8) $E = (z/(z+n))(m_2/m_1)V/R.$

Thus, the electric field needed to transmit $M_2^{(z+n)+}$ through the electrostatic analyzer must be adjusted by the ratio of the charges and masses relative to the electric field needed to transmit M^{z+} through the electric sector.

The doubly charged ions are generally much weaker than the CID peaks so one must use increased electron multiplier gain to observe them. Oxygen generates a greater abundance of doubly charged ions than helium.[15] Oxygen also generates a higher yield of doubly charged parent ions relative to doubly charged fragment ions than does helium.[15] A problem may exist where the doubly charged peaks are obscured by intense CA peaks.

Section 2.1.4a Ion Structure and Charge Stripping

Charge stripping is useful for distinguishing isomers whose CA mass spectra are very similar. If an ion has a relatively low barrier for isomerization then it may freely interconvert to its isomer in the ion source. The ions which interconvert are closer to the fragmentation threshold than those ions which do not interconvert. Therefore, since the most probable gain in energy following collisional activation is a few electron volts,[50] the fragment ions in a CA mass spectrum will arise mostly from interconverting ions. Charge stripping, which requires much more energy (>10eV) than fragmentation, produces doubly charged ions arising much more uniformly from all ions (both those which interconvert and those which do not interconvert). Thus, the CS mass spectrum better reflects the structure of the non-interconverting ions than does the CA mass spectrum.

For example, of the four stable $[C_2H_5O]^+$ ions ($[CH_3CHOH]^+$, $[CH_3OCH_2]^+$, $[CH_2(OH)-CH_2]^+$ and $CH_2=CHOH_2]^+$) only the first three could be distinguished on the basis of their CA mass spectra.[51,52] However, all four isomers had distinct CS mass spectra indicating that all four exist as separate, stable species in the gas phase.[52]

Section 2.1.5 Collisionally Induced Dissociative Ionization - CIDI

One may study the neutral product(s) produced by the unimolecular dissociation of a metastable ion using the technique known as collisionally induced dissociative ionization (CIDI). These experiments can be performed with the ZAB. An ion is mass selected via the first magnetic analyzer. Some of the ions will dissociate unimolecularly in the 2FFR prior to the deflector electrode. A positive charge is placed on the electrode such that all the ions are deflected away and only the fast neutrals, produced during the unimolecular dissociation, continue on to collision cell II. A gas (He or O_2) is placed in collision cell II. When the fast beam of neutrals collides with the gas, sufficient translational energy may be converted to internal energy so that ionization and/or fragmentation take place. The CIDI mass spectrum is then obtained by scanning the electrostatic analyzer. The ions are detected at the second detector.

The majority of workers believe ionization occurs by the electron detachment mechanism (Equation 2.9) rather than by the electron transfer mechanism (Equation 2.10).

(2.9) $M + T \rightarrow M^{+\cdot} + T + e$

(2.10) $M + T \rightarrow M^{+\cdot} + T^{-}$

The internal energy of the neutrals produced in a metastable dissociation can generally be accurately determined by measuring the AE. For metastable dissociations which occur at their thermodynamic threshold, the neutral should be in its ground state and the CIDI spectrum should illustrate this.[53]

Section 2.1.5a Factors Influencing the CIDI Mass Spectrum

The width of the neutral beam is not significantly changed by ionization and so the peak width of the ionized neutrals closely resembles that of the corresponding metastable peak. In cases where the neutral suffers dissociative ionization, the widths of the fragment ion beams will be broadened by the resultant release of kinetic energy. Therefore, fragment peaks are much broader than the peak corresponding to ionized neutrals which do not fragment. Increasing the resolution will have the effect of increasing the height of the narrower ionized neutral peak with respect to the fragment peaks.

The CIDI mass spectrum will depend on the collision gas and pressure (see Section 2.1.3a). Helium will cause more fragmentation than O_2. It is best to use collision gas pressure such that the main beam is reduced by 10%. In addition to ensuring that mostly single collision conditions are achieved this also prevents collision gas from leaking to the region preceding the deflector electrode. In the event the gas does leak to the region preceding the deflector electrode the resulting CA processes will also produce neutrals which will continue past the electrode and be ionized along with the desired neutral beam. This will produce extraneous peaks in the CIDI mass spectrum. For aniline, increasing the He pressure produced neutral species by CID which confused the CIDI mass spectrum of HNC.[54] Peaks at m/z 24 and 25 appeared and the ratio of m/z 26:m/z 27 rose rapidly due to collisionally generated C_2H_2. This danger is most severe when the

mass selected ion has only a weak metastable process but a large cross-section for CID.

The efficiency of the ionization step and the relative intensities of the signals will also depend on the translational energy of the metastably produced neutral. Therefore, when comparing CIDI spectra it is important to adjust the accelerating voltage such that the neutrals have identical translational energies. The He CIDI mass spectrum of $\cdot CH_2OH$ recorded with V_{acc} = 2kV and 8kV and with equal main beam widths (no effect due to resolution) illustrates this point.[55] At 2kV, m/z 29 is more intense than m/z 30. This situation is reversed at 8kV.

(2.11) $\cdot CH_2OH + He \rightarrow [CH_2OH^{+\cdot}]^* \rightarrow HCO^+$ m/z 29) + H_2

(2.12) $\cdot CH_2OH + He \rightarrow [CH_2OH^{+\cdot}]^* \rightarrow CH_2O^{+\cdot}$ (m/z 30) + $H\cdot$

Formation of m/z 29 (Equation 2.11) requires less energy than formation of m/z 30 (Equation 2.12).[56] Therefore, the lower energy fragmentation was preferred at the lower translational energy.[55]

In addition to the effects of resolution, collision gas and pressure, and neutral translational energy, problems may be encountered when interpreting a CIDI mass spectrum if the mass selected ion has two or more metastable dissociation channels which generate neutrals possessing common fragment ions. This situation is especially serious when one of the neutral species has a much higher cross-section ror collisional ionization than the other neutral(s). For instance, the $[H_3,C,O]\cdot$ flux generated from metastable methyl acetate molecular ions produces a CIDI mass

spectrum resembling that of pure $\cdot CH_2OH$ while it has been shown that only 25% of the neutrals have the $\cdot CH_2OH$ structure (the remaining 75% of the neutrals have the $CH_3O\cdot$ structure).[57] This situation occurs since the cross-section for ionization of $\cdot CH_2OH$ (Ionization Energy = 7.56 eV^2) was measured to be 12 and 18 times greater than the cross-section for ionization of $CH_3O\cdot$ (Ionization Energy = 8.6 eV^2) with He and O_2 respectively.[57]

Section 2.1.5b Neutral Structure and CIDI

CIDI is particularly useful for identifying the neutral structure in cases where it may be in doubt.[58] It was demonstrated that loss of HNC (not the thermodynamically more stable HCN) from metastable ionized aniline, $[C_6H_5NH_2]^{+\cdot}$, was responsible for the peak at m/z 66, $[C_5H_6]^{+\cdot}$.[58] This was shown by comparing the CIDI mass spectrum of HCN generated from pyridine with the CIDI mass spectrum of the [H,C,N] isomer generated from ionized aniline as shown in Figure 2.6.[58]

Figure 2.6 CIDI Mass Spectra of Neutral HCN and HNC

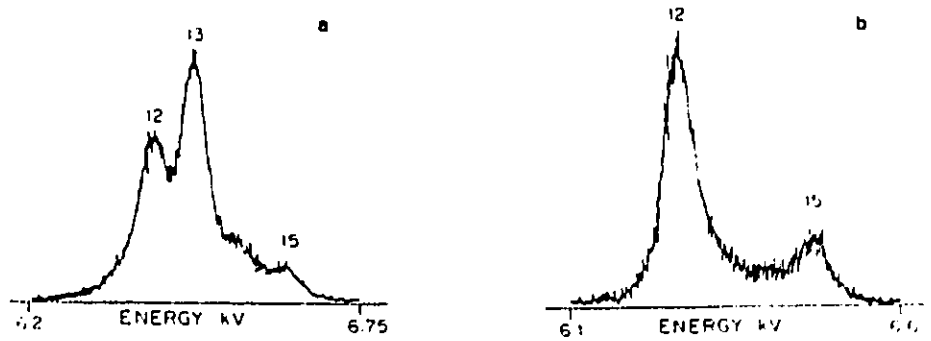

(a) HCN Generated from Ionized Pyridine
(b) HNC Generated from Ionized Aniline

Ionization will occur vertically in the Franck-Condon sense. In some cases, vertical ionization may lead to a dissociative state of the ion or the ion may not lie in a potential well so that no ion with the same mass as the neutral will be observed. For instance, the CIDI mass spectrum of neutral $[CH_3O]^{\cdot}$, m/z 31, produced from $[CH_3CH_2COOCH_3]^{+\cdot}$ has very little recovery at m/z 31.[58] This indicates that the neutral is mostly $CH_3O^{\cdot}$ since CH_3O^{+} exists as a stable species only in its triplet state and in a shallow well.[59] The CIDI mass spectrum of $^{\cdot}CH_2OH$ has a much more intense recovery peak.[58]

Section 2.1.6 Neutralization Reionization Mass Spectrometry - NRMS

NRMS is a versatile technique which has been used to generate and characterize the neutral counterpart of new and unconventional ions. NRMS experiments take place in five steps. First the desired ion is mass selected using the first magnetic sector. The ion beam is then neutralized by charge exchange with a target gas, T, in the first collision cell. All remaining ions are deflected from the flight path by applying a positive voltage to the deflector electrode. The neutrals are collisionally reionized in the second collision cell. Finally the reionized neutrals and their fragment ions are separated based on their kinetic energy by scanning the ESA and the ions are detected at the second detector.

The peak width of recovered $M^{+\cdot}$ ions has been found to be only slightly broader than the initial peak width of the mass selected ions. Therefore, the kinetic energies released in the

fragmentations of neutral M are reflected in the broadening of the fragment peaks.[53] The relative peak heights will therefore depend greatly on the resolution used.

Section 2.1.6a Neutralization and Reionization

Let us consider the neutralization and reionization steps in more detail.

A. Neutralization

As previously stated neutralization will occur via charge exchange (Equation 2.13)

(2.13) $M^{+\cdot} + T \rightarrow M + T^{+\cdot}$

For ions (m/z < 100) with 8kV translational energy, interaction with the target, over a range of a few Ångstroms, will occur during ~ 10^{-15} seconds.[53] Therefore, charge exchange may be considered to occur vertically. The energy balance, Q_N, for the above reaction is therefore given by Equation 2.14. See Figure 2.7.

(2.14) $Q_N = IE_v(T) - NE_v(M)$

Figure 2.7 Relationship Between the Vertical Neutralization Energy of $M^{\cdot}$, the Ionization Energy of the Target and the Energy Balance for Neutralization

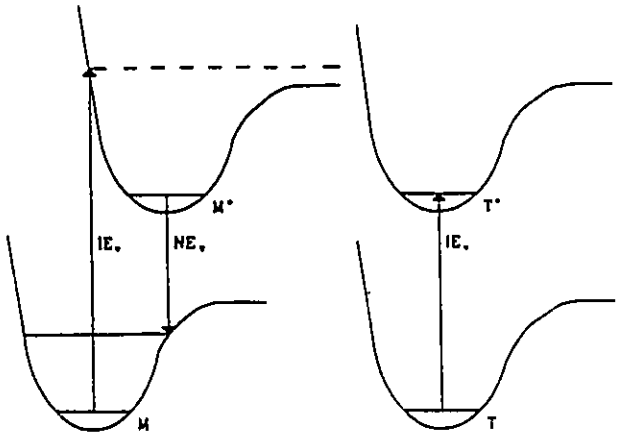

There are three situations to consider: resonant electron transfer, endothermic electron transfer and exothermic electron transfer.

(i) Resonant electron transfer ($Q_N \sim 0$)

Near resonant electron transfer has been shown to be very efficient for both monatomic and diatomic species as well as for polyatomic molecules. However, for polyatomic molecules, where there is a significant geometry change, use of M as target in order to neutralize $M^{+\cdot}$ will not be resonant since $IE_v \neq NE_v$. This situation occurs for acetone.[60]

(ii) Endothermic electron transfer ($Q_N > 0$)

In these situations the extra energy required for electron transfer comes from the translational energy of $M^{+\cdot}$. Thus, Xe (IE = 12.1 eV) is an excellent neutralization target and has been effectively used to neutralize ions whose corresponding neutrals have ionization energies as low as ~ 6eV.[53]

(iii) Exothermic Electron Transfer ($Q_N < 0$)

These conditions can be achieved by using alkali metal vapours as target. These metal vapours have low ionization energies (Na = 5.1 eV, K = 4.3 eV). This will very often cause neutralization to a dissociative state (no recovery observed). However, if electron transfer is resonant with a stable excited state of the neutral, this state is also accessible. Exothermic neutralization of $N_2^{+\cdot}$ with NO (which produces N_2 in a stable electronic state, 6.2 eV above its ground state) is almost as efficient as resonant neutralization.[53]

B. Reionization

Reionization with a collision gas occurs in the same manner as in a CIDI experiment. The most important difference being that with CIDI the neutral will mostly be in its ground state whereas in NRMS the neutrals will often be formed with an excess of energy. CIDI and NRMS will often (but certainly not always) produce similar spectra. The fragmentation pattern of the reionized neutral may be used to identify the neutral. Reionization is usually with O_2 or He depending on the desired amount of fragmentation.

Vertical neutralization may lead to a dissociative state of the neutral or vertical reionization following vertical neutralization may lead to a dissociative state of the ion (see Figure 2.7). Thus, the absence of a recovery signal does not disprove the existence of a stable neutral.

Section 2.1.6b Problems Encountered in the Interpretation of NRMS

A NRMS experiment may be considered a success when a recovery signal at the same m/z ratio as the mass selected ion is recorded (i.e. a stable neutral is produced which survives over a sufficient period of time for it to traverse the distance between the two collision cells) and when the observed fragments can be used to support or assign the desired structure to the reionized neutral. Thus, the hypervalent radical, $ND_4\cdot$, was shown to be a stable species by NRMS.[61] Also, the methene ammonium ylide, $\cdot CH_2{}^+NH_3$, has been shown to be stable[53,62] in agreement with theory.[63]

The interpretation of a neutralization reionization mass spectrum is much more complex than it may at first appear.

The first major problem is ensuring that the ions of known m/z ratio consist solely of the correct molecular formula. Interference may come from a 1FFR metastable daughter ion with the same apparent mass, m_2^2/m_1, as the mass selected ion or from an ion of the same nominal mass but with a different molecular formula. For example, the m/z 41 ion from oxazole, $[C_3H_3NO]$, is a mixture of C_2HO^+ and $C_2H_3N^{+\cdot}$.[53] It is easy to check for these interferences and they are relatively uncommon. Most difficulties arise from ions with the same nominal mass arising from naturally occurring isotopes (^{13}C, ^{18}O etc). In several cases the NRMS spectrum must be corrected as described in Section 2.1.7. Thus, the apparent recovery of $\cdot CH_2^+FH$ indicating the generation of stable CH_2FH was entirely due to interference from $^{13}CH_2F^+$ ions.[64]

Another difficulty is the possibility that the mass selected ion beam does not contain only one ion structure. Due to the probability of rearrangement this is indeed an important consideration. It is often possible to confidently assign structure to ions based on thermochemistry, metastable ion characteristics, CA/CS, and isotopic labelling. For instance, it was shown that $ClCH_2CO_2H$ generates the ylid ion $[\cdot CH_2^+ClH]$ together with $[CH_3Cl]^{+\cdot}$ and that the recovery at m/z 72 in the NRMS was due solely to the $[CH_3Cl]^{+\cdot}$ ions.[64] However, in several studies these experiments have not been performed, leaving the interpretation of the NRMS in question.

Where isomeric species interfere it may be possible to isolate the one desired ion by performing ionization at low electron energy, or if possible and if there is enough intensity, by selecting the 1FFR metastable daughter ion with the desired structure.

Fragment ions are not solely formed by dissociative reionization. They may also occur from other processes. Metastable dissociation prior to the deflector electrode will result in neutrals which may be collisionally ionized in cell II. Collisionally induced dissociation and dissociative neutralization of the mass selected ions in cell I will produce fast neutrals which will also be ionized in cell II.

One can see that there are many complications to consider before rashly jumping to the conclusion that you have observed the presence of some hitherto unknown neutral.

Section 2.1.7 Corrections For Naturally Occurring Isotopes

Corrections for naturally occurring isotopes may often have to be performed in MIKES, CA, CS, CIDI and NRMS experiments.

The procedure used to correct for ^{13}C overlap is best understood by use of an appropriate example. Consider

(1) $C_4H_8^{+\cdot}$ (m/z56) $\rightarrow$ $C_3H_4^{+\cdot}$ (m/z40) + CH_4

(2) $C_4H_7^{+\cdot}$ (m/z55) $\rightarrow$ $C_3H_3^{+\cdot}$ (m/z39) + CH_4

(3) $^{13}CC_3H_7^{+\cdot}$ (m/z56) $\rightarrow$ $^{13}CC_2H_3^{+\cdot}$ (m/z40) + CH_4

The problem is to determine how much m/z 40 from process (3) is observed in the MIKES of $C_4H_8^{+\cdot}$. This is achieved as follows:

(a) The signal at m/z 40 in the MIKES of $C_4H_8^{+\cdot}$ is recorded.

(b) The signal at m/z 39 in the MIKES of $C_4H_7^+$ is recorded using only the calibrated divisions of the amplifier to adjust the signal intensity.

(c) The signal intensity measured in step (b) is multiplied by the difference in amplification gain, the number of carbon atoms in the ion, 3, and the natural abundance of ^{13}C, 1.1%, in order to determine the amount of signal at m/z 40 which is due to process (3).

(d) Finally the amount of contribution from process (3) as calculated in step (c) is subtracted from the peak recorded in step (a).

The same type of reasoning may be used for other isotopes.

Section 2.1.8 Negative Ions

Up to now only positive ions have been discussed. Most of the work in mass spectrometry has been concerned with positive ions; however, negative ions are also formed in the ion source and can be studied using mass spectrometry. The formation and fragmentation of negative ions was the subject of a review article by Bowie in 1984.[65] It has only been in the last 15 years that interest in negative ions has significantly grown. One of the major drawbacks is the lack of sensitivity when working with negative ions (unless the molecule of interest contains an extended π system and/or

strongly electron withdrawing substituents such as NO_2, CN, CO_2R, or COR in which case the negative ion current may be greater than that of the analogous positive ion current). The behaviour of negative ions is different from that of positive ions as will be seen in the sections below.

Section 2.1.8a Formation of Negative Ions

Negative ions may be formed in the ion source by electron impact or by chemical ionization.

Negative ions are formed following electron impact by one of two mechanisms: resonant electron capture (Equation 2.15) or ion pair production (Equation 2.16).

(2.15)A $AB + e \rightarrow AB^{-\cdot}$

B $AB + e \rightarrow A^{\cdot} + B^{-}$

(2.16) $AB + e \rightarrow A^{+} + B^{-} + e$

To form a negative ion by electron capture, the molecule must have a vacant, low lying orbital which the electron may occupy. Electron capture may be either non-dissociative (Equation 2.15A) or dissociative (Equation 2.15B). Note that there is no electron to carry off excess energy, hence the term "resonant" electron capture. Non-dissociative electron capture involves the capture of a low energy electron (<3eV) by a molecule with a positive electron affinity. This process will increase in importance as the pressure in the ion source is increased due to thermal stabilization of the ions by collision. Dissociative electron capture is an important process at electron energies <15eV and provided the molecular

anion, $AB^{-\cdot}$, is prone to fragmentation.[66] Resonant electron captures in an ion source utilizing 70 eV electrons are formed by secondary electrons (electrons produced at metal surfaces or ejected during positive ionization).

Ion-pair formation is a non-resonant process since excess energy can be carried off by the electron. This process occurs over a large range of energies >10 eV.

Production of negative ions by electron impact is usually much less favourable than that of positive ions (relative intensities are usually ~ 10^3 less than those of positive ions).[67]

Negative ions may also be produced by chemical ionization. Chemical ionization is a process by which a molecule and an ion react to form a new charged species. For sufficient ion/molecule reactions to take place, the source pressure must be considerably higher (0.1-1.0 torr) than under normal conditions (~ 10^{-6} torr). Negative ion chemical ionization occurs during the reaction of a molecule, MH, with thermally equilibrated reactant ion, R^- (often OH^-). Several types of ion-molecule reactions may take place; the most common is proton abstraction (Equation 2.17).

(2.17) $MH + R^- \rightarrow M^- + RH$

The exothermicity of the reaction is often carried off as vibrational energy in the newly formed RH bond leaving a relatively stable M^- ion.

Water may be used as a source of reagent negative ions. Secondary electrons react with H_2O by dissociative electron capture to form H^- and O^- ions which react via ion/molecule reactions to

give an excellent yield of OH^-. Negative ion chemical ionization greatly increases the yield of negative ions with respect to formation by electron impact.

In order to create a fast beam of negative ions it is necessary to have a negative charge on the repeller and to use a negative accelerating voltage. A wide variety of experiments may be performed using the beam of negative ions.

Section 2.1.8b Normal Mass Spectrum

In order to switch from working with positive ions to working with negative ions it is necessary to reverse the polarity of the magnet and the direction of the electric field. Once this is done, negative ions may be focused through the magnetic and electrostatic analyzers. In order to detect negative ions the conversion dynode carries a positive charge.

The appearance of the normal mass spectrum of negative ions will depend on the mode of ionization. The electron impact normal mass spectrum will usually contain a parent negative ion, $M^{-\cdot}$. Molecular negative ions may undergo consecutive and competitive fragmentations in the ion source as well as metastable processes. Rearrangement reactions are quite common and often give more abundant peaks than those produced by simple bond cleavage. This behaviour is due to the low internal energy of the negative ions formed upon electron capture.

The most abundant ion formed upon negative ion chemical ionization is usually $[M-H]^-$ formed following proton abstraction by OH^-. Since a high pressure is used, the excess energy for this proton abstraction reaction is dissipated by many collisions.

Therefore, there is generally very little fragmentation observed in the Normal Mass Spectrum.

Section 2.1.8c Negative Ion MIKES

Metastable ions are abundant in the negative ion spectra of organic compounds. Similar reasoning as that used for positive ions may be applied to negative ions.[65] Metastable ions formed by rearrangement are more abundant than those formed by simple bond cleavage. It is also known that autodetachment of an electron will often occur in the metastable timeframe (10^{-5}-10^{-4} sec).[68] Time of flight mass spectrometry has been used to measure autodetachment lifetimes.[69]

Section 2.1.8d Collision Induced Processes

A non-decomposing, polyatomic, negative ion may be forced to fragment by collisional activation.[70] Collisional activation of negative ions is a useful technique which provides information concerning the anion structures.

Collision processes which induce a change in the charged state of the ion are of great interest. A non-decomposing negative ion may be converted to a positive ion by charge reversal[71,44] (Equation 2.18).

T is the target or collision gas.

(2.18) $AB^- + T \rightarrow AB^+ + T + 2e$

The energy required for this process is equal to the sum of the electron affinity and the ionization energy of AB. This energy

is provided from the translational energy of AB^-.[72] Peaks corresponding to AB^+ are usually small or absent. The major peaks are due to fragmentation of the parent positive ion (Equation 2.19).[65]

(2.19) $AB^- + T \rightarrow [AB^+]^* \rightarrow A^+ + B$

In a charge reversal mass spectrum the magnetic analyzer transmits negative ions while the electrostatic analyzer is set to transmit only positive ions.

The charge reversal reaction is a vertical process.[73] Provided that the geometry difference between the positive and the negative ions is not too large, the cation will retain the structure of the anion. Negative ions often have an unstable positive analogue and thus charge reversal allows the study of species not available by any other method.[66,74] The dissociation characteristics of the newly formed cation are structure characteristic and should be expected to be similar to the collisional activation mass spectrum of the corresponding cation generated (if possible) directly by electron impact.[75,76]

Information concerning the negative ion is also available provided that the anion does not undergo rearrangement during the collision process and that the parent positive ion does not rearrange prior to fragmentation.[77] Collision transforms enough translational energy into internal energy such that simple cleavages in the highly excited ions are usually rapid with respect to rearrangement. Thus, peaks resulting from rearrangement prior to fragmentation have been found to be of low relative intensity (~15-20% of total intensity) with few exceptions.[76]

Section 2.18e Neutrals Produced From Negative Ions

As stated previously, negative ions may undergo unimolecular electron loss in the metastable time frame in addition to unimolecular fragmentation. It has been pointed out that electron loss from negative ions should prove to be an excellent source of fast neutrals for CIDI experiments.[78] Neutral $C_6H_5NO_2$ and $CH_3\cdot$ have been produced by metastable electron loss and their CIDI mass spectra recorded.[78] In this study, the positive ions formed upon collision of the neutral with He were detected. The CIDI mass spectrum of nitrobenzene was similar to the charge reversal mass spectrum of $C_6H_5NO_2^{-\cdot}$. The CIDI mass spectrum of the methyl radical produced by electron loss was identical to the CIDI mass spectrum of the methyl radical produced by the metastable dissociation of acetone (Equation 2.20).

(2.20) $(CH_3)_2CO^{+\cdot} \rightarrow CH_3CO^+ + \cdot CH_3$

Anions should give excellent yields of neutrals upon collision because of the low electron affinity of many molecules and radicals.[68] NRMS of negative ions is therefore possible and has been reported in the literature.[68,79]

A negative ion may be converted to a positive ion of the same structure by the two steps:

(2.21) $X^- + T_1 \rightarrow X\cdot + T_1 + e$

(2.22) $X\cdot + T_2 \rightarrow [X^+]^* + T_2 + e$

This has been termed a $^-NR^+$ mass spectrum since a negative ion is converted to a positive ion. For C_1-C_3 alkoxide ions, the $^-NR^+$ experiments produced spectra similar to the charge reversal mass spectra of the alkoxide anions.[79] Therefore, it was concluded that alkoxyl radicals were produced upon neutralization.

Section 2.1.8f Formation of Negative Ions From a Fast Beam of Neutrals by Collision

In CIDI and NRMS experiments it is also possible to generate anions upon (re)ionization. Negative ions may be formed by electron transfer during a collision between a fast beam of neutrals and a target gas (Equation 2.23).

(2.23) $AB + T \rightarrow [AB^-]^* + T^-$

Wesdemiotis and Feng[79] performed neutralization-reionization experiments involving the neutralization of a cation followed by reionization to an anion ($^+NR^-$). Neutralization was with Hg and reionization was with Xe. For C_3H_n (n=0-6) species they found that the reionization efficiency increased in parallel with the electron affinity.[80] Reionization to negative ions was always less efficient than reionization to positive ions with oxygen (by at best a factor of seven).[80]

$^+NR^-$ mass spectrometry has also been used to distinguish between isomeric neutrals and cation.[81] Reionization of $CH_3O\cdot$ gives an intense parent anion, CH_3O^-, while reionization of $\cdot CH_2OH$ produces no detectable $^-CH_2OH$.[81] The hydroxycarbene, :CH(OH) gives rise to an intense recovery at m/z 30 in the $^+NR^-$ mass spectrum while its isomer, formaldehyde, does not generate a detectable $H_2CO^-\cdot$ signal.[81]

$H_2C{=}CCl_2^{+\cdot}$ and (E) and (Z) $ClHC{=}CHCl^{+\cdot}$ can be unequivocally distinguished by their $^+NR^-$ mass spectra while all other attempts to distinguish the isomers by mass spectrometry have met with only limited success. $H_2C{=}CCl_2^{+\cdot}$ yields predominantly CCl_2^- (m/z 82) while (E) and (Z) $ClHC{=}CHCl^{+\cdot}$ generate mostly $CHCl^-$ (m/z 48).[81] Also, the peak corresponding to H loss is about eight times more intense for the (E) isomer than for the (Z) isomer.[81]

Section 2.2 Experiments Performed with the MS-9 Mass Spectrometer

The following sections will describe experiments performed with the MS-9 mass spectrometer: normal mass spectrum, accelerating voltage scan, and metastable peak appearance energy measurements.

Section 2.2.1 Normal Mass Spectrum

The normal mass spectrum run on the MS-9 involves maintaining the electric field at a constant value such that all ions with kinetic energy = zV_{acc} are focused through the electrostatic analyzer. V_{acc} is typically 7000V on the MS-9. After travelling across the 2FFR these ions are mass analyzed by scanning the magnetic analyzer. Finally the ions are detected and the spectrum recorded. Note that metastable peaks will appear in the normal mass spectrum. These peaks will appear at an apparent mass of m_2^2/m_1, due to decompositions taking place in the 2FFR. They are easily distinguishable by their increased width with respect to source generated ions (see Section 2.1.2a).

Section 2.2.2 Scanning the Accelerating Voltage

Assume that the electrostatic analyzer is tuned to focus ions with kinetic energy = zV_{acc} and the magnetic analyzer is tuned to focus ions with kinetic energy = zV_{acc} and mass m_y. Therefore, source generated m_y will pass through the whole mass spectrometer and be detected. However, consider an ion which fragments in the 1FFR as shown:

(2.24) $M_x^{+\cdot} \rightarrow M_y^{+} + M_z$

M_y^{+} formed in the 1FFR will have a kinetic energy = $(m_y/m_x)V_{acc}$ and will therefore not pass through the electrostatic analyzer. If V_{acc} is increased to $(m_x/m_y)V_{acc}$, the metastably generated M_y^{+} will have a kinetic energy = $(m_x/m_y)[(m_y/m_x)V_{acc}] = V_{acc}$ and will now pass through the electrostatic analyzer and the magnetic analyzer.

In this way, any metastable ion which fragments to give M_y^{+} may be detected by scanning the accelerating voltage.

The spectrum one obtains appears as a large peak at the initial accelerating voltage $[V_{acc}]_i$ corresponding to source generated M_y^{+}. As the accelerating voltage is increased each peak which appears will be due to M_y^{+} generated metastably in the 1FFR from a different precursor ion, $M_x^{+\cdot}$. The mass of $M_x^{+\cdot}$ may be calculated using the simple formula shown below.

(2.25) $m_x = \{V_{acc}/[V_{acc}]_i\}m_y$

V_{acc} = accelerating voltage at which the peak appears.

Section 2.2.3 Metastable Peak Appearance Energies

Metastable peak appearance energies are obtained using the extrapolated voltage difference technique described in Section 1.6.3.

It is necessary that the ion of interest is generated from a metastable ion in the 1FFR of the MS-9.

(2.26) $M_1^{+\cdot} \xrightarrow{*} M_2^{+} + M_3^{\cdot}$

The accelerating voltage is initially set at 7000V and the electric field at an appropriate value to transmit the source generated

ions. Both these values are adjusted by a factor of m_2/m_1 and so source generated ions are still transmitted through the electrostatic sector. The magnet is then tuned to focus the source generated M_2^+ ions having an accelerating voltage of $(m_2/m_1)7000$. The accelerating voltage is then retuned back to 7000V in order to transmit the M_2^+ ions generated in the 1FFR from $M_1^{+\cdot}$ ions.

This procedure is followed for both the standard and the unknown in order to ensure that both metastable ions are accelerated by the same voltage (identical ion source conditions).

The unknown is run first. One follows several steps.

(1) Once the metastable peak has been selected the energy of the ionizing electrons is lowered until the signal is just visible on the recorder.

(2) The energy is then increased by 2 eV in the hope that the signal will be full scale.

(3) If it is not, the signal intensity is adjusted using the amplifier or the multiplier (increased if it is less than full scale, decreased if it is off scale). This step will alter the energy at which the signal is just visible.

Steps (1) to (3) are repeated until an increase of 2 eV is the difference between the point at which the signal is just visible and the point at which it is full scale.

Once this requirement is achieved, the signal is measured at 0.2 eV step intervals from the onset to full scale.

Once the unknown has been run, the calibrant is run using the same criteria with the exception that in step (3) the signal

intensity is adjusted using only the sample pressure in the ion source. The amplifier and multiplier are put to the settings used for the unknown so that the unknown and the calibrant are recorded under identical experimental conditions. This is very important because the absolute energy of the electron beam is sensitive to the source conditions.

The signal heights for the unknown and calibrant are plotted as a function of electron energy as shown in Figure 2.8.

Figure 2.8 Ionization Efficiency Curves for Metastably Generated m/z 59 from Diethyl Ether and m/z 42 from Propanol

$d_{Unknown}/d_{Calibrant}$ = 107/85 = 1.26

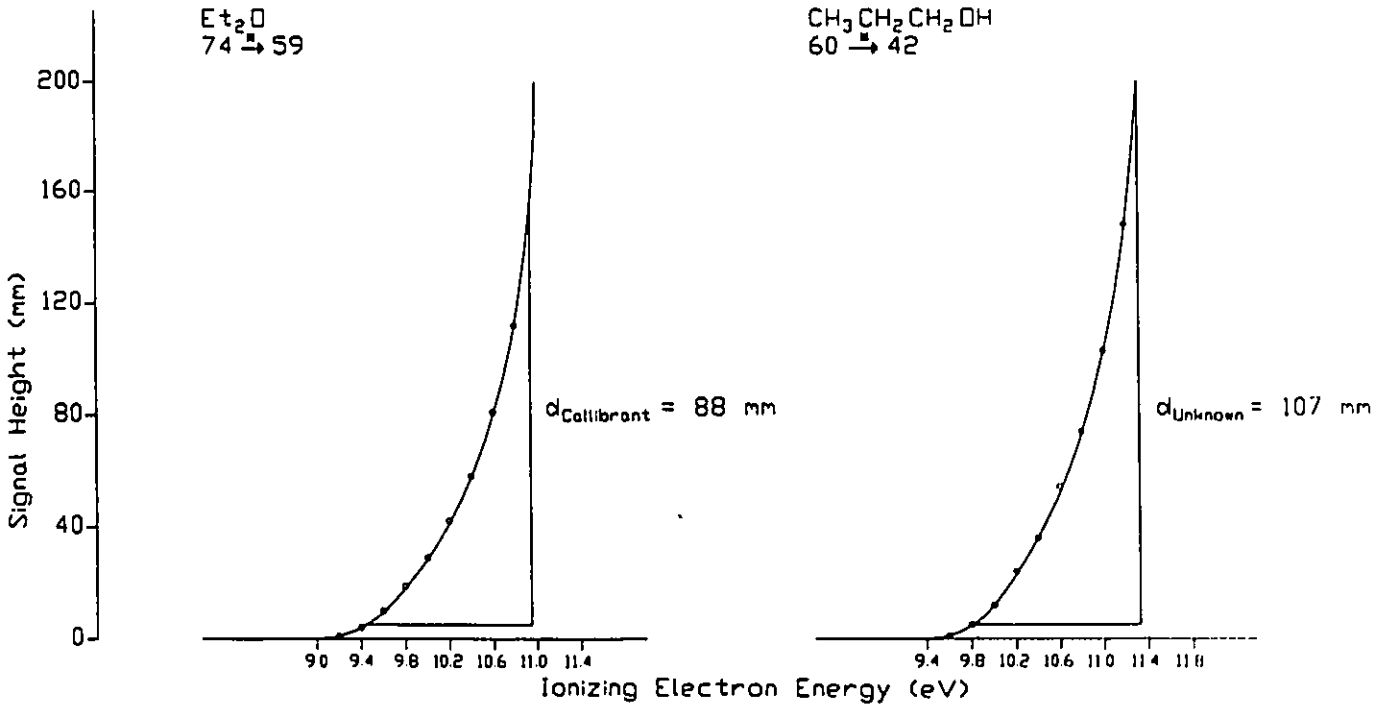

The two curves are normalized by taking a point on the unknown curve and going to a new point displaced to the right by a fixed value. A vertical line is drawn from this point to the point where it crosses the curve. The distance, $d_{UNKNOWN}$, between these two points is measured and recorded (see Figure 2.8). This procedure is repeated for the calibrant curve (ensuring that the original point is at the same height and that the new point is displaced to the right by the same fixed value) in order to obtain $d_{CALIBRANT}$. Normalization of the unknown curve and the calibrant curve is then achieved by multiplying the calibrant curve by $d_{UNKNOWN}/d_{CALIBRANT}$ (see Figure 2.9).

Figure 2.9 Normalized Ionization Efficiency Curves for Metastably Generated m/z 59 from Diethyl Ether and m/z 42 from Propanol

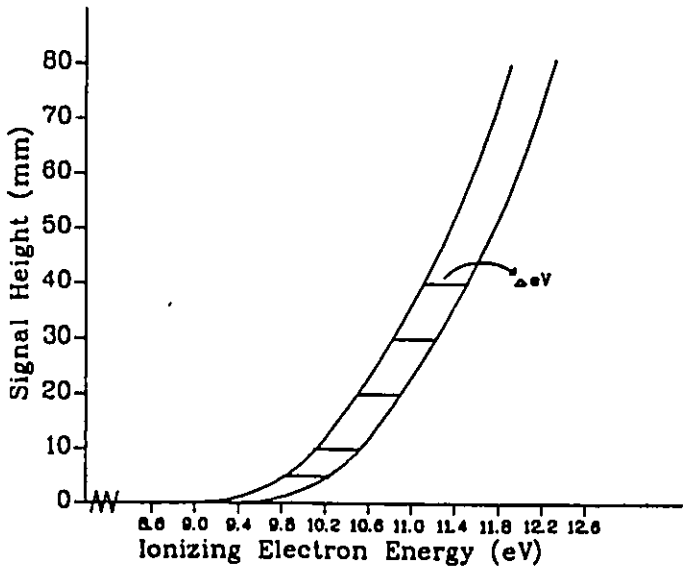

A plot of ΔeV versus signal height, SH, is made and extrapolated to SH = 0 (see Figure 2.10) to obtain the difference between the appearance energy of the unknown and the calibrant. Uncertainty in this method is estimated to be not greater than ± 0.1 eV.[82]

Figure 2.10 Calculation of the Appearance Energy of Metastably Generated m/z 42 from Propanol by the Extrapolated Voltage Difference Technique with Metastably Generated m/z 59 from Diethyl Ether as the Callibrant
The Plot of △eV Versus Signal Height

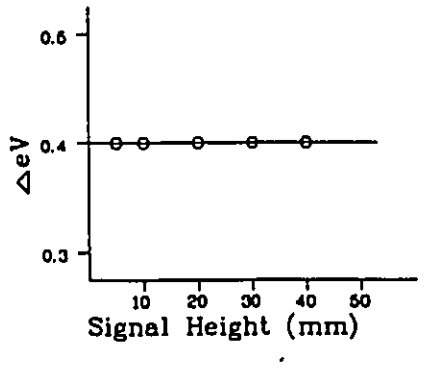

$AE_{Callibrant}$ = 10.26 eV

$AE_{Unknown}$ = 10.26 + 0.4 = 10.66 eV

The calibrant most often used is the peak at m/z 59 from diethyl ether.

(2.27) $CH_3CH_2OCH_2CH_3^{+\cdot} \xrightarrow{*} CH_3CH_2OCH_2^{+} + {\cdot}CH_3$

$d_{UNKNOWN}/d_{CALIBRANT}$ is normally measured twice and the average value used for normalization. The original points chosen are usually at signal heights of 5mm and 10mm and these points are displaced to the right by 2.4 eV. A large difference in the two values of $d_{UNKNOWN}/d_{CALIBRANT}$ indicates that the ionization efficiency curves have dissimilar behaviour near threshold which will decrease the accuracy of the measured AE.

Section 2.3 Appearance and Ionization Energies Measured Using a Monoenergetic Beam of Electrons

Ionization and appearance energies are measured using the energy-selected electron ion source and quadrupole mass filter. The ionization efficiency curve of the desired ion (selected using the quadrupole mass filter) is recorded. The electron energy is increased in 0.02 eV steps. The energy scale is calibrated from the ionization energy of H_2O which is admitted into the ion source together with the sample.

The limiting rate constant for detection of a fragment ion with this apparatus is of the order of $k = 10^3$ sec^{-1}.[83] Therefore, the maximum time between ionization and fragmentation in which the ion may still be observed is $\leq 10^{-3}$ sec (the ion must fragment before reaching the mass filter in this time). Fragmentation occurs in the 1FFR of the MS-9 ~ $2X10^{-6}$ sec after ionization (corresponding to a rate constant of ~ $5X10^{-5}$ sec^{-1}). This rate constant is two orders of magnitude larger than the limiting rate constant for the energy-selected electron appearance energy measurements. Therefore, the appearance energy measured with the MS-9 will have a larger kinetic shift (see Section 1.6.2) and thus a higher appearance energy than the energy-selected electron appearance energy measurements.

Section 2.4 Isotopic Labelling Studies

Isotope labelling studies are used to clarify fragmentation sequences and to investigate fragmentation mechanisms. For example, the molecular weight of a methylester, RCO_2CH_3, may be

increased by three mass units by labelling the methyl group with deuterium, RCO_2CD_3. By comparing the spectrum from each compound one may conclude that all fragment ions in the mass spectrum of the labelled compound which are increased by three mass units relative to the fragment ions in the mass spectrum of the unlabelled compound incorporate the methyl group. The use of labelling to elucidate reaction mechanisms will be demonstrated in Chapters 3 and 4.

Every man seeks for truth, but God
only knows who has found it.

LORD CHESTERFIELD
Letters

ION-RADICAL COMPLEXES IN THE GAS PHASE: STRUCTURE AND MECHANISM IN THE FRAGMENTATION OF IONIZED ALKYL PHENYL ETHERS

Section 3.1 Introduction

The base peak in the normal mass spectrum of any alkyl phenyl ether (with the exception of anisole) occurs at m/z 94 $[C_6,H_6,O]^{+\cdot}$ and is due to the loss of a neutral olefin from the molecular ion. This reaction also occurs during the metastable ion time frame.

1-Butyl phenyl ether, $C_6H_5O\overset{\alpha}{C}H_2\overset{\beta}{C}H_2\overset{\gamma}{C}H_2\overset{\delta}{C}H_3$, was one of the first alkyl phenyl ethers studied.[84,85] Using specifically deuterium labelled compounds, it was discovered that hydrogen from all four positions of the butyl sidechain were involved in transfer to the phenoxy group prior to the elimination of C_4H_8. It was also discovered that H-transfer became more specific as the internal energy of the molecular ions decreased: with $C_6H_5OCH_2CH_2CD_2CH_3$ 34%, 43% and 53% of H/D-transfer occurred from C_γ for ions generated in the source with 70 eV electrons, ions generated in the source with 12 eV electrons and ions generated in the 2FFR respectively.[85] These results led to the conclusion that hydrogen was transferred from each position of the butyl group (rather than involving randomization of the alkyl hydrogens prior to transfer from one particular position) since rearrangement reactions with prior H-scrambling generally show a decrease in specificity of the transferred hydrogen with decreasing internal energy.

Specifically deuterium labelled 1-propyl phenyl ethers were studied by Benoit and Harrison.[86] The amount of deuterium transfer

from each position of the propyl chain was measured. The results are listed in Table 1. Labelled 1-propyl phenyl ethers were also studied by Chronister and Morton[87] and the results are in agreement with those of Benoit and Harrison.[86]

Table 1 % D^+ transfer from labelled 1-propyl phenyl ethers

D-position	Ion Energy	Observed % D	Calculated % D
1,1-d_2	Metastable	28	33[b]
	70 eV[a]	27	29[c]
2,2-d_2	Metastable	19	17[b]
	70 eV[a]	35	29[c]
3,3,3-d_3	Metastable	53	50[b]
	70 eV[a]	38	43[c]

a. Source Ions
b. Assumes a single 1,2-H shift followed by rapid $\beta(H^{\cdot})$ transfer
c. Assumes complete H/D randomization

A field ionization source allows the measurement of the intensities of fragment ions as a function of decomposition time within the range of 10^{-11}-10^{-5} seconds. The amount of H-transfer from each position of the propyl group was measured as a function of the time of decomposition using a field ionization source.[88] H-transfer became more specific (transfer from C_γ preferred) as the precursor ion lifetime increased in agreement with the results from 1-butyl phenyl ether.[88] Scrambling is normally expected to increase with longer lifetimes (hydrogen scrambling and subsequent decomposition are consecutive reactions which should always take longer than the competing decomposition without scrambling). Thus, it was concluded that specific transfer from each position of the propyl sidechain occurred and not label scrambling.

There is no doubt that hydrogen is transferred to the oxygen and that the $[C_6,H_6,O]^{+\cdot}$ ion formed has the phenol molecular ion structure as will be described below. The ratio of H-transfer from each position of D-labelled 2,6-dimethyl phenyl 1-propyl ether ions was the same as for similarly labelled 1-propyl phenyl ether ions.[86] Since blocking the ortho positions did not effect the ratio of H-transfer it was concluded that transfer of H^+ to the ortho carbon forming cyclohexadienone does not occur. The CA mass spectra of m/z 94 ions produced from 1-propyl, 2-propyl and 1-butyl phenyl ethers were identical to the CA mass spectrum of the phenol molecular ion.[88] Moreover, these spectra contained significant differences from the CA mass spectrum of ionized cyclohexadienone.[89] The CA mass spectra of $[C_6H_5OD]^{+\cdot}$ ions produced from deuterated 1-propyl phenyl ethers (deuteration at the various positions of the propyl group) showed only OD loss (no OH loss).[88] OH loss would be expected if D was transferred to an ortho carbon forming cyclohexadienone which rapidly rearranged to a phenol ion prior to CA. Therefore, there can be no doubt that phenol ions are produced following H-transfer to oxygen. $C_6D_5OCH(CH_3)CH_2CH_2CH_3$ produced only $[C_6D_5OH]^{+\cdot}$ ions indicating that mixing of the aromatic and alkyl hydrogens does not occur.[90]

Morton[91] suggested a mechanism for C_4H_8 loss from 1-butyl phenyl ether involving a complex between a phenoxy radical and an alkyl cation (Scheme 3.1). The $O-C_\alpha$ bond is stretched to an extent that the coupling of the degrees of freedom between the phenoxy radical and butyl cation ceases. The butyl cation may then freely rotate

and behave as an isolated species. The 1-butyl cation rearranges to a 2-butyl cation via a 1,2 H-shift. Rapid 2,3 H-shifts may then occur prior to transfer of a $\beta(H^+)$, a proton on C_β, from the 2-butyl ion to the phenoxy radical.[91]

Scheme 3.1

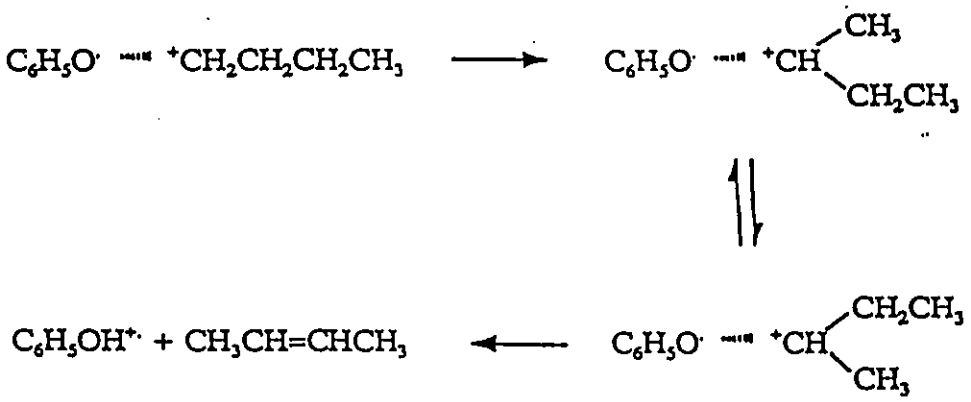

Morton sought confirmation for this mechanism by probing a system which contained an alkyl group which is known to undergo a characteristic rearrangement. For instance, Morton studied neopentyl phenyl ether[91] using a technique, electron bombardment flow radiolysis, developed by Burns and Morton.[92] This technique allowed them to study the neutral species produced in their mass spectrometer. The neutral species were isolated and condensed in a liquid nitrogen trap. The contents of the trap were then studied by combined gas-chromatography/mass spectrometry.

It has been shown that neopentyl cations rearrange to t-pentyl cations, $^+CH_2C(CH_3)_3 \rightarrow {}^+C(CH_3)_2CH_2CH_3$.[93] The neopentyl phenyl ether produced neutral alkenes with a product ratio which was consistent with that produced following the deprotonation of t-pentyl

cations.[93] This result was in agreement with Morton's proposed ion/radical pair mechanism.

Morton prepared and studied three monodeuterio 2-butyl phenyl ethers: (1) 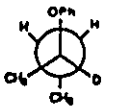 (2) 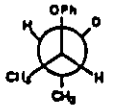 (3) 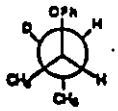

His results are shown in Table 2.[94]

Table 2 % D^+ transfer from labelled 2-butyl phenyl ethers

D-position	Ion Energy	Observed % D	Calculated % D
2-d_1 (1)	Metastable	3	33[b]
	70 eV[a]	5	11[c]
3-d_1 (2)	Metastable	30	33[b]
	70 eV[a]	18	11[c]
3-d_1 (3)	Metastable	23	33[b]
	70 eV[a]	14	11[c]

a Source Ions
b Assume rapid 2,3-H shifts followed by secondary $\beta(H^+)$ transfer
c Assumed complete H/D randomization

If an ion/radical complex was formed, then according to Morton, rapid 2,3 H-shifts would eliminate stereochemical and regiochemical distinctions among the three isomers. However, Table 2 clearly shows that the isomers are distinguishable. Morton failed to provide any explanation for the different behaviour of 1-butyl and 2-butyl phenyl ethers.

Deuterium labelled derivatives of 2-butyl, t-pentyl, and 2-pentyl phenyl ethers were prepared and their metastable ions studied by MIKES.[90] It was found that transfer of a $\beta(H^+)$ is the most important process and that transfer of a secondary $\beta(H^+)$ is preferred over transfer of a primary $\beta(H^+)$. For 2-pentyl phenyl

ether the observed distribution of secondary H(α):H(β):H(γ) transfer was 5.7:88.6:5.7. For t-pentyl phenyl ether, transfer of a secondary β(H^+) was 99% selective. It was also noted that the KER ($T_{0.5}$ values) of the m/z 94 peaks depended on the primary, secondary or tertiary nature of the alkyl group.

The above results are in keeping with a possible distonic ion intermediate, $C_6H_5\overset{H}{\overset{+}{O}}CH(CH_3)\dot{C}HCH_2CH_3$, which was first proposed by Yeo and Djerassi,[85] or a proton bound intermediate as suggested by Audier,[90] [$PhO^{\cdot}$ ... H^+ ... $CH_3CH{=}CHCH_2CH_3$].

There was however no understanding as to why primary ethers apparently behaved quite differently from secondary or tertiary ethers until the energetics were studied.[95] In that paper, the appearance energies of m/z 94 were measured for ethyl, n-propyl, and the four butyl phenyl ethers. It was noted that although the $T_{0.5}$ values are relatively small the dissociations proceed with quite large reverse energy barriers. Apparently, the threshold for dissociation for secondary and tertiary ethers is <u>below</u> the energy required for rearrangement of the alkyl group in an ion/radical complex while the threshold for dissociation from the unrearranged ion of a primary ether lies <u>above</u> the energy required for rearrangement of the alkyl group to a more stable secondary or tertiary group, thus providing a lower energy pathway to the observed products.

The aim of the present study is to understand the mechanism by which olefin expulsion occurs and to relate the mechanism to the energy requirements for the reaction and to specific characteristics of the ether ions.

Section 3.2 Results and Discussion

Fourteen alkyl phenyl ethers and some deuterium labelled isotopomers have been studied.

I	$C_6H_5OCH_2CH_3$
II	$C_6H_5OCH_2CH_2CH_3$
III	$C_6H_5OCH(CH_3)_2$
IV	$C_6H_5OCH_2CH_2CH_2CH_3$
V	$C_6H_5OCH(CH_3)CH_2CH_3$
VI	$C_6H_5OCH_2CH(CH_3)_2$
VII	$C_6H_5OC(CH_3)_3$
VIII	$C_6H_5OCH_2CH_2CH_2CH_2CH_3$
IX	$C_6H_5OCH(CH_3)CH_2CH_2CH_3$
X	$C_6H_5OCH(CH_2CH_3)_2$
XI	$C_6H_5OCH_2CH_2CH(CH_3)_2$
XII	$C_6H_5OCH_2C(CH_3)_3$
XIII	$C_6H_5OC(CH_3)_2CH_2CH_3$
XIV	C_6H_5O-cyclo-C_6H_{11}

Section 3.2.1 Energetics

The results of IE, AE and KER measurements are shown in Table 3 together with other appropriate thermochemical data.

As noted earlier,[95] the $T_{0.5}$ values are small relative to the reverse energy barriers. This indicates that the products are formed with a large excess of internal energy and that this energy is not converted into translational degrees of freedom.

There is a definite trend in the excess energy of the transition state above the energy of the reacting ion (E_a, the activation energy for the reaction $[C_6H_5OR]^{+\cdot} \rightarrow [C_6H_5OH]^{+\cdot} + [R\text{-}H]$).

Primary ethers have the largest Ea.

232 kJmol^{-1} - no rearrangement of alkyl cation

187 ± 7 kJmol^{-1} - rearrangement to a more stable secondary alkyl cation

133 ± 4 kJmol^{-1} - rearrangement to a more stable tertiary alkyl cation

Secondary ethers have a smaller E_a.

144 ± 5 kJmol^{-1} - no rearrangement

Tertiary ethers have the smallest E_a.

85 ± 1 kJmol^{-1} - no rearrangement

Table 3 Appearance Energies and Related Thermochemical Data for Alkyl Phenyl Ethers

Compound Studied (M)	$\Delta H_f(M)$[a] ($kJmol^{-1}$)	IE (eV)	$\Delta H_f(M^{+\cdot})$ ($kJmol^{-1}$)	AE[b] (eV)	AE[c] (eV)	Energy of TS[d] ($kJmol^{-1}$)	Product Energy[e] ($kJmol^{-1}$)	Excess Energy ($kJmol^{-1}$)	$T_{0.5}$ (meV)	E_a ($kJmol^{-1}$)
I	-101.7	8.12	682	10.30	10.5	911	774[f]	137	30	232
II	-126	8.12	657		10.0	839	742[g]	97	21	181
III	-143	8.10	638		9.64	787	742[g]	45	15	149
IV	-150	8.18	639	9.85	10.04	815	710[h]	108	24	180
V	-163	8.17	625	9.38	9.64	765	710[h]	57	17	142
VI	-158	8.18	631	9.44	9.6	768	705[i]	63	22	137
VII	-174	8.16	613		9.05	699	705[i]	0	6.5	86
VIII	-168	8.15	618		10.16	812	691[j]	121	26	194
IX	-186	8.15	600		9.62	742	691[j]	51	14	142
X	-186	8.15	600		9.70	750	691[j]	59	15	150
XI	-177	8.15	609		10.06	793	680[k]	113	23	184
XII	-190	8.18	599		9.52	728	680[k]	48	19	129
XIII	-194	8.15	592		9.02	676	680[k]	0	6.0	84
XIV	-161	8.10	620		9.54	759	717[l]	42	17	139

a. By Additivity (Reference 19)
b. Monoenergetic Electron AE
c. Metastable Peak AE
d. $\Delta H_f(M)$ + Metastable Peak AE
e. $C_6H_5OH^{+\cdot}$ (ΔH_f = 722 $kJmol^{-1}$ [2]) + Alkene
f. Ethene ΔH_f = 52 $kJmol^{-1}$ [2]
g. Propene ΔH_f = 20 $kJmol^{-1}$ [2]
h. But-2-ene ΔH_f = -12 $kJmol^{-1}$ [2]
i. iso-Butene ΔH_f = -17 $kJmol^{-1}$ [2]
j. Pent-2-ene ΔH_f = -32 $kJmol^{-1}$ [2]
k. 2-Methyl-but-2-ene ΔH_f = -42 $kJmol^{-1}$ [2]
l. Cyclohexene ΔH_f = -5 $kJmol^{-1}$ [2]

These E_a values are consistent with the ion/radical complex mechanism. An ion/radical pair is produced by elongation of the $[C_6H_5O^{\cdot} \ldots {}^{+}alkyl]$ bond until the internal degrees of freedom of the radical and ion effectively cease to interact. Such an extension has been identified as greater than ca 3Å.[87]

The strength of $O\text{-}C_\alpha$ bonds decrease in the order primary, secondary, tertiary. This trend is related to the greater delocalization of charge in the larger methyl substituted alkyl groups.

The value of E_a for $[C_6H_5OCH_2CH_3]^{+\cdot}$ is related to the primary $O-C_\alpha$ bond separation which is required before transfer of a $\beta(H^+)$ may occur and is dependant on the $O-C_\alpha$ bond strength. Clearly, for the other primary ethers a lower energy pathway exists. The isomerization to an energy rich secondary or tertiary alkyl ion can take place at a lower energy (shorter bond elongation) than a direct $\beta(H^+)$ transfer (no isomerization of the ethyl cation is possible).

Secondary and tertiary ethers do not undergo rearrangement prior to $\beta(H^+)$ transfer and so E_a is strongly related to the energy required to elongate the $O-C_\alpha$ bond to the point at which transfer occurs which in turn is dependant on the strength of the bond.

Section 3.2.2 Reaction Mechanisms and Ion Structures

Deuterium labelling studies and a variety of mass spectrometric techniques have been used in order to understand the behaviour of ion/radical pairs as well as to obtain a clearer picture of such an intermediate. Of particular interest are four of the pentyl ethers in which other low energy complex-mediated reactions compete with proton transfer in their MIKE spectra.

Section 3.2.2.a Ethyl Phenyl Ether

The possible observation of the involvement of the classical and non-classical ethyl cations in the loss of ethene from ionized ethyl phenyl ether was examined using $C_6H_5OCH_2CD_3$. High level ab initio molecular orbital theory calculations indicate that the

classical ethyl cation, $CH_3CH_2^+$, is not the global minimum on the $[C_2,H_5]^+$ hypersurface but lies some 27 $kJmol^{-1}$ above the thermodynamically most stable configuration, symmetrically proton bridged ethene.[96] They are not separated by an energy barrier. Metastable peak AE measurements indicated that fragmentation of $C_6H_5OCH_2CH_3$ takes place at an energy ca 137 $kJmol^{-1}$ above the product energies. This result was confirmed by Riley and Baer who showed that the excess energy is made up from a reverse energy barrier and a sizeable kinetic shift.[97] Their favoured model involved a relatively tight transition state with a small negative entropy of activation, $\Delta S^{\ddagger} = -2.1$ $calmol^{-1}K^{-1}$. However, a better fit to the observed rate constant versus internal energy curve resulted when a looser transition state (lower vibrational frequencies) with $\Delta S^{\ddagger} = 4.1$ $calmol^{-1}K^{-1}$ was employed. The looser transition state appears to be more in keeping with an ion/radical pair transition state.

The KER for loss of ethene, $T_{0.5} = 6.3$ $kJmol^{-1}$, shows that little of the excess energy of the fragmenting ion is partitioned among translational degrees of freedom of the products. That the ethene is not generated in its ground state is shown by its collision induced ionization efficiency and its subsequent fragmentation characteristics (see Chapter 5).

The degree of H^+ versus D^+ transfer to the phenoxy radical as a function of ion lifetime (and hence internal energy) for $C_6H_5OCH_2CD_3$ is shown in Table 4.

Very little H/D mixing occurs: formal $\beta(D^+)$ transfer predominates for all metastable ions in spite of the high excess of

internal energy of these ions above the products. The metastable ions therefore do not consist of a significant amount of a complex between an ethyl cation and a phenoxy radical in which the classical and non-classical forms are in equilibrium. The transition state is then best represented as a symmetrical deuterium bridged complex, 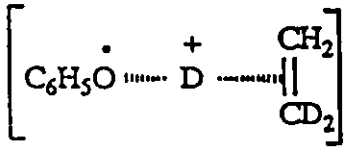 , which is looser than the cyclic transition state leading to $\beta(H^+)$ transfer preferred by Riley and Baer.[97]

Table 4 Effect of Ion Lifetime on the Production of $C_6H_5OD^{+\cdot}$ (m/z95) and $C_6H_5OH^{+\cdot}$ (m/z94) from $C_6H_5OCH_2CD_3$

Ion Lifetime (μsec)	m/z94	m/z95
<1[a]	23	77
2[b]	9	91
15[c]	6	94
30[d]	4	96
(random)	40	60

a Ion Source, ZAB
b 1FFR, MS-9
c 2FFR, ZAB
d 3FFR, ZAB

The ratio m/z 94:m/z 95 ($C_6H_5OH^{+\cdot}$:$C_6H_5OD^{+\cdot}$) was measured for $C_6H_5OCH_2CH_2D$. For metastable ions which dissociate in the 2FFR of the ZAB the ratio was 76:24. For source generated ions the ratio was 74:26. These ratios correspond to an unremarkable isotope effect for H^+ versus D^+ transfer of about 1.5.

Section 3.2.2.b 2-Propyl Phenyl Ether

Deuterium labelled 2-propyl phenyl ether was studied. Ionized $C_6H_5OCH(CD_3)_2$ showed no $[C_6H_5OH]^{+\cdot}$, m/z 94, (< 0.02 relative to m/z 95 = 100) in its MIKE spectrum. Species fragmenting in the ion source displayed m/z 94:m/z 95 = 3:100.

Clearly, there is no loss of positional identity of H and D atoms in labelled 2-propyl phenyl ether. These observations are in keeping with those reported by Uggerud et al.[98] on the behaviour of ionized 2-propyl trimesitylvinyl ether.

The excess energy of the transition state above the products has been measured to be 45 $kJmol^{-1}$ for 2-propyl phenyl ether (see Table 3). According to the most recent ab initio calculations[99] hydrogen atom scrambling in the 2-propyl cation involves interconversion between the 1-propyl and 2-propyl cations, $^+CH_2CH_2CH_3 \rightleftharpoons {}^+CH(CH_3)_2$, and requires an energy of 86 $kJmol^{-1}$. Therefore, the observed excess energy cannot be expected to produce any H-scrambling.

Section 3.2.2.c 1-Propyl Phenyl Ether

For 1-propyl phenyl ether, the excess energy of the transition state above the products for $[C_6H_5OH]^{+\cdot}$ generation from metastable ions is 97 $kJmol^{-1}$ (an energy sufficient for isomerization and H-scrambling in <u>isolated</u> 1-propyl cations).[99] This observation has already been discussed in detail by Chronister and Morton[87] whose results on labelled $C_6H_5OCD_2CH_2CD_3$ and $C_6H_5OCH_2CD_2CH_3$ were compatible with incomplete H/D scrambling in 2-propyl ions produced via a

phenoxy radical/1-propyl cation complex in which the primary carbocation rearranges via a single 1,2-H shift (Scheme 3.2).

However, H/D scrambling is not necessary tc explain their results. They may be explained equally as well by participation of $\beta(H^+)$ transfer from a non-rearranged 1-propyl cation in competition with $\beta(H^+)$ transfer from a 2-propyl cation formed by a single 1,2-H shift. Also note that Chronister and Morton observed a peak at m/z 77 in their MIKE spectra: a peak which was totally absent in our MIKE spectrum of 1-propyl phenyl ether but was an intense peak in our CA mass spectrum. Therefore, their m/z 94:m/z 95 ratios may have been effected by CA processes.

Scheme 3.2

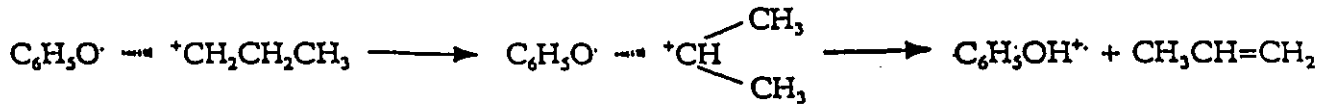

Section 3.2.2.d Butyl Phenyl Ethers

Ionized 1-butyl phenyl ether has an E_a = 180 kJmol^{-1} for C_4H_8 loss which is less than that required for $\beta(H^+)$ transfer from ethyl phenyl ether, 232 kJmol^{-1}. The former value corresponds to the energy required for isomerization of the 1-butyl cation to an energy rich 2-butyl cation in an ion/radical complex. The transition state energy for the metastable fragmentation of 1-butyl phenyl ether (815 kJmol^{-1}) is greater than the transition state energy required for $\beta(H^+)$ transfer from ionized 2-butyl phenyl

ether (765 $kJmol^{-1}$) and similar to the energy required for complete separation of the phenoxy radical plus 2-butyl cation (ΔH_f $C_6H_5O^{\cdot}$ = 48 $kJmol^{-1}$ [100], ΔH_f $^{+}CH(CH_3)CH_2CH_3$ = 766 $kJmol^{-1}$ [2]). See Figure 3.1.

Figure 3.1 Energy Diagram for the Metastable Fragmentation of Butyl Phenyl Ethers

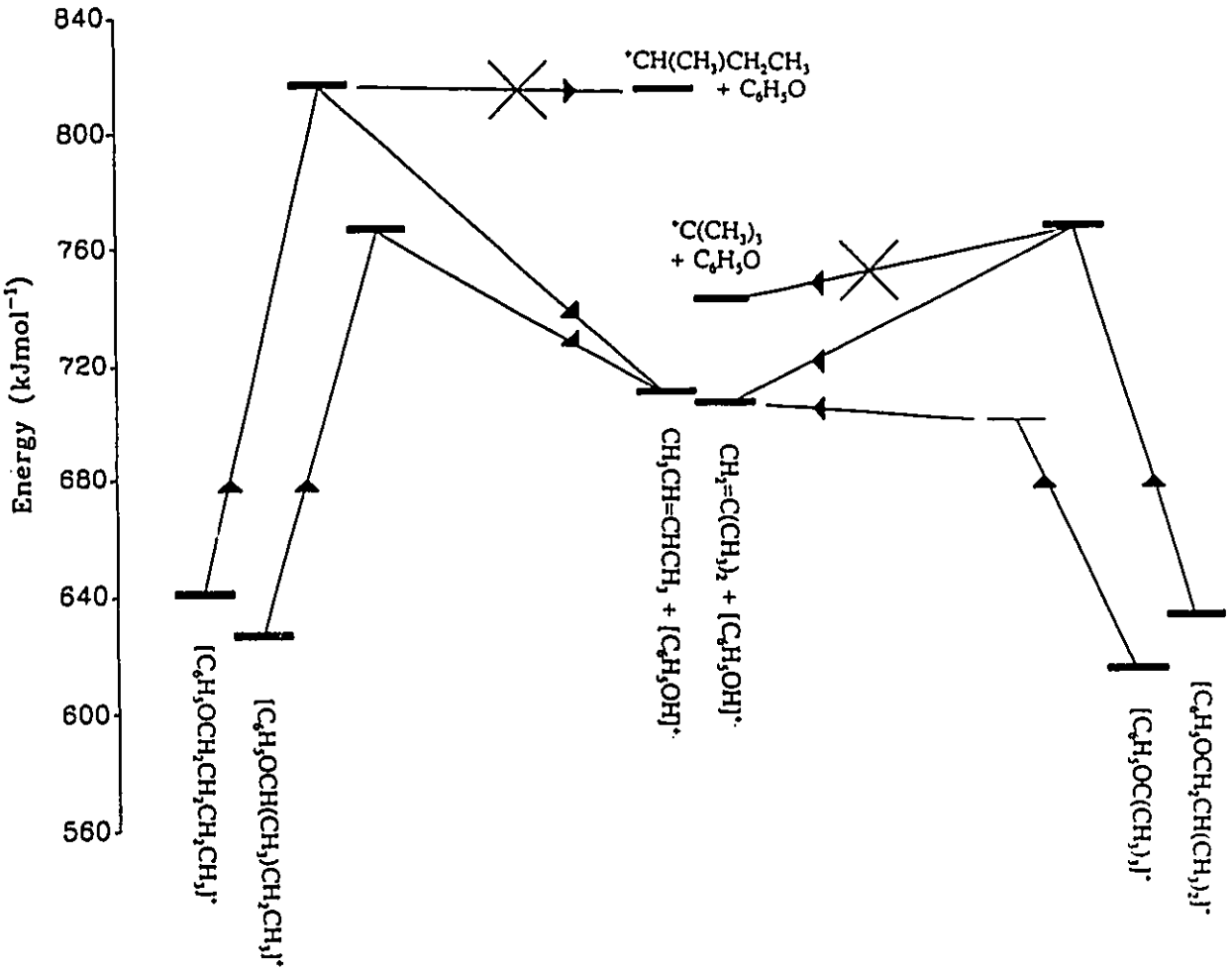

For iso-butyl phenyl ether, metastable ions fragment to produce $C_6H_5OH^{+\cdot}$ at an energy 27 $kJmol^{-1}$ above that required for the simple bond cleavage to $C_6H_5O^{\cdot}$ + $^{+}C(CH_3)_3$ ($\Delta H_f[C_6H_5O]^{\cdot}$ = 48 $kJmol^{-1}$ [100],

$\Delta H_f[C(CH_3)_3]^+$ = 694 kJmol^{-1} [2]) and 63 kJmol^{-1} above the thermochemical minimum for $C_6H_5OH^{+\cdot}$ + CH_2=$C(CH_3)_2$ (see Figure 3.1). The m/z 57 peak, $(CH_3)_3C^+$, in the Normal Mass Spectrum of iso-butyl phenyl ether was very weak and a peak at m/z 57 in the MIKE spectrum was totally absent. That the simple bond cleavage did not occur even though energetically feasible was taken as an indication that the iso-butyl cation does <u>not</u> isomerize via a 1,2-H shift to a t-butyl cation but that $\beta(H^+)$ transfer occurs from an unrearranged ion. The low E_a value (137 kJmol^{-1}) with respect to ethyl phenyl ether (232 kJmol^{-1}) being due to greater ease for transfer of a <u>tertiary</u> $\beta(H^+)$ than for transfer of a <u>primary</u> $\beta(H^+)$. Note that in (free) even-electron ions, such as the alkyl ions, the difference between primary and secondary, and between secondary and tertiary [C-H] bonds can be as much as 40-60 kJmol^{-1}.[101]

Two labelled compounds were synthesized, $C_6H_5OCH_2CD(CH_3)_2$ & $C_6H_5OCHDCH(CH_3)_2$, to test for rearrangement. In the metastable time frame, the H^+ versus D^+ transfer results of the two isotopomers were <u>identical</u>, m/z 94:m/z 95 = 89:11. This result is solely compatible with complete isomerization to the t-butyl ion prior to fragmentation with no isotope effect for H^+ versus D^+ transfer to the phenoxy radical (Scheme 3.3). The lack of any isotope effect at this modestly elevated internal energy, 63 kJmol^{-1} above the product energies, is in contrast to the ethyl analogue, which has an isotope effect of ca 1.5, where the $\beta(H^+)$ transfer rather than an isomerization is the rate determining step. Therefore, it must be concluded that the $\beta(H^+)$ transfer from the tertiary ion, $(CH_3)_3C^+$,

to the phenoxy radical is very fast, even relative to simple O-C_α bond fission.

Scheme 3.3

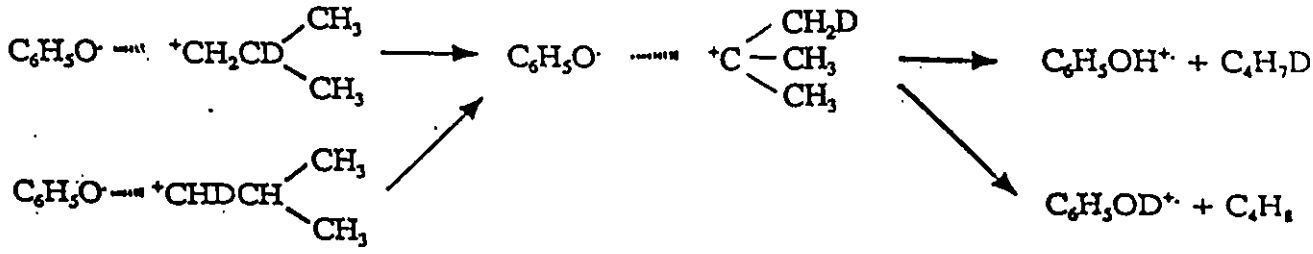

A conventional picture of a t-butyl cation with the formal charge located at the central carbon atom is not the best representation. The charge density calculations by Bader[102] show that the positive charge resides in the methyl groups, that the tertiary carbon atom is weakly negatively charged (-0.098e) and that the ground state of the ion is planar. In the ion/radical complex, the nearby presence of the electronegative phenoxy oxygen atom should distort the ion, attracting the positively charged methyl groups into closer proximity to oxygen while repelling the central carbon atom. $C_6H_5O^{\cdot}$ ····· 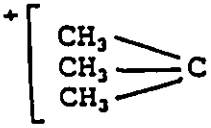 This should facilitate proton transfer. It is worth remarking that a similar picture obtains with the 2-propyl cation[102] and so the ion-radical complex involving a point positive charge at carbon-2, as depicted in the calculations of Chronister and Morton (see Figure 10 in reference 87) may well be inappropriate. Recently,

Perrin[103] has criticized Bader's calculations and has shown that they tend to exaggerate electron densities at electronegative atoms. However this does not invalidate the above qualitative description of the ion/radical complex.

t-Butyl phenyl ether transfers a $\beta(H^+)$ without rearrangement. It is a threshold reaction. The lack of a reverse energy barrier is due to the weak tertiary $O-C_\alpha$ bond which requires little energy to elongate.

Section 3.2.2.e 2- and 3-Pentyl Phenyl Ethers

These molecules showed only m/z 94 in their MIKE spectra. The labelling experiments of Sozzi et al.[90] are compatible with the formation of pent-2-ene as the neutral olefin. The excess energy of the products are 52 and 64 $kJmol^{-1}$. The E_a values for 2- and 3-pentyl phenyl ethers (142 and 150 $kJmol^{-1}$ respectively) are similar to those observed for the other metastable secondary ions (see Table 3).

Section 3.2.2.f 1-Pentyl and 2-Methyl-2-Butyl (t-pentyl) Phenyl Ethers

These two isomers lose both $[C_5,H_{10}]$ and $CH_3CH_2\cdot$ in the metastable time frame. For 1-pentyl phenyl ether the AE for both processes were identical. For t-pentyl phenyl ether, $CH_3CH_2\cdot$ loss takes place at a higher energy than $[C_5,H_{10}]$ loss (see Table 5).

Table 5 Metastable Peak Appearance Energies and Related Thermochemical Data for Pentyl Phenyl Ethers

Compound Studied [M]	$\Delta H_f[M]$[a] ($kJmol^{-1}$)	AE m/z94 (eV)	$T_{0.5}$ (meV)	Energy of TS Above Products ($kJmol^{-1}$)	AE m/z135 (eV)	$T_{0.5}$ (meV)	Energy of TS Above Products ($kJmol^{-1}$)	AE m/z70 (eV)	$T_{0.5}$ (meV)	Energy of TS Above Products ($kJmol^{-1}$)
VIII	-168	10.16	26	122[b]	10.14	27	158[d]	/	/	/
XI	-177	10.06	23	114[c]	/	/	/	10.02	22	91[e]
XII	-190	9.52	19	48[c]	/	/	/	9.52	17	29[e]
XIII	-194	9.02	6	0[c]	9.34	13	55[d]	/	/	/

a. By Additivity (Reference 19)
b. Products are $C_6H_5OH^{+\cdot}$ (ΔH_f = 722 $kJmol^{-1}$ [2]) + Pent-2-ene (ΔH_f = -32 $kJmol^{-1}$ [2])
c. Products are $C_6H_5OH^{+\cdot}$ (ΔH_f = 722 $kJmol^{-1}$ [2]) + 2-Methyl-but-2-ene (ΔH_f = -42 $kJmol^{-1}$ [2])
d. Products are $C_6H_5OC^+(CH_3)_2$ (ΔH_f = 534 $kJmol^{-1}$ see text) + $\cdot CH_2CH_3$ (ΔH_f = 118 $kJmol^{-1}$ [2])
e. Products are Ionized 2-Methyl-but-2-ene (ΔH_f = 795 $kJmol^{-1}$ [2]) + C_6H_5OH ΔH_f = -96 $kJmol^{-1}$ [2])

The fragment ions formed by $CH_3CH_2\cdot$ loss from these two ethers have the same structure as that generated by loss of $CH_3\cdot$ from t-butyl phenyl ether: $C_6H_5O^+C(CH_3)_2$, m/z 135. This was shown by comparing the CA mass spectra of the peaks at m/z 135 from the pentyl ethers with the CA of $C_6H_5O^+C(CH_3)_2$ (generated by methyl loss from $C_6H_5OC(CH_3)_3$) and with the CA of $C_6H_5{}^+CHCH_2CH_3$ (generated by methyl loss from $C_6H_5OCH(CH_3)CH_2CH_3$ (Table 6). The metastable peaks were not considered when comparing the CA mass spectra as already discussed in Section 2.1.3. The two $[C_{9,}H_{11,}O]^+$ isomers may be distinguished on the basis of the peaks at m/z 43 ($C_3H_7^+$) and m/z 106 ($\cdot CH_2CH_3$ loss). The peak at m/z 106 is absent in the CA mass spectrum of the $C_6H_5O^+C(CH_3)_2$ isomer which does not contain an ethyl group but is present in the CA mass spectrum of the $C_6H_5O^+CHCH_2CH_3$ isomer which does contain an ethyl group. The AE of the $C_6H_5O^+C(CH_3)_2$ ion, m/z 135, from $C_6H_5OC(CH_3)_3$ was measured using energy selected electrons. The value was 8.85 ± 0.05 eV. This value, together with $\Delta H_f[CH_3\cdot]$ = 146 $kJmol^{-1}$ [2] and $\Delta H_f[C_6H_5OC(CH_3)_3]$ = -174 $kJmol^{-1}$ [19] gives $\Delta H_f[C_6H_5OC^+(CH_3)_2]$ = 534 $kJmol^{-1}$ (note the

destabilizing effect of phenoxy relative to methoxy, $\Delta H_f[CH_3OC^+(CH_3)_2]$ = 477 $kJmol^{-1}$ [2]).

Table 6 The Partial CA Mass Spectra of $[C_9,H_{11},O]^+$ Ions, m/z 135. Peak Intensities are Relative to m/z 77 = 100.

m/z	t-Butyl Phenyl Ether	2-Butyl Phenyl Ether	1-Pentyl Phenyl Ether[a]	t-Pentyl Phenyl Ether[a]
39	18	10	17	15
41	23	14	25	21
43	14	1	10	12
50	18	15	20	20
51	25	22	28	26
63	9	7	10	9
65	23	19	26	29
76	28	31	30	30
77	100	100	100	100
91	21	30	21	23
94	30	30	28	29
95[b]	490	140	160	240
105	7	13	8	8
106	/	9	/	/
107[b]	2100	1200	1600	1900
117[b]	32	19	85	72
119	18	17	22	21
120	7	15	8	12

a. m/z 135 ions produced metastably in the 1FFR
b. Also a metastable peak

The calculated threshold energies for the $CH_3CH_2^\cdot$ (ΔH_f = 118 $kJmol^{-1}$ [2]) loss from 1-pentyl and 2-methyl-2-butyl phenyl ethers (8.50 and 8.77 eV respectively) both lie well below the observed values. For 1-pentyl phenyl ether the energy required for both $[C_5,H_{10}]$ loss and $CH_3CH_2^\cdot$ loss is governed by the isomerization of the 1-pentyl to a 2-pentyl cation (hence the identical appearance energies).

For metastable 1,1-d_2-1-pentyl phenyl ether ions, $[C_6H_5OCD_2CH_2CH_2CH_2CH_3]^{+\cdot}$, the ratio of m/z 94:m/z 95 = 90:10 (2FFR ZAB-ion lifetime ca 15μsec) and m/z 135 was wholly shifted to m/z 137 showing that <u>only</u> $CH_3CH_2\cdot$ was lost. At shorter ion lifetimes, ca 1μsec (1FFR MS-9), the m/z 137 peak remained alone, but the m/z 94:m/z 95 ratio fell to 78:22. By analogy with the 1-propyl and 1-butyl phenyl ethers it is proposed that the metastable 1-pentyl phenyl ether ion rearranges to the energy rich 2-pentyl isomer prior to loss of pent-2-ene. The increase in $C_6H_5OD^{+\cdot}$ production at shorter lifetimes (higher internal energies) reflects the increase in primary β(D•) transfer relative to the thermodynamically favoured secondary β(H•) transfer (see Scheme 3.4).

Scheme 3.4

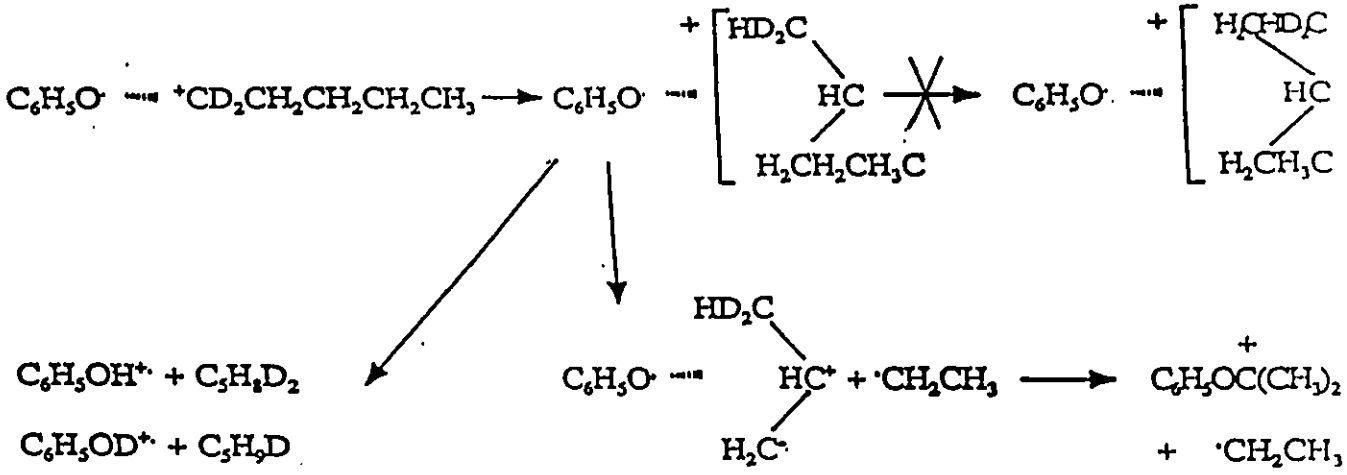

For the ethyl loss to remain so isotope specific, it follows that further rearrangement to the symmetrical 3-pentyl species cannot take place (see Scheme 3.4). In addition, to generate the observed peak at m/z 135, the $C_6H_5OC^+(CH_3)_2$ ion, a further 1,2-H shift must accompany (or follow) the loss of the ethyl radical, $CH_3CH_2^{\cdot}$ (see Scheme 3.4). In spite of the low enthalpy requirement for the overall reaction leading to $C_6H_5OC^+(CH_3)_2$, it should be noted that the bond $[CH_3^+CHCH_2 - CH_2CH_3]$ in the isolated secondary ion is very strong: 345 $kJmol^{-1}$ ($\Delta H_f[CH_3^+CHCH_2CH_2CH_3]$ = 732 $kJmol^{-1}$ [2], $\Delta H_f[CH_3CH{=}CH_2]^{+\cdot}$ = 959 $kJmol^{-1}$ [2], $\Delta H_f[CH_3CH_2^{\cdot}]$ = 118 $kJmol^{-1}$ [2]).

For the tertiary pentyl phenyl ether it appears that the $\beta(H^+)$ transfer is <u>less</u> energy demanding than the enthalpy favoured simple C-C bond cleavage. This must relate to the structure and charge distribution in the ion-radical complex.

<u>Section 3.2.2.q</u> 3-Methyl-1-Butyl and 2,2-Dimethyl Propyl Phenyl Ethers

These two isomers lose both $[C_5,H_{10}]$ and C_6H_5OH in the metastable time frame: $\beta(H^+)$ transfer competes with $\beta(H^{\cdot})$ transfer from the carbocation to phenoxy at the same internal energy (see Table 5) for each isomer.

3-Methyl-1-butyl phenyl ether, $C_6H_5OCH_2CH_2CH(CH_3)_2$, is expected to rearrange to the 3-methyl-2-butyl isomer prior to $\beta(H^+)$ or $\beta(H^{\cdot})$ transfer (Scheme 3.5). $\beta(H^{\cdot})$ transfer can yield two products, ionized 2-methyl-2-butene, $(CH_3)_2C{=}CH(CH_3)^{+\cdot}$, ($\Delta H_f$ = 795 $kJmol^{-1}$ [2]) from tertiary $\beta(H^{\cdot})$ transfer and 3-methyl-1-butene, $(CH_3)_2CHCH{=}CH_2^{+\cdot}$, ($\Delta H_f$ = 891 $kJmol^{-1}$ [2]) from primary $\beta(H^{\cdot})$ transfer. The metastable

peak AE, 10.02 eV, leads to $\Delta H_f[C_5,H_{10}]^{+\cdot}$ = 886 $kJmol^{-1}$. This threshold energy is governed by the rearrangement energy barrier and is typical of a primary to secondary isomerization in other primary ethers.

Scheme 3.5

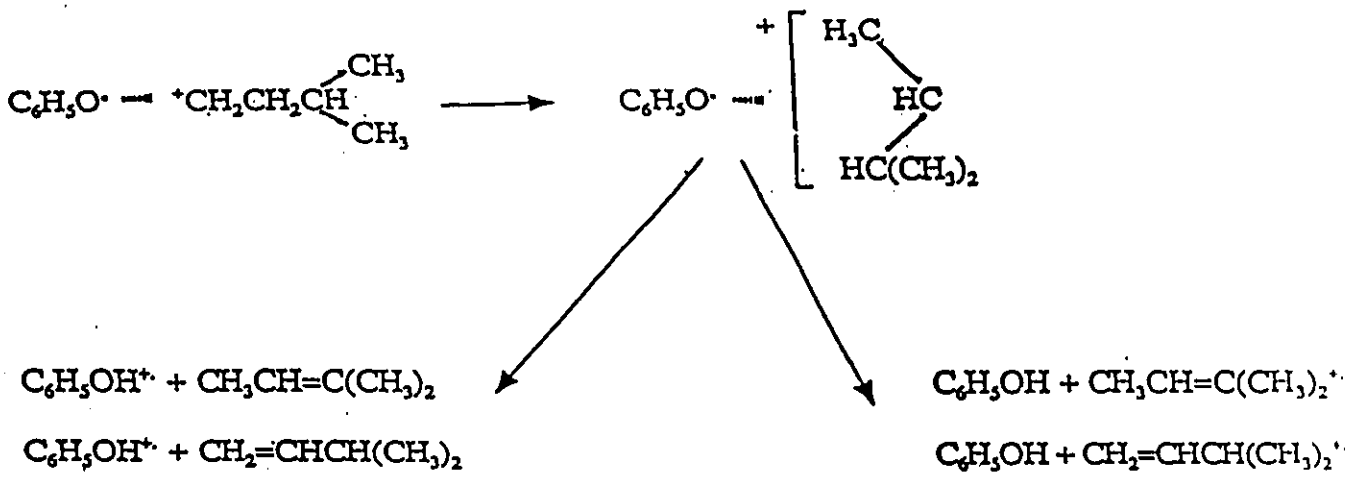

The identity of isomeric $[C_5,H_{10}]^{+\cdot}$ ions can be determined (see Table 13 Section 4.4) by CS mass spectrometry. The CS mass spectrum of the ion source generated m/z 70 ions was recorded and the relative abundances of the doubly charged ions are shown in Table 7. The predominant source generated ions are 3-methyl-1-butene ($\beta(H^{\cdot})$ transfer from unrearranged 3-methyl-1-butyl phenyl ether ions) and/or 1,1-dimethylcyclopropane ($\gamma(H^{\cdot})$ transfer from unrearranged 3-methyl-1-butyl phenyl ether ions). Note that the CS mass spectra of ionized 1,1-dimethylcyclopropane (ΔH_f = 858 $kJmol^{-1}$ from ΔH_f[1,1-dimethylcyclopropane] = -8 $kJmol^{-1}$ [2] and IE = 8.98 eV[104]) and 3-methyl-1-butene are indistinguishable. However, the 2-

methyl-2-butene ion must also be present based on the abundance of the peaks at m/z 69^{++} and m/z 70^{++}. Efforts were made to record the CS mass spectrum of the m/z 70 ions generated in the 1FFR where the ion-radical complex and rearrangement should predominate but the doubly charged peaks were too weak to measure, even by accumulated signal averaging.

Table 7 CS Mass Spectra of Ion Source Generated $[C_5,H_{10}]^{+\cdot}$ Ions, m/z70

	Precursor Molecules		
m/z	3-Methyl-1-butyl Phenyl Ether	2,2-Dimethylpropyl Phenyl Ether	t-Pentyl Phenyl Ether
31	19	19	19
31.5	4	5	5
32	9	9	10
32.5	9	8	8
33	15	15	15
33.5	10	11	9
34	10	11	9
34.5	<0.5	0	1.5
35	2.5	0	7

2,2-dimethyl propyl phenyl ether, $C_6H_5OCH_2C(CH_3)_3$, has no $\beta(H^+)/\beta(H^\cdot)$ to transfer and rearrangement of the alkyl group via a 1,2-H shift is not possible. Therefore, it is proposed that a 1,2-methyl shift is the governing process yielding an energy rich 2-methyl-2-butyl (t-pentyl) cation from which $\beta(H^+)$ and $\beta(H^\cdot)$ transfer may occur at the same energy. The E_a for the 1,2-methyl shift to form the t-pentyl cation was similar to the E_a for the 1,2-H shift in the isobutyl phenyl ether ion to form the t-butyl cation. This proposal is supported by experimental results.

$C_6H_5OCD_2C(CH_3)_3$ was synthesized. The MIKE spectrum showed almost equal transfer of H^+ and D^+. This is explained by the slightly less energy demanding transfer of (one of) the two secondary $\beta(D^+)$ to form $(CH_3)_2C{=}CH(CH_3)$ (ΔH_f = -42 kJmol^{-1} [2]) being preferred relative to transfer of (one of) the six primary $\beta(H^+)$ to form $CH_2{=}C(CH_3)CH_2CH_3$ (ΔH_f = -36 kJmol^{-1} [2]) from the tertiary ion (see Scheme 3.6). More strikingly, only $D^\cdot$ was transferred in the MIKE spectrum. This result is easily rationalized on energetic grounds. $\beta(D^\cdot)$ transfer from the tertiary pentyl ion produces the $[C_5,H_{10}]^{+\cdot}$ ion of lowest enthalpy, $(CH_3)_2C{=}CH(CH_3)^{+\cdot}$, ($\Delta H_f$ = 795 kJmol^{-1} [2]). $\beta(H^\cdot)$ transfer would form $CH_2{=}C(CH_3)CH_2CH_3^{+\cdot}$ (ΔH_f = 845 kJmol^{-1} [2]) at an energy 50 kJmol^{-1} higher (only 6 kJmol^{-1} lies between the neutral olefin products produced by primary or secondary $\beta(H^+)$ transfer).

Scheme 3.6

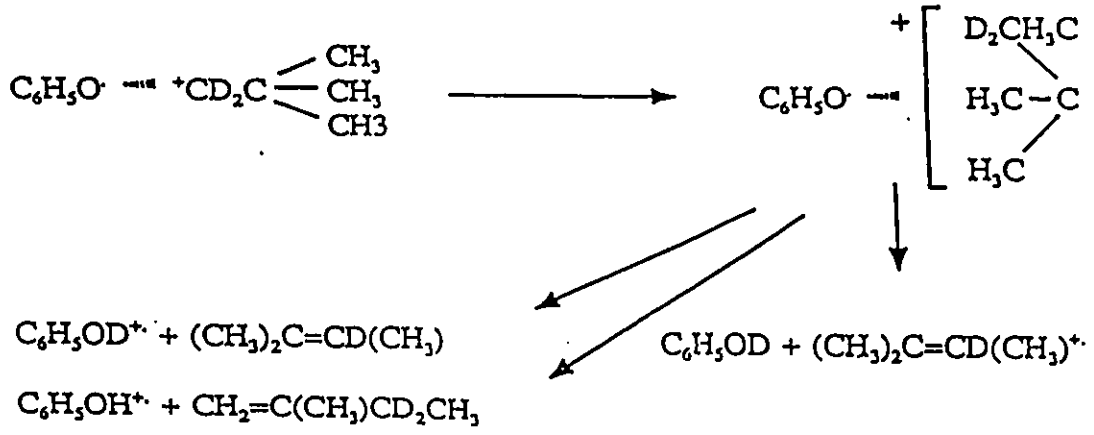

The CS mass spectrum of the m/z 70 ions formed metastably in the 1FFR was again too weak to be recorded and so only the CS mass

spectrum for the source generated ions was obtained (Table 7). The source generated m/z 70 ions can be identified as ionized 1,1-dimethylcyclopropane or its higher energy, ring opened form, ionized 3-methyl-1-butene. The reaction shown in Scheme 3.6 predicts formation of ionized 2-methyl-2-butene by $\beta(D^{\cdot})$ transfer. Therefore, in the ion source other reaction paths leading to formation of m/z 70 ions predominate.

The CS mass spectrum of source generated m/z 70 ions from t-pentyl phenyl ether was recorded (Table 7). $\beta(H^{\cdot})$ transfer should give the thermodynamically most stable $[C_5,H_{10}]^{+\cdot}$ isomer, $(CH_3)_2C{=}CH(CH_3)^{+\cdot}$. However, from Table 7, one can see that a mixture of $[C_5,H_{10}]^{+\cdot}$ ions must be generated with only ca 40% having the 2-methyl-2-butene structure (based on the doubly charged ion peak for m/z 70^{++} ions). Thus, m/z 70 ions must be formed by other than $\beta(H^{\cdot})$ transfer in the ion source.

In an attempt to determine the fragmentation behaviour of ionized 2,2-dimethylpropyl phenyl ether in the ion source, the labelled ether, $C_6H_5OCD_2C(CH_3)_3$ was studied over a range of internal energies and observation times. The results are shown in Table 8.

For metastable ions, in dissociations at intermediate times (1-2μsec) the transfer of $D^{\cdot}$ becomes internal energy dependant, being the most specific at the lower energy. These observations reflect an increase in primary $\beta(H^{\cdot})$ transfer to phenoxy from the rearranged (tertiary) ion. The CS mass spectrum for ion source generated m/z 70 ions showed that $D^{\cdot}$ transfer from a <u>tertiary</u> ion must be rejected. The transfer of a $\gamma(H^{\cdot})$ from a non-rearranged

ion suffices to explain the above CS result (formation of 1,1-dimethylcyclopropane); however, it is not reconcilable with the deuterium labelling results. One proposal which satisfies the observed D· transfer in the source invokes an ylidion (an ion in which the radical and charge bearing sites are on adjacent atoms), $C_6H_5\overset{D\cdot}{\underset{+}{O}}CDC(CH_3)_3$, in which a 1,3-H shift followed by dissociation could yield 1,1-dimethylcyclopropane. The CS mass spectrum produced no evidence for significant production of any other ionized branched olefin or cycloalkane and so extensive isomerization of the carbon skeleton can be ruled out. The change in label atom retention in the ion source as the ionizing electron energy is reduced would result from $\gamma(H\cdot)$ transfer becoming kinetically favoured over the ylidion route.

Table 8 The Effect of Ionizing Electron Energy and Observational Timeframe on the Generation of $[C_5H_9D]^{+\cdot}$ Ions, m/z 71, and $[C_5H_8D_2]^{+\cdot}$ Ions, m/z 72, from $C_6H_5OCD_2C(CH_3)_3$

Ionizing Electron Energy (eV)	Observation Timescale	m/z71	m/z72
70	0-1 µsec[a]	71	29
20	0-1 µsec[a]	53	47
13.8	0-1 msec[b]	38	62
12.9	0-1 msec[b]	35	65
12.3	0-1 msec[b]	33	67
11.6	0-1 µsec[b]	30	70
11.4	0-1 µsec[b]	20	80
11.1	0-1 µsec[b]	17	83
70	1-2 µsec[c]	70	30
12	1-2 µsec[c]	91	9
70	11-14 µsec[d]	100	0

a Ion source, MS-9
b Quadrupole mass spectrometer with electron energy selector
c 1FFR Metastable ions, MS-9
d 2FFR Metastable ions, ZAB

Section 3.2.2.h Cyclohexyl Phenyl Ether

The E_a value for cyclohexyl phenyl ether, 139 $kJmol^{-1}$, is similar to that for other secondary ethers. Therefore, it is proposed that there is no ring opening or rearrangement and that the neutral product produced following $\beta(H^+)$ transfer is cyclohexene.

Section 3.3 Conclusions

This work has clearly indicated the limits of isomerization in these systems at low internal energies, where the ion-radical complex plays a major role. At higher (ion source) energies, complex formation is much less important, as other dissociation processes become apparent. When complex ions are involved, their dissociation energies are governed solely by the nature of the alkyl ion portion. For primary ions, the energy required for isomerization to a secondary or tertiary ion is rate determining, whereas for secondary and tertiary ions the $\beta(H^+)$ transfer energy controls the rate of fragmentation. In general, among metastable ions there is little, if any, loss of positional identity (scrambling) of hydrogen atoms prior to fragmentation. Finally, the geometry of the complex will be governed by the charge distribution in the alkyl cation.

Section 3.4 Pentyl Methyl Ethers

Metastable fragmentations of four of the pentyl methyl ethers (2-pentyl methyl ether, 1-pentyl methyl ether, 2-methyl-2-butyl

methyl ether, 2,2-dimethylpropyl methyl ether) were studied in order to compare their behaviour with that of the corresponding pentyl phenyl ethers. The four pentyl methyl ethers studied all lost CH_3OH in the metastable time frame to produce ions at m/z 70. It is proposed that these reactions involve a $\beta(H^{\cdot})$ transfer from a pentyl cation in a methoxy radical/pentyl cation complex.

The results of IE, AE and KER measurements are shown in Table 9 together with other appropriate thermochemical data.

Table 9 Appearance Energies and Related Thermochemical Data for Pentyl Methyl Ethers

Compound Studied (M)	$\Delta H_f(M)$ ($kJmol^{-1}$)	IE (eV)	$\Delta H_f(M^{+\cdot})$ ($kJmol^{-1}$)	Metastable Peak AE m/z70 (eV)	Energy of TS[a] ($kJmol^{-1}$)	Product Energy[d] ($kJmol^{-1}$)	Excess Energy ($kJmol^{-1}$)	$T_{0.5}$ (meV)	E_a ($kJmol^{-1}$)
2-Pentyl Methyl Ether	-296[a]	9.30	601	10.16	684	638[e]	46	18	83
1-Pentyl Methyl Ether	-277[b]	9.45	635	9.98	685	638[e]	47	18	50
2-Methyl-2-Butyl Methyl Ether	-303[a]	9.15	580	10.06	668	593[f]	75	16	88
2,2-Dimethyl Propyl Methyl Ether	-297[b]	9.30	600	10.0	675	593[f]	82	15	75

a. By Additivity (Reference 19)
b. Reference 2
c. $\Delta H_f(M)$ + Metastable Peak AE m/z70
d. CH_3OH (ΔH_f = -202 $kJmol^{-1}$ [2]) + $[C_5H_{10}]^{+\cdot}$
e. $[CH_3CH{=}CHCH_2CH_3]^{+\cdot}$ ΔH_f = 840 $kJmol^{-1}$ [2]
f. $[(CH_3)_2C{=}CH(CH_3)]^{+\cdot}$ ΔH_f = 795 $kJmol^{-1}$ [2]

Section 3.4.1 2-Pentyl Methyl Ether

Ionized 2-pentyl methyl ether loses only CH_3OH in the metastable time frame producing a $[C_5,H_{10}]^{+\cdot}$ ion at m/z 70. The identity of the source generated m/z 70 ions could not be determined by their CS mass spectrum (shown in Table 10). This CS

mass spectrum is unlike any of the CS mass spectra of the $[C_5,H_{10}]^{+\cdot}$ isomers. The most obvious difference is the relatively large proportion of doubly charged 70^{++} and 69^{++} ions when compared with any of the $[C_5,H_{10}]^{+\cdot}$ isomers. There is no correction necessary for ^{13}C contributions. Therefore, the m/z 70 region in the Normal Mass Spectrum was examined under conditions of high mass resolution. It was found that in addition to $[C_5,H_{10}]^{+\cdot}$ two other ions of m/z 70 were present, $[C_4,H_6,O]^{+\cdot}$ and $[C_3,H_2,O_2]^{+\cdot}$, which were 30% and 10% as abundant as the $[C_5,H_{10}]^{+\cdot}$ ions based on peak heights. These interference peaks were present on several different days. The m/z 70 peak is very weak in the normal mass spectrum, so the $[C_4,H_6,O]^{+\cdot}$ and $[C_3,H_2,O_2]^{+\cdot}$ peaks are most probably due to background interference and not impurities in the compound.

Table 10 CS Mass Spectra of Ion Source Generated $[C_5,H_{10}]^{+\cdot}$ Ions, m/z70

	Precursor Molecules			
m/z	2-Pentyl Methyl Ether	1-Pentyl Methyl Ether	2-Methyl-2-Butyl Methyl Ether	2,2-Dimethyl Propyl Methyl Ether
31	9	20	14	16
31.5	2	5	6	8
32	6	10	10	6
32.5	7	10	9	6
33	12	19	16	14
33.5	9	11	10	8
34	21	24	31	23
34.5	11	1	1	4
35	23	0	3	15

The metastable peak appearance energy for the CH_3OH loss was 10.16 eV corresponding to a transition state energy of 684 $kJmol^{-1}$ which is 46 kJmol-1 above the energy of the products (See Table 9) assuming that the products are methanol and ionized pent-2-ene produced following a $\beta(H^{\cdot})$ transfer from a 2-pentyl cation to a methoxy radical in an ion/radical complex (similar to 2-pentyl phenyl ether). The value of E_a for this reaction is 83 $kJmol^{-1}$.

Section 3.4.2 1-Pentyl Methyl Ether

Ionized 1-pentyl methyl ether loses both CH_3OH and $\cdot CH_2CH_3$ in the metastable timeframe to produce ions at m/z 70 and m/z 73. The ratio m/z 70:m/z 73 in the MIKE spectrum was 100:61.

The source generated m/z 70 ions may be identified by their CS mass spectrum as ionized pent-2-ene with some ionized 1,1-dimethylcyclopropane (Table 10). These products may be simply explained by rearrangement of the 1-pentyl cation to a 2-pentyl or 3-pentyl cation prior to $\beta(H^{\cdot})$ transfer to give ionized pent-2-ene or rearrangement of the 1-pentyl cation to a 2-pentyl cation prior to $\gamma(H^{\cdot})$ transfer to give ionized 1,1-dimethylcyclopropane.

The metastably generated m/z 73 ions had a CA mass spectrum similar to that of $CH_3O^{+}CHCH_2CH_3$ (generated by $CH_3^{\cdot}$ loss from $CH_3OCH(CH_3)CH_2CH_3^{+\cdot}$) but had distinctive differences when compared to the CA mass spectrum of $CH_3O^{+}C(CH_3)_2$ (generated by $CH_3^{\cdot}$ loss from $CH_3OC(CH_3)_3^{+\cdot}$). Therefore the metastably generated m/z 73 ions are $CH_3O^{+}CHCH_2CH_3$. There is no metastable peak at m/z 73 in the MIKE spectrum of 2-pentyl methyl ether and the m/z 73 ions from

metastable 1-pentyl methyl ether ions have been assigned the $CH_3O^+CHCH_2CH_3$ structure. Therefore, it is proposed that an initial 1-2 H-shift in the 1-pentyl cation produces a 2-pentyl cation in which equilibrium with the 3-pentyl cation is established by successive 1-2 H-shifts. Further it is proposed that ethyl loss occurs from the 3-pentyl cation since ethyl loss from the 2-pentyl cation would give $CH_3O^+C(CH_3)_2$. See Scheme 3.7.

Scheme 3.7

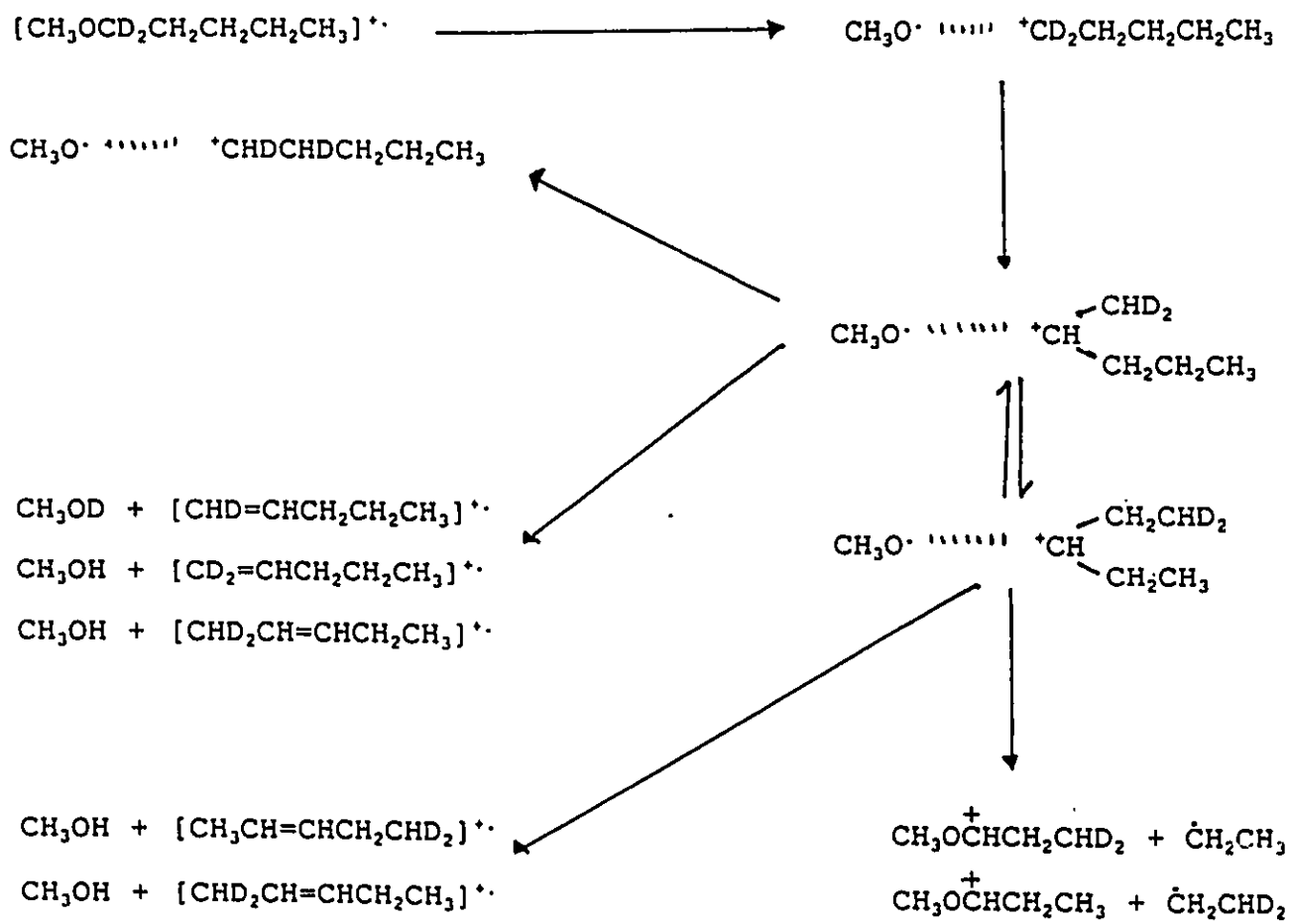

The metastable peak appearance energy of m/z 70 was 9.98 eV corresponding to a transition state energy of 685 $kJmol^{-1}$ which is 47 $kJmol^{-1}$ above the energy of the products (see Table 9). The value of E_a for this reaction is 51 $kJmol^{-1}$.

The energy (and E_a) for this reaction is not governed by the rearrangement/O-C_α bond strength (as per 1-pentyl phenyl ether) since the transition state energy for 1-pentyl methyl ether (685 $kJmol^{-1}$) is nearly identical to that of 2-pentyl methyl ether (684 $kJmol^{-1}$) and the value of E_a for 1-pentyl methyl ether (51 $kJmol^{-1}$) is less than that of 2-pentyl methyl ether (83 $kJmol^{-1}$). The rearrangement from the 1-pentyl cation to the 2-pentyl cation in the methoxy radical/pentyl cation complex must occur at an energy less than that required to directly transfer a $\beta(H\cdot)$ from the methoxy/2-pentyl cation complex. Therefore, it is the $\beta(H\cdot)$ transfer which controls the energy required for CH_3OH loss for both 1-pentyl and 2-pentyl methyl ethers.

The metastable peak appearance energy of m/z 73 was 9.91 eV corresponding to a transition state energy of 679 $kJmol^{-1}$. The heat of formation of $CH_3O^+CHCH_2CH_3$ has been estimated to be 522 ± 10 $kJmol^{-1}$. This is based on the approximation that $\cdot CH_3$ substitution lowers the heat of formation of $CH_3O^+CHCH_3$, 562 $kJmol^{-1}$ [2], by about 40 $kJmol^{-1}$. {$\cdot CH_3$ substitution lowers the heat of formation of $CH_3CH_2O^+CHCH_3$, 521 $kJmol^{-1}$ [2], by 45 $kJmol^{-1}$ ($\Delta H_f[CH_3CH_2O^+CHCH_2CH_3]$ = 476 $kJmol^{-1}$ [2]). $\cdot CH_3$ substitution lowers the heat of formation of $CH_3CH_2^+CHCH_3$, 766 $kJmol^{-1}$ [2], by 34 $kJmol^{-1}$ ($\Delta H_f[CH_3CH_2^+CHCH_2CH_3]$ = 732 $kJmol^{-1}$ [2]).} The heat of formation of $\cdot CH_2CH_3$ = 118 $kJmol^{-1}$ [2].

Therefore, the energy of the transition state above the products is about 39 $kJmol^{-1}$.

$CH_3OCD_2CH_2CH_2CH_2CH_3$ was synthesized. The ratio of the metastable peaks in the MIKE spectrum of this deuterated methyl pentyl ether were m/z 71:m/z 72:m/z 73:m/z 75 = 17:100:27:40. The peaks at m/z 73 and m/z 75 result from $\cdot CD_2CH_3$ loss and $\cdot CH_2CH_3$ loss respectively. The occurrence of both these losses must be due to interconversion between the isoenergetic 2-pentyl and 3-pentyl cations (see Scheme 3.7). Note that interconversion between the 2-pentyl and 3-pentyl cations does not occur from 1-pentyl phenyl ether. The absence of a peak at m/z 74 ($[C_2,H_4,D]\cdot$ loss) proves that the reverse rearrangement from the 2-pentyl cation to the 1-pentyl cation does not occur (see Scheme 3.7).

Section 3.4.3 2-Methyl-2-Butyl Methyl Ether

In the Normal Mass Spectrum, the molecular ion of 2-methyl-2-butyl methyl ether (t-pentyl methyl ether) is extremely weak. The base peak is due to loss of $\cdot CH_2CH_3$ (ΔH_f = 118 $kJmol^{-1}$ [2]) to produce an ion, $CH_3O^+C(CH_3)_2$ (ΔH_f = 477 $kJmol^{-1}$ [2]), at m/z 73. The threshold for this reaction is 595 $kJmol^{-1}$; only 15 $kJmol^{-1}$ above the heat of formation of the molecular ion. This reaction is not metastable. Note that ethyl loss from ionized t-pentyl phenyl ether is metastable but that this reaction occurs at an energy 115 $kJmol^{-1}$ above the heat of formation of the molecular ion (see Table 5).

CH_3OH and CH_3CH_3 are both lost from ionized t-pentyl methyl ether in the metastable time frame to produce ions at m/z 70 and

m/z 72. The ratio is m/z 70:m/z 72 = 49:100 after correction for ^{13}C contributions.

The source generated m/z 70 ions may be identified by their CS mass spectrum (Table 10) as a mixture of ionized 2-methyl-but-2-ene and ionized 1,1-dimethylcyclopropane. The formation of these products are easily explained by $\beta(H^{\cdot})$ transfer and $\gamma(H^{\cdot})$ transfer from the t-pentyl group.

The metastable peak appearance energy of m/z 70 was 10.06 eV corresponding to a transition state energy of 684 $kJmol^{-1}$ which is 89 $kJmol^{-1}$ above the energy of the products (see Table 9). The value of E_a for this reaction is 82 $kJmol^{-1}$.

The metastable peak appearance energy of m/z 72 was 10.28 eV corresponding to a transition state energy of 689 $kJmol^{-1}$ which is 85 $kJmol^{-1}$ above the energy of the products ($\Delta H_f[CH_3OC(CH_3)=CH_2]^{+\cdot}$ = 688 $kJmol^{-1}$ [2], $\Delta H_f[CH_3CH_3]$ = -84 $kJmol^{-1}$ [2]).

Section 3.4.4 2,2-Dimethylpropyl Methyl Ether

Ionized 2,2-dimethylpropyl methyl ether (neopentyl methyl ether) loses both CH_3OH and CH_3OCH_3 in the metastable time frame to produce ions at m/z 70 and m/z 56. The ratio m/z 70:m/z 56 = 57:100 in the MIKE spectrum.

The source generated m/z 70 ions may be identified by their CS mass spectrum (Table 10) as ionized 2-methyl-but-2-ene. The formation of ionized 2-methyl-but-2-ene is consistent with $\beta(H^{\cdot})$ transfer from a t-pentyl cation produced following a 1,2-methyl shift from the neopentyl cation in a methoxy radical/neopentyl

cation complex (similar to the loss of neutral phenol from metastable neopentyl phenyl ether ions).

The metastable peak appearance energy of m/z 70 was 10.0 eV corresponding to a transition state energy of 675 $kJmol^{-1}$ which is 82 $kJmol^{-1}$ above the energy of the products (see Table 9). This transition state energy is close to that of t-pentyl methyl ether, 668 $kJmol^{-1}$ (and the other two pentyl methyl ethers). Similar to 2-pentyl and 1-pentyl methyl ethers it is suggested that neopentyl and t-pentyl methyl ethers possess a common transition state and that the $\beta(H^{\cdot})$ transfer controls the energy required for CH_3OH loss.

The metastable peak appearance energy of m/z 56 was 10.1 eV corresponding to a transition state energy of 685 $kJmol^{-1}$. This reaction is a threshold process ($\Delta H_f[CH_3OCH_3]$ = -184 $kJmol^{-1}$ [2], $\Delta H_f[(CH_3)_2C{=}CH_2]^{+\cdot}$ = 874 $kJmol^{-1}$ [2]).

Hammerum and Audier[105] previously studied deuterium labelled neopentyl methyl ethers. They noted that in the metastable fragmentation of $CH_3OCD_2C(CH_3)_3^{+\cdot}$ and $CD_3OCH_2C(CH_3)_3^{+\cdot}$ there was extensive incorporation of D into the $[C_4,H_8]^{+\cdot}$ product ions.

Three labelled neopentyl methyl ethers were synthesized and studied. The MIKE spectrum of $^{13}CH_3OCH_2C(CH_3)$ contains three peaks at m/z 70, m/z 71 and m/z 56. The peaks at m/z 70 and m/z 71 are of equal intensity and correspond to $^{13}CH_3OH$ loss and CH_3OH loss respectively. The peak at m/z 56 corresponds to $^{13}CH_3OCH_3$ loss. The MIKE spectrum of $CH_3OCD_2C(CH_3)_3$ contains peaks at m/z 70, m/z 71 and m/z 72 (in the ratio 7:66:100) and peaks at m/z 56, m/z 57 and m/z 58 (in the ratio 63:100:54). The MIKE spectrum of $CD_3OCH_2C(CH_3)_3$

contains peaks at m/z 70, m/z 71, m/z 72 and m/z 73 (in the ratio 9:26:100:83) and peaks at m/z 56, m/z 57, m/z 58 and m/z 59 (in the ratio 28:100:93:19).

The extensive label scrambling observed is contrary to the behaviour of neopentyl phenyl ether. The scrambling may best be explained by invoking a mechanism for dimethyl ether loss (similar to that proposed for methanol loss from neopentyl alcohol[106]) which is in competition with CH_3OH loss via a methoxy radical/t-pentyl cation complex (see Scheme 3.9).

It is suggested that partial separation of the t-butyl cation and the $CH_3OCH_2\cdot$ radical allows rotation of the methoxy methyl radical to produce the ylid ion (a). H/D mixing may be explained via 1,4 H-shifts and involves the equilibrium between structures (a) and (b). A 1,3-methyl shift from the oxygen to the methylene radical in structure (b) produces the methoxy radical/t-pentyl complex. This complex then transfers a $\beta(H\cdot)$ to produce ionized 2-methyl-but-2-ene, m/z 70. Since the methoxy carbon and the α-carbon are indistinguishable in structure (b) they have an equal probability of being transferred. Therefore the carbon atom in the methanol loss may be either the original methoxy carbon or the original α-carbon (this proposal explains the presence of m/z 70 and m/z 71 in the MIKE spectrum of ^{13}C labelled neopentyl methyl ether). Structure (b) may also undergo simple bond cleavage to produce ionized iso-butene, m/z 56, and dimethyl ether.

There is no evidence that the methoxy radical/t-pentyl cation complex is produced by the isomerization of the neopentyl cation in

a methoxy radical/neopentyl cation complex (in the same manner that a phenoxy radical/t-pentyl cation complex is formed from ionized neopentyl phenyl ether).

Scheme 3.8

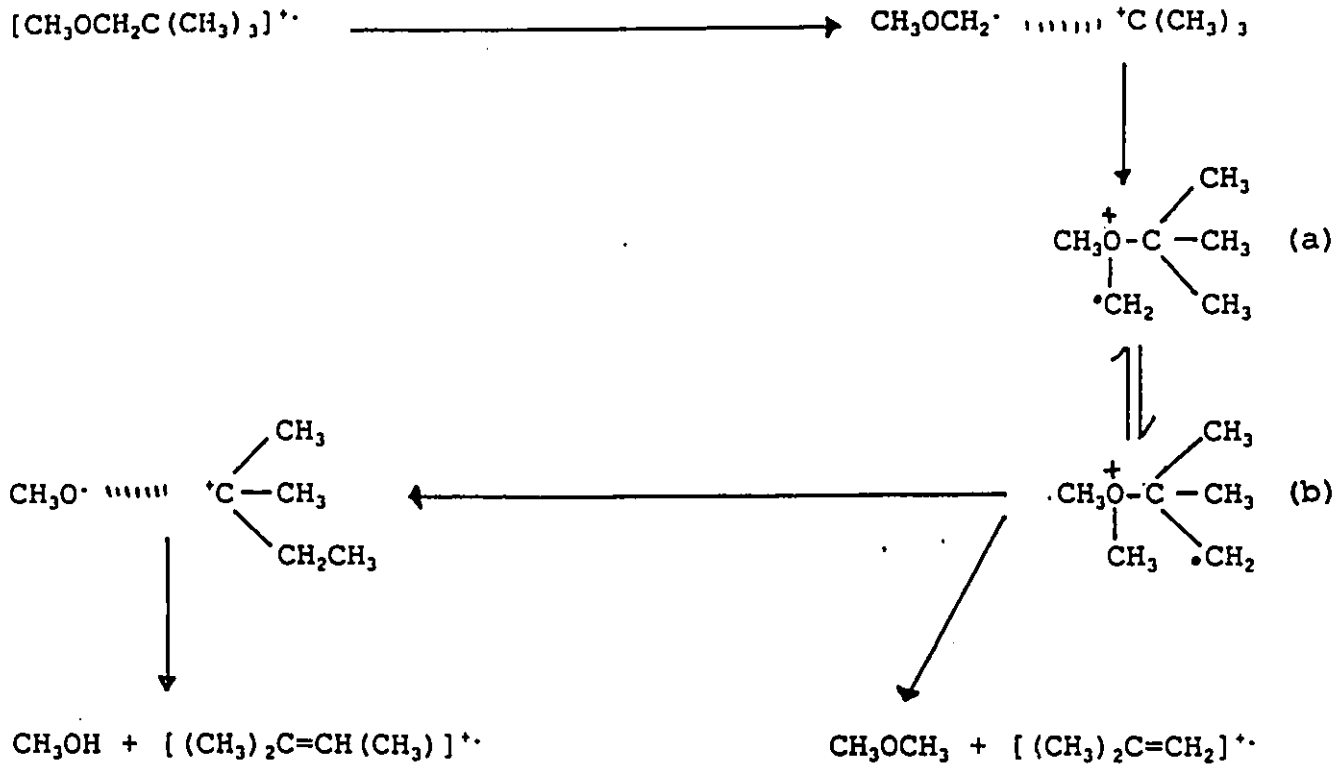

Section 3.4.5 Conclusions

The factors which govern the fragmentation of the metastable methyl pentyl ethers are different than those which control the fragmentation of the phenyl pentyl ethers.

The energy of the transition states for CH_3OH loss are similar for all the pentyl methyl ethers. This observation indicates that rearrangements occur below the energy required for $\beta(H\cdot)$ transfer

(unlike the primary alkyl phenyl ethers where rearrangement of the alkyl group produces a complex with a large excess of energy over that required for $\beta(H^+)$ transfer) and also explains why there is no relationship between the E_a values for the pentyl methyl ethers.

As illustrated for 1-pentyl methyl ether, $\beta(H^\cdot)$ transfer does not occur from the methoxy radical/2-pentyl cation complex immediately following a single 1,2-H shift but occurs only after further 1,2-H shifts have established equilibrium between the 2-pentyl and 3-pentyl isomers. Therefore the $\beta(H^\cdot)$ transfer is the rate determining step unlike the phenyl ethers where the rate determining step is the rearrangement.

Section 3.5 Experimental

The collisional activation (CA) mass spectra, charge stripping (CS) mass spectra and mass analyzed ion kinetic energy (MIKE) spectra were recorded on the VG-ZAB 2F mass spectrometer described in Chapter 1. The ionizing electron energy was 70 eV and the accelerating voltage was 8 kV. O_2 was used as collision gas in the CA and CS mass spectra at a pressure corresponding to 10% beam reduction. Metastable peak abundances were measured as relative peak heights with the energy resolving slits fully open. Kinetic energy release ($T_{0.5}$) values were recorded under conditions of good energy resolution such that the width at half-height of the main beam was less than 3V.

Ionization and appearance energy (AE) measurements were recorded using the energy selected electron impact ion source and quadrupole mass filter described in Chapter 1.

Metastable peak AE measurements were measured on the Kratos-AEI MS-902S mass spectrometer described in Chapter 1. The reference AE was the metastable loss of $CH_3\cdot$ from diethyl ether (AE = 10.26 eV).[30]

Ethyl phenyl ether, 1-butyl phenyl ether, and t-pentyl methyl ether were obtained from Aldrich Chemical Co., Inc. and were of research grade purity. 1-pentyl phenyl ether was obtained from Columbia Organic Chemical Co., Inc. and was of 97% purity.

A sample of $C_6H_5OCH(CD_3)_2$ was provided by Prof. T.H. Morton. A sample of $CH_3OCH(CH_3)CH_2CH_2CH_3$ was provided by Prof. R.D. Bowen.

2-Methyl-2-butyl phenyl ether was synthesized as described by Camps et al..[107] 2,2-Dimethyl propyl phenyl ether was synthesized according to the method of Dandrée and Seyden-Penne.[108] All the other alkyl phenyl ethers were prepared by standard Williamson syntheses (reaction of C_6H_5ONa with the appropriate alkyl bromide in ethanol).

$C_6H_5OCH_2CH_2D$ and $C_6H_5OCH_2CD_3$ were prepared by reacting the appropriate bromide ($BrCH_2CH_2D$ & $BrCH_2CD_3$ from MSD Isotopes) with C_6H_5ONa in ethanol.

$C_6H_5OCHDCH(CH_3)_2$ and $C_6H_5OCH_2CD(CH_3)_2$ were synthesized by reacting the appropriate tosylate ($TsOCHDCH(CH_3)_2$ & $TsOCH_2CD(CH_3)_2$) with C_6H_5ONa in ethanol. $TsOCHDCH(CH_3)_2$ was prepared by the reduction of $(CH_3)_2CHCHO$ with $LiAlD_4$ (MSD Isotopes) to the labelled alcohol followed by tosylation. $TsOCH_2CD(CH_3)_2$ was prepared by the reduction of $(CH_3)_2CDCHO$ (MSD Isotopes) with $LiAlH_4$ to the labelled alcohol followed by tosylation.

$C_6H_5OCD_2CH_2CH_2CH_2CH_3$ was synthesized by reacting $TsOCD_2CH_2CH_2CH_2CH_3$ with C_6H_5ONa in ethanol. $TsOCD_2CH_2CH_2CH_2CH_3$ was prepared by the reduction of $CH_3CH_2CH_2CH_2CO_2H$ with $LiAlD_4$ (MSD Isotopes) to the labelled alcohol followed by tosylation.

$C_6H_5OCD_2C(CH_3)_3$ was synthesized by reacting $TsOCD_2C(CH_3)_3$ with C_6H_5ONa in ethanol. $TsOCD_2C(CH_3)_3$ was prepared by the reduction of $(CH_3)_3CCO_2Cl$ with $LiAlD_4$ (MSD Isotopes) to the labelled alcohol followed by tosylation.

All the phenyl ethers were purified by vacuum distillation prior to use.

1-Pentyl methyl ether and 2,2-dimethylpropyl methyl ether were prepared by standard Williamson syntheses (reaction of CH_3I with the appropriate sodium alkoxide in ether).

$CH_3OCD_2CH_2CH_2CH_2CH_3$ was synthesized by reacting $NaOCD_2CH_2CH_2CH_2CH_3$ with CH_3I in ether. $NaOCD_2CH_2CH_2CH_2CH_3$ was prepared by the reduction of $CH_3CH_2CH_2CH_2CO_2H$ with $LiAlD_4$ (MSD Isotopes) to the labelled alcohol. The alcohol was then reacted with sodium metal in ether.

$CH_3OCD_2C(CH_3)_3$ was synthesized by reacting $NaOCD_2C(CH_3)_3$ with CH_3I in ether. $NaOCD_2C(CH_3)_3$ was prepared by the reduction of $(CH_3)_3CCO_2Cl$ with $LiAlD_4$ (MSD Isotopes) to the labelled alcohol. The alcohol was then reacted with sodium metal in ether. $CD_3OCH_2C(CH_3)_3$ was synthesized by reacting $NaOCH_2C(CH_3)_3$ with CD_3I (MSD Isotopes) in ether. $^{13}CH_3OCH_2C(CH_3)_3$ was synthesized by reacting $NaOCH_2C(CH_3)_3$ with $^{13}CH_3I$ (MSD Isotopes) in ether.

The contemplation of truth and beauty is the proper object for which we were created, which calls forth the most intense desires of the soul, and of which it never tires.

WILLIAM HAZLITT
Criticisms on Art

ASSIGNING STRUCTURES TO ISOMERIC $[C_5,H_{10}]^{+\cdot}$ IONS: THE GENERATION OF IONIZED ETHYLCYCLOPROPANE FROM PENTAN-1-OL AND 1-CHLOROPENTANE

Section 4.1 Introduction

The base peaks in the normal mass spectra of pentan-1-ol and 1-chloropentane occur at m/z 70, $[C_5,H_{10}]^{+\cdot}$ (H_2O loss & HCl loss respectively). The purpose of this study was to identify the $[C_5,H_{10}]^{+\cdot}$ ions produced from pentan-1-ol and 1-chloropentane. The various techniques (Ion thermochemistry, Metastable Peak Observations and Collision-Induced Fragmentation) used to assign structures to ions in the gas phase have been discussed by Holmes.[15] It was concluded that 'no method alone can suffice for an ion structure determination, but that in combination, the various techniques provide a powerful tool by means of which ion structure may be confidently assigned.' The identity of the $[C_5,H_{10}]^{+\cdot}$ isomers has proved difficult to determine since the metastable peak observations and CA mass spectra of all the isomers are similar. Therefore another technique(s) for distinguishing the various $[C_5,H_{10}]^{+\cdot}$ isomers had to be found.

Deuterium labelling studies of butan-1-ol[109] and some higher alcohols[110] showed that the elimination of water occurred predominantly by 1,4-elimination, through a six-centred transition state (Scheme 4.1). For pentan-1-ol ($R=CH_3$) the 1,4-elimination would produce methylcyclobutane ions. A study of deuterated long-chain alkan-1-ols by Bukovits and Budzikiewicz[111] led to the conclusion that production of ionized alkyl cycloalkanes by water loss is a general reaction.

Scheme 4.1

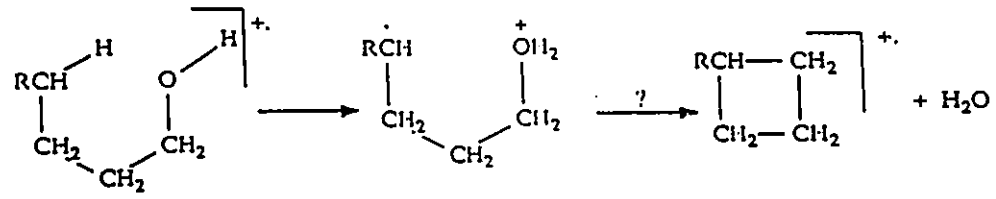

In contrast to the alkan-1-ols, deuterium labelling of 1-chlorobutane[112] showed that 93% of the HCl loss from the molecular ion took place via a 1,3-elimination. It was also determined that 72% of HCl loss from 1-chloropentane occurred via a 1,3-elimination and 18% occurred via a 1,4-elimination.[112] Thus, for 1-chloropentane a 1,3-elimination would produce ethylcyclopropane ions.

In this study, the results of ion thermochemistry, low-energy mass spectra and CS mass spectra have been used to distinguish among the $[C_5,H_{10}]^{+\cdot}$ isomers. These results have been used to identify the m/z 70 ions produced from pentan-1-ol and 1-chloropentane.

Section 4.2 Thermochemistry

Table 11 shows the enthalpies of formation, ΔH_f, for the isomeric $[C_5,H_{10}]^{+\cdot}$ ions. The values are mostly from reference 2 but modified to include new results. It has been shown that the adiabatic ionization energies for homologous and related series of compounds fall linearly with (1/n) where n = the number of atoms.[113] For instance, ΔH_f[cyclopropane] = 9.86 eV, ΔH_f[methylcyclopropane] = 9.46 eV, ΔH_f[1,1,2-trimethylcyclopropane] = 8.90 eV.[113] Therefore, the values for the ionization energies of the ethyl and dimethyl

substituted cyclopropanes given in the most recent data collection[2] appear to be inconsistent: ΔH_f[ethylcyclopropane] = 9.50 eV, ΔH_f[1,1-dimethylcyclopropane] = 9.08 eV, ΔH_f[cis/trans-1,2-dimethylcyclopropane] = 9.75 eV. The reason for the discrepancies lies in the difficulty of obtaining the adiabatic ionization energies for these molecules. The adiabatic ionization energies for these and other cycloalkanes have recently been measured and the values discussed in detail.[104] The new values have been used to determine the ΔH_f of the $[C_5,H_{10}]^{+\cdot}$ ions shown in Table 11. Therefore, the values assigned to the heats of formation for ethylcyclopropane, 1,1-dimethylcyclopropane and cis/trans-1,2-dimethylcyclopropane are quite similar; their adiabatic ionization energies being 8.98 eV, 9.02 eV and 8.95 eV respectively.[104] The results shown in Table 11 allow a clear thermochemical distinction, in terms of ΔH_f, between most of the $[C_5,H_{10}]^{+\cdot}$ isomers.

The AE values for $[C_5,H_{10}]^{+\cdot}$, m/z 70 ions, from pentan-1-ol and 1-chloropentane were measured using energy selected electrons and were found to be 10.04 ± 0.05 eV and 10.56 ± 0.05 eV respectively. These values together with $\Delta H_f[C_5H_{12}O]$ = -295 kJmol^{-1} [114], $\Delta H_f[C_5H_{11}Cl]$ = -175 kJmol^{-1} [114], $\Delta H_f[H_2O]$ = -242 kJmol^{-1} [2], ΔH_f[HCl] = -92 kJmol^{-1} [2] give apparent heats of formation of 916 and 936 kJmol^{-1} for the $[C_5,H_{10}]^{+\cdot}$ daughter ions from pentan-1-ol and 1-chloropentane respectively. These appearance energies are barely above the ionization energies of the parent molecules (IE$[C_5H_{12}O]$ = 10.00 eV[114], IE$[C_5H_{11}Cl]$ = 10.50 eV[115]) and so must give upper limits for the ΔH_f of the $[C_5,H_{10}]^{+\cdot}$ fragment ions.

Table 11 Thermochemistry of $[C_5,H_{10}]^{+\cdot}$ Ions[a]

$[Ion]^{+\cdot}$	ΔH_f ($kJmol^{-1}$)
Pent-1-ene	897
2-Methylbut-1-ene	845
3-Methylbut-1-ene	891
1,1-Dimethylcyclopropane	858[b]
Pent-2-ene	840
2-Methylbut-2-ene	795
1,2-Dimethylcyclopropane	866[b]
Ethylcyclopropane	859[b]
Methylcyclobutane	920
Cyclopentane	870[b]

a. All values from reference 2 except where noted
b. New values,[104] see text for discussion

The apparent heats of formation of the $[C_5,H_{10}]^{+\cdot}$ ions from both pentan-1-ol and 1-chloropentane lie above ΔH_f for most of the isomers in Table 11 and so the thermochemistry does little to aid their structure assignment.

There is a very weak metastable peak for loss of H_2O from ionized pentan-1-ol, m/z88 → m/z70, but half of the intensity arises from the ^{13}C contribution of the much stronger m/z87 → m/z69 dissociation. 1-Chloropentane shows a Gaussian type metastable peak for HCl loss having a kinetic energy release, measured from the peak width at half height ($T_{0.5}$) of 50 meV. The metastable peak was sufficiently intense that a CS mass spectrum of the $[C_5,H_{10}]^{+\cdot}$ ions generated in the 1FFR could be recorded (see Table 15).

Section 4.3 Low Energy Mass Spectra

The low energy mass spectra (ionizing electron energy = 12 eV) of the $[C_5,H_{10}]^{+\cdot}$ isomers are given in Table 12. The last column lists the percentage of fragmentation defined as $f = 100\Sigma f_i/(\Sigma f_i + M)$. f_i is the relative intensity of the fragment ion, i. M is the relative intensity of the molecular ion. These spectra differ from the low-energy spectra reported by Li et al.[116] from charge exchange with $COS^{+\cdot}$.

From Table 12, one can say that the spectrum of pentan-1-ol most resembles that of ethylcyclopropane (not methylcyclobutane as predicted). This result is in keeping with the CS results (see below) and may be rationalized in terms of a 1,2-H shift in the intermediate distonic ion to yield ionized ethylcyclopropane (Scheme 4.2).

Scheme 4.2

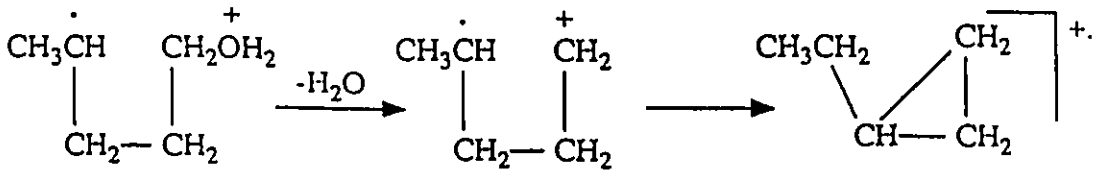

The spectrum of 1-chloropentane most closely resembles that of pent-1-ene. This result does not agree with the CS results (see below).

The percentage of fragmentation is greater for pentan-1-ol (39%) than for 1-chloropentane (30%). This observation may be explained by considering their ionization energies. The ionization

energy of pentan-1-ol is 10.00 eV[114] and the ionization energy of 1-chloropentane, estimated by the method of Holmes et al.,[116] is ca 10.5 eV. Therefore, with an ionizing electron energy of 12 eV the molecular ions of pentan-1-ol will be formed with a greater internal energy than the molecular ions of 1-chloropentane.

Table 12 The Low Energy Mass Spectra of the $[C_5,H_{10}]^{+\cdot}$ Isomers

Molecule	% Relative Intensity						%f[a]
	42^+	43^+	54^+	55^+	56^+	70^+	
Pent-1-ene	25	1	/	19	/	100	31
2-Methylbut-1-ene	5	/	/	10	/	100	13
3-Methylbut-1-ene	12	/	/	28	1	100	29
Pent-2-ene (Z)	9	/	/	16	1	100	21
Pent-2-ene (E)	15	/	1	31	1	100	32
2-Methylbut-2-ene	6	/	/	12	/	100	15
1,1-Dimethylcyclopropane	9	/	/	18	/	100	21
1,2-Dimethylcyclopropane	11	1	/	19	/	100	24
Ethylcyclopropane	34	/	/	22	/	100	36
Methylcyclobutane	100	6	/	37	/	75	66
Cyclopentane	55	4	2	39	/	100	50
Pentan-1-ol	38	2	/	24	/	100	39
1-Chloropentane	21	3	/	18	/	100	30

a. The % fragmentation, $f = 100\Sigma f_i/(\Sigma f_i + M)$.

Section 4.4 Charge Stripping

An earlier study by Miller and Gross[117] showed that CS mass spectra are more effective than CA mass spectra for distinguishing among $[C_5,H_{10}]^{+\cdot}$ isomers. This conclusion is in keeping with the work of Bowen et al.[118] and Holmes et al.[119] who were able to differentiate between propene and cyclopropane by their Helium CS mass spectra. McLafferty et al.[120] showed that O_2 was the most efficient CS target gas. Apart from increasing the total abundance

for doubly charged ions, O_2 also altered the relative abundance of the doubly charged ion peaks, showing a greater abundance of the doubly charged parent ions (relative to Helium).

It had been supposed that the work of Miller and Gross[117] would provide the necessary reference spectra for assigning structures to the $[C_5,H_{10}]^{+\cdot}$ product ions. However, their spectra showed very little difference on going from He to N_2 as collision gas, an unusual result in view of the substantial differences observed in other systems.[118] Also, they only reported the relative intensities of five of the nine observable CS peaks. Therefore, we remeasured the CS mass spectra of all the $[C_5,H_{10}]^{+\cdot}$ isomers using oxygen as the collision gas in order to enhance any contribution from $[C_5,H_{10}]^{2+}$ ions. The $[C_5,H_{10}]^{2+}$ ions were mentioned by Miller and Gross[117] but their relative intensities were not recorded. A few experiments were also performed with He and N_2. It was found that these two gases produced spectra having <u>fewer</u> structure significant features than those produced with oxygen. The He and N_2 results did not agree with those of Miller and Gross[117] in that the small differences in their spectra could not be reproduced. The CS mass spectra of four $[C_5,H_{10}]^{+\cdot}$ isomers with He as collision gas have also been reported by Sozzi et al..[121] Their results were in poor agreement with those of Miller and Gross[117] and again only five of the nine observable peaks were recorded. As will be seen below, inclusion of all nine peaks makes structure assignment much more certain.

In the earlier work[117] (performed on a Kratos triple sector mass spectrometer) the status of the final energy resolving slit was not given. In the present work it was found that only the relatively narrow m/z 70^{2+} peak was significantly affected by narrowing the final energy resolving slit.

The CS mass spectra of the $[C_5,H_{10}]^{+\cdot}$ isomers have been recorded with the accelerating voltage equal to 8 kV, 6 kV, 5 kV and 4 kV. The results are shown in Tables 13-16. The 8kV CS mass spectrum of 2-methyl-but-2-ene is shown in Figure 4.1.

Table 13 Charge Stripping Mass Spectra (O_2) of the $[C_5,H_{10}]^{+\cdot}$ Ions[a] Accelerating Voltage = 8 kV

Precursor	62^{2+}	63^{2+}	64^{2+}	65^{2+}	66^{2+}	67^{2+}	68^{2+}	69^{2+}	70^{2+}
Pent-1-ene	18	4	9	10	29	13	10	6	/
2-Methylbut-1-ene	20	5	9	10	19	12	18	7	/
3-Methylbut-1-ene	19	5	10	9	15	10	32	/	/
1,1-Dimethylcyclopropane	20	5	10	11	14	9	31	/	/
(E)-Pent-2-ene	20	5	9	10	19	12	20	5	/
2-Methylbut-2-ene	15	4	7	7	16	10	23	2	17
(Z)-1,2-Dimethylcyclopropane	15	4	9	9	16	10	27	4	5
Ethylcyclopropane	21	5	10	11	19	10	24	<1	/
Methylcyclobutane	22	5	11	11	17	9	25	<1	/
Cyclopentane	23	5	13	13	18	10	18	/	/
Pentan-1-ol	22	5	12	10	16	10	24	1	/
1-Chloropentane	26	5	11	10	15	10	22	<1	/

Table 14 Charge Stripping Mass Spectra (O_2) of the $[C_5,H_{10}]^{+\cdot}$ Ions[a] Accelerating Voltage = 6 kV

Precursor	62^{2+}	63^{2+}	64^{2+}	65^{2+}	66^{2+}	67^{2+}	68^{2+}	69^{2+}	70^{2+}
Pent-1-ene	18	3	8	10	28	14	11	8	/
2-Methylbut-1-ene	19	3	8	10	20	14	18	8	/
3-Methylbut-1-ene	16	3	9	9	15	11	36	/	/
1,1-Dimethylcyclopropane	17	3	10	10	15	10	35	/	/
(E)-Pent-2-ene	18	5	10	11	19	16	18	3	/
2-Methylbut-2-ene	10	2	6	7	16	12	28	2	17
(Z)-1,2-Dimethylcyclopropane	13	3	9	11	17	12	27	3	5
Ethylcyclopropane	16	4	10	13	20	12	25	/	/
Methylcyclobutane	17	4	11	13	18	11	26	/	/
Cyclopentane	17	4	13	15	21	11	19	/	/

Table 15 Charge Stripping Mass Spectra (O_2) of the $[C_5,H_{10}]^{+\cdot}$ Ions[a] Accelerating Voltage = 5 kV

Precursor	62^{2+}	63^{2+}	64^{2+}	65^{2+}	66^{2+}	67^{2+}	68^{2+}	69^{2+}	70^{2+}
Pent-1-ene	18	3	7	11	27	16	10	8	/
2-Methylbut-1-ene	18	3	8	11	21	16	15	8	/
3-Methylbut-1-ene	13	3	9	12	17	11	35	/	/
1,1-Dimethylcyclopropane	15	3	10	11	17	10	34	/	/
(E)-Pent-2-ene	17	4	10	12	19	18	18	2	/
2-Methylbut-2-ene	8	2	5	7	16	13	32	2	15
(Z)-1,2-Dimethylcyclopropane	12	3	9	11	17	12	29	3	4
Ethylcyclopropane	14	3	10	13	21	13	26	/	/
Methylcyclobutane	14	3	11	14	21	11	26	/	/
Cyclopentane	15	3	13	16	22	12	19	/	/
1-Chloropentane[b]	20	5	10	11	18	16	19	1	/

Table 16 Charge Stripping Mass Spectra (O_2) of the $[C_5,H_{10}]^{+\cdot}$ Ions[a] Accelerating Voltage = 4 kV

Precursor	62^{2+}	63^{2+}	64^{2+}	65^{2+}	66^{2+}	67^{2+}	68^{2+}	69^{2+}	70^{2+}
Pent-1-ene	13	3	7	11	28	18	11	9	/
2-Methylbut-1-ene	13	4	6	14	19	19	16	9	/
3-Methylbut-1-ene	12	3	9	13	16	11	36	/	/
1,1-Dimethylcyclopropane	15	3	10	11	18	10	35	/	/
(E)-Pent-2-ene	12	4	10	14	19	19	19	3	/
2-Methylbut-2-ene	5	2	4	9	16	15	33	3	13
(Z)-1,2-Dimethylcyclopropane	11	3	9	11	18	12	28	3	4
Ethylcyclopropane	11	2	10	14	24	13	26	/	/
Methylcyclobutane	11	3	10	15	22	11	28	/	/
Cyclopentane	11	2	12	18	24	13	20	/	/

a. The peak heights for 69^{2+} and 70^{2+} were obtained from an estimated baseline, since they appear on the skirt of an intense CA signal. Correction for ^{13}C overlap is not necessary for any of the $[C_5,H_{10}]^{+\cdot}$ ions. The values are an average of not less than three measurements. Estimated uncertainty ± 5%.

b. $[C_5,H_{10}]^{+\cdot}$ ions produced by metastable molecular ions. Estimated uncertainty ± 1.

Figure 4.1 The 8 kV Charge Stripping Mass Spectrum of Ionized 2-Methyl-but-2-ene

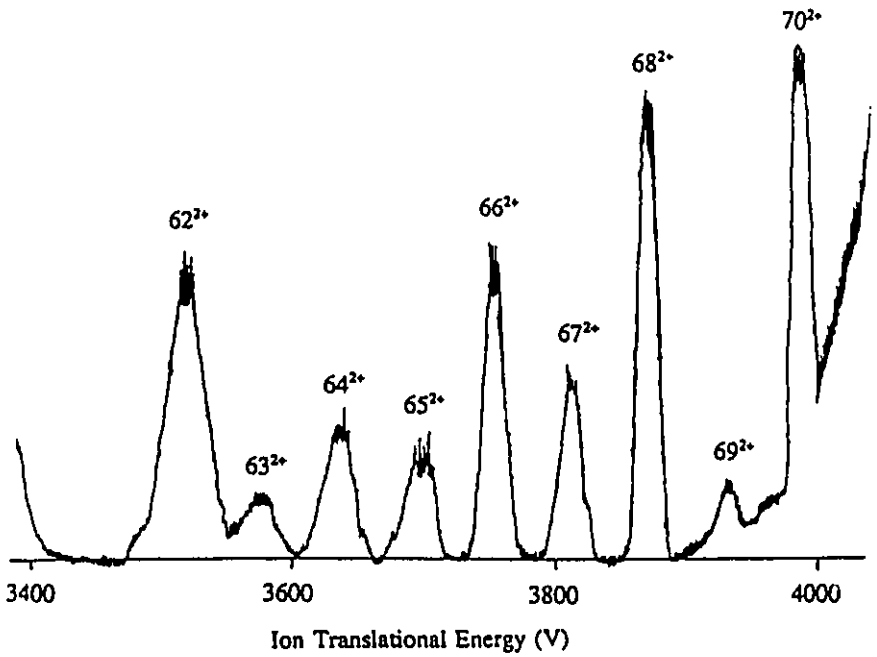

The general effect of lowering the accelerating voltage is to decrease the relative intensities of the lower mass (62-66) doubly charged ions and to increase the relative intensity of the higher mass (67-69) doubly charged ions. For 1,2-dimethylcyclopropane and 2-methylbut-2-ene the relative intensities of the 70^{2+} peaks are slightly decreased even though the effect of lowering the accelerating voltage increases the intensity of narrow peaks relative to broad peaks similar to increasing resolution.

It is therefore important that the translational energy of the $[C_5,H_{10}]^{+\cdot}$ isomers used to make the reference spectra is equal to the translational energy of the unknown $[C_5,H_{10}]^{+\cdot}$ ions in order to make the correct identification. For example, the CS mass spectrum of

an unknown ion, $M_2^{+\cdot}$, produced in the 1FFR (by the metastable dissociation of $M_1^{+\cdot}$) will have a kinetic energy of $(m_2/m_1)(8kV)$ where 8kV is the accelerating voltage. Therefore, the accelerating voltage of the reference spectra of the $M_2^{+\cdot}$ isomers should be equal to $(m_2/m_1)(8kV)$.

From Table 13 it can be seen that only 1,2-dimethylcyclopropane and 2-methylbut-2-ene show a peak for the doubly charged molecular ion. This result makes them quite distinct from all the other isomers and in view of the general similarity of their spectra it seems likely that the ring in the former compound opens to a significant extent to give the latter. There are three pairs of isomers that cannot be distinguished on the basis of their CS mass spectra: 3-methylbut-1-ene & 1,1-dimethylcyclopropane, pent-2-ene & 2-methylbut-1-ene, and ethylcyclopropane & methylcyclobutane. Distinctions within these pairs must therefore rest upon evidence from other experimental techniques. The thermochemistry clearly distinguishes between the members in each of the three pairs.

The CS mass spectra of the source generated $[C_5,H_{10}]^{+\cdot}$ daughter ions from both the alcohol and the chloride are most similar to those of ionized ethylcyclopropane and methylcyclobutane. These two isomers may be distinguished by their low energy mass spectra. The low energy mass spectrum of methylcyclobutane is dominated by m/z 42, ionized propene, formed by a simple C_2H_4 elimination from the four membered ring.

The low energy mass spectrum of pentan-1-ol is similar to that of ethylcyclopropane and bears little resemblance to that of methylcyclobutane as has already been discussed. For the fragmentation of pentan-1-ol, the 1,2 H-shift in the intermediate distonic ion (see Equation 4.2) may be driven by the significant energy difference (61 $kJmol^{-1}$) between the molecular ions of methylcyclobutane and ethylcyclopropane (Table 11).

The formation of source generated ionized ethylcyclopropane from 1-chloropentane is in keeping with the 1,3 HCl elimination previously observed.[112] However, the metastably generated $[C_5,H_{10}]^{+\cdot}$ ions from 1-chloropentane (kinetic energy = 5.185 kV) when compared to the CS mass spectra of the $[C_5,H_{10}]^{+\cdot}$ isomers with an accelerating voltage of 5kV (Table 15) no longer resemble ethylcyclopropane but now resemble pent-2-ene. The formation of pent-2-ene may be rationalized in terms of a 1,2 H-shift in the intermediate distonic ion (see Scheme 4.3) to yield ionized pent-2-ene (19 $kJmol^{-1}$ more stable that ionized ethylcyclopropane - see Table 12).

Scheme 4.3

$$CH_3CH_2CH_2CH_2CH_2Cl^{+\cdot} \xrightarrow{-HCl} CH_3CH_2\dot{C}HCH_2\overset{+}{C}H_2 \xrightarrow{1,2\ H\text{-shift}} CH_3\dot{C}H_2CH{=}CHCH_3^{+\cdot}$$

The low energy mass spectrum of 1-chloropentane is similar to that of pent-1-ene. However, it is also compatible with a mixture of ethylcyclopropane and pent-2-ene which would be in keeping with the CS results.

Section 4.5 Experimental

Ionization and appearance energy measurements were recorded using the energy selected electron impact ion source and quadrupole mass filter described in Chapter 1.

The low energy mass spectra (12 eV,350K) were recorded on the MS-9 mass spectrometer described in Chapter 1.

The CS mass spectra were obtained on the ZAB-2F mass spectrometer described in Chapter 1 at an ionizing electron energy of 70 eV. Oxygen was used as collision gas at a pressure corresponding to 90% transmission of the parent ion beam. The collision cell was situated in the second field free region of the instrument between the magnet and the electric sector. The CS mass spectrum of m/z 70 ions selected by the magnet was obtained by scanning the electric sector in the energy range close to that corresponding to transmission of ions having one half the m/z 70 ions' translational energy. The doubly charged ion peaks were sufficiently intense to be recorded by a single scan. The ionizing electron energy was 70 eV and the energy resolving slits were fully open. Corrections for ^{13}C overlap were carried out where necessary.

All samples, except for methylcyclobutane, were obtained from Wiley Organics Inc. and were at least 99% pure as determined by their mass spectra and NMR spectra. Methylcyclobutane was prepared by Dr. M. George by reduction of methylenecyclobutane (Aldrich) using H_2 and platinum oxide. The labelled pentanol, $CD_3CD_2CH_2CH_2CH_2OH$ was prepared by Dr. L.C. Leitch by the reaction of trimethylene oxide (Aldrich) with deuterated ethyl Grignard in ether. The Grignard was prepared from C_2D_5Br (MSD Isotopes) in the usual way.

Science is for those who learn;
poetry, for those who know

JOSEPH ROUX
Meditations of a Parish Priest

THE COLLISION INDUCED IONIZATION EFFICIENCY OF FAST NEUTRALS: NEUTRAL INTERNAL ENERGY & NEUTRAL TRANSLATIONAL ENERGY

Section 5.1 Introduction

The Collisionally Induced Dissociative Ionization mass spectra of metastably generated neutrals have been discussed in Section 2.1.5. In the second collision cell the neutrals are ionized by collision with a target gas, usually He or O_2.

McLafferty et al.[60] and Porter et al.[122] examined the efficiency of collision induced ionization. The ionization efficiency of species with low ionization energies (< 7 eV) increased with the electron affinity of the target indicating that electron transfer (Equation 2.10) may be the dominant ionization process with electron detachment (Equation 2.9) as a minor ionization process. It was concluded[122] that the ionization efficiency of species with ionization energies over ca 7 eV are not simply related to the electron affinity of the target. In general it was found[55] that for these species O_2 was the most efficient target. Also, if the ionization energy of the neutral is greater than the ionization energy of the target then ionization of the target will be a major process[55] and hence the ionization efficiency of the fast neutral will be relatively low.

The pressure of the target has a great effect on the ionization efficiency of fast neutrals. Upon increasing the pressure, the absolute abundance of the signals in the CIDI mass spectrum increases as is shown in Figure 5.1. Even though maximum intensity is achieved at about 30% mainbeam transmission for best

results, the mainbeam transmission is usually maintained between 85-90%. This ensures that there are mostly single collision conditions and that the spectrum is not affected by CA processes due to gas which has diffused out of the collision cell.

Figure 5.1 Relative Collision Induced Ionization Efficiency as a Function of the Reduction of the Mainbeam Intensity (Target Gas = O_2) Metastably Generated H_2O (from Ionized Propanol), Metastably Generated HCN (from Ionized Pyridine) and Metastably Generated $Br^{\cdot}$ (from Ionized Bromopropane) Were Used as the Sources of Fast Neutrals

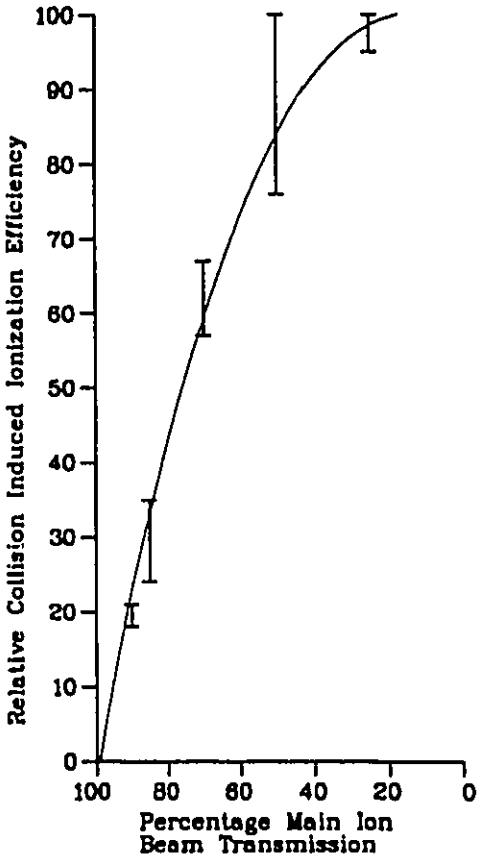

The translational energy required for maximum ionization cross-section may be estimated (Equation 5.1) using Massey's adiabatic criterion.[48]

(5.1) $V_{max} = (Q \cdot a)/h$

V_{max} = velocity of the incident particle corresponding to maximum cross section for the electronic transition (m/s)
Q = energy deficit/surplus of the electronic transition at the point of separation between the incident particle and the target molecule where the transition takes place (J)
a = distance over which interaction occurs between the incident particle and the target molecule (5-10 x 10^{-10} m)
h = Planck's constant (J·s)

Typically, V_{max} > 100 kV.[55] Hence, the accelerating voltages used in the CIDI experiments (< 10 kV) are much smaller than V_{max}. An increase in the neutral translational energy is therefore expected to increase the ionization cross-section.

The collision induced ionization cross-section of Na, K, Rb and Cs using H_2 and D_2 as target gas increased dramatically as the translational energy was increased from 150 to 2000 V.[123] In contrast with O_2 and Cl_2 as target gas the maximum cross-section occurred at translational energies between 150 and 1500 V.[123,124] With the latter targets it was shown that ionization occurred by both the electron transfer mechanism (V_{max} < 500 V) and the electron detachment mechanism (V_{max} > 2000 V).

McLafferty et al.[60] examined the O_2 ionization efficiency of fast CH_3Cl, $\cdot CH_2NH_2$, $\cdot S$ and $\cdot CH_3$. They found an increase of less than a factor of two upon raising the translational energy of the incident particle from 3 to 10 kV.

The collision induced ionization efficiency of CO, C_2H_4 and $CH_3CO\cdot$ were measured earlier in this laboratory with O_2 as the target gas.[55] For CO and C_2H_4 the cross-section increased as the accelerating voltage was increased from 2-9.8 kV. However, $CH_3CO\cdot$ had a maximum cross-section corresponding to an accelerating voltage of about 8 kV. These results were interpreted as indicating that ionization of CO (IE = 14.01 eV^2) and C_2H_4 (IE = 10.51 eV^2) occurred by the electron detachment mechanism while ionization of $CH_3CO\cdot$ (IE = 7.0 eV^2) occurred by both the electron detachment mechanism and the electron transfer mechanism. At higher accelerating voltages, the electron transfer mechanism is less efficient and contribution from the electron detachment mechanism will increase.

It was also shown[55] that the ionization efficiency of metastably generated neutrals depends on the internal energy of the neutrals. For example, the kinetic energy releases for metastable $Br\cdot$ loss from $[CH_2BrCH{=}CH_2]^{+\cdot}$, $[CH_3CH{=}CHBr]^{+\cdot}$ and $[HC{\equiv}CCH_2Br]^{+\cdot}$ were $T_{0.5}$ = 0.4, 6.0 and 570 meV respectively and the relative O_2 collision induced ionization efficiencies of the $Br\cdot$ atoms were 1.0, 1.5 and 2.5 respectively.[55] It was proposed that the degree of electronic excitation of the $Br\cdot$ atoms increased with increasing kinetic energy release resulting in higher ionization efficiencies. Appearance energy measurements have shown that $[CH_2BrCH{=}CH_2]^{+\cdot}$ and $[CH_3CH{=}CHBr]^{+\cdot}$ both lose $Br\cdot$ near their thermochemical thresholds[125] while $[HC{\equiv}CCH_2Br]^{+\cdot}$ loses $Br\cdot$ at an energy 0.83 eV above its

thermochemical threshold.[21,75] The lowest lying excited state of Br·, $^2P_{1/2}$, lies some 0.46 eV above the ground state, $^2P^{\bullet}_{3/2}$.[126] Therefore, the great majority of Br· atoms produced from the metastable dissociation of $[CH_2BrCH{=}CH_2]^{+\cdot}$ and $[CH_3CH{=}CHBr]^{+\cdot}$ must be in the ground state and hence the difference in the measured ionization efficiencies must be due to some reason other than electronic excitation, such as target gas pressure (one target gas pressure was not used for all measurements, rather target gas pressures corresponding to 10% mainbeam reduction for each metastable precursor ion were used). Br· produced from the metastable dissociation of $[HC{\equiv}CCH_2Br]^{+\cdot}$ may well have been generated in the $^2P_{1/2}$ state which could account for the observed increase in ionization efficiency.

Section 5.2 Results and Discussion

The effects of varying the internal energy of the neutral and the translational energy of the neutral upon the collision induced ionization efficiencies of CO and $CH_2{=}CH_2$ were studied.

The ionization efficiencies could be directly measured by observing the metastable reaction $M_1^+ \rightarrow M_2^+ + M_3$. The ratio of the intensity of ionized M_3 in the CIDI mass spectrum to the intensity of M_2^+ in the MIKE spectrum was recorded. Since the flux of neutral M_3 is equal to the flux of M_2^+ the ionization efficiency could be determined.

The internal energy and translational energy of the fast neutrals will vary according to the method of preparation. In this study the fast neutrals were prepared by the metastable dissociation of various precursor ions. Fast CO was generated by the metastable dissociation of three ions: CH_3CO^+ (m/z 43), $CH_2{=}CHCO^+$ (m/z 55) & $C_6H_5OH^{+\cdot}$ (m/z 94). Fast $CH_2{=}CH_2$ was generated by the metastable dissociation of two ions: $CH_3(CO)CH_2CH_2CH_3^{+\cdot}$ (m/z 86) & $C_6H_5OCH_2CH_3^{+\cdot}$ (m/z 122).

The relative amount of internal energy was related to the kinetic energy release ($T_{0.5}$) and/or the AE for the dissociation (see Section 2.1.2a). The results of kinetic energy release measurements are shown in Table 17.

Table 17 Kinetic Energy Releases for Loss of CO and C_2H_4

Metastable Ion	Precursor Molecule	Neutral Lost	$T_{0.5}$ (meV)
CH_3CO^+	$CH_3C(O)CH_3$	CO	1.4 (1.5[127], 1.6[128])
CH_3CO^+	$CH_3C(O)CH_2CH_3$	CO	1.9
CH_3CO^+	$CH_3C(O)CH{=}CH_2$	CO	1.6
CH_3CO^+	$CH_3C(O)C(O)CH_3$	CO	2.0
CH_3CO^+	$CH_3C(O)OCH_2CH_3$	CO	2.7
$CH_2{=}CHCO^+$	$CH_2{=}CHC(O)CH_3$	CO	2.3 (2.1[129])
$CH_2{=}CHCO^+$	$CH_2{=}CHC(O)CH_2CH_3$	CO	2.3
$CH_2{=}CHCO^+$	$CH_2{=}CHCO_2H$	CO	2.4
$CH_2{=}CHCO^+$	$CH_2{=}CHC(O)OCH_2CH_3$	CO	3.6
$C_6H_5OH^{+\cdot}$	C_6H_5OH	CO	530 (530[130], 520[131])
$C_6H_5OH^{+\cdot}$	$C_6H_5OCH_2CH_3$	CO	540 (544[132])
$CH_3(CO)CH_2CH_2CH_3^{+\cdot}$	$CH_3C(O)CH_2CH_2CH_3$	$CH_2{=}CH_2$	14 (14[133], 13[134], 18[135])
$C_6H_5OCH_2CH_3^{+\cdot}$	$C_6H_5OCH_2CH_3$	$CH_2{=}CH_2$	30 (16[136])

CO loss from CH_3CO^+ and $CH_2{=}CHCO^+$ both produce narrow, Gaussian metastable peaks indicating that these reactions proceed near threshold. However, CO loss from $C_6H_5OH^{+\cdot}$ produces a broad, dished metastable peak indicating a large reverse energy barrier. These predictions were tested by measuring the appearance energies for Reactions (1)-(3) below. The appropriate heats of formation are given underneath the reactants and products in $kJmol^{-1}$.

(1) $CH_3C(O)CH_3 \rightarrow CH_3CO^+ + \cdot CH_3 \text{ -*-> } {}^+CH_3 + CO + \cdot CH_3$
ΔH_f -217^2 1093^2 -111^2 146^2

Calculated AE = 1093 + (-111) + 146 - (-217) = 1345 $kJmol^{-1}$
= 13.95 eV
Measured AE (metastable peak appearance energy)
= 13.9 ± 0.1 eV

(2) $CH_2{=}CHC(O)OCH_2CH_3 \rightarrow CH_2{=}CHCO^+ + \cdot OCH_2CH_3 \text{ -*-> } CH_2{=}CH^+ + CO + \cdot OCH_2CH_3$
ΔH_f -377^2 1112^2 -111^2 -17^{100}

Calculated AE = 1112 + (-111) + (-17) - (-377) = 1361 $kJmol^{-1}$
= 14.11 eV
Measured AE (metastable peak appearance energy)
= 14.3 ± 0.1 eV

(3) $C_6H_5OH \rightarrow C_6H_5OH^{+\cdot} \text{ -*-> } C_5H_6^{+\cdot}$ (cyclopentadiene) + CO
ΔH_f -96^2 957^2 -111^2

Calculated AE = 957 + (-111) - (-96) = 942 $kJmol^{-1}$
= 9.76 eV
Measured AE (monoenergetic electron appearance energy)
= 10.76 ± 0.05 eV

As can be seen from the above results, CO loss from CH_3CO^+ and $CH_2{=}CHCO^+$ do proceed near their thermochemical thresholds while CO loss from C_6H_5OH has a large reverse energy barrier and/or kinetic shift ≤ 1 eV.

$CH_2{=}CH_2$ loss from $CH_3C(O)CH_2CH_2CH_3^{+\cdot}$ produces a Gaussian metastable peak ($T_{0.5}$ = 14 meV). The appearance energy for Reaction (4) was 10.08 eV which is equal to the calculated value showing that the reaction proceeds near its thermochemical threshold.

(4) $CH_3C(O)CH_2CH_2CH_3 \rightarrow CH_3C(O)CH_2CH_2CH_3^{+\cdot} \text{ -*-> } CH_3C(OH){=}CH_2^{+\cdot} + CH_2{=}CH_2$
ΔH_f -259^2 661^2 52^2

Calculated AE = 661 + 52 - (-259) = 972 $kJmol^{-1}$
= 10.08 eV
Measured AE (monoenergetic electron appearance energy)
= 10.08 ± 0.05 eV

CH_2=CH_2 loss from $C_6H_5OCH_2H_3$ produces a Gaussian metastable peak with a small kinetic energy release ($T_{0.5}$ = 30 meV). However, the appearance energy for Reaction (5) was 10.3 eV which is 1.22 eV above the calculated value, 9.03 eV. Therefore, there is a large reverse energy barrier and/or kinetic shift even though the magnitude of the kinetic energy release does not reflect this.

(5) $C_6H_5OCH_2CH_3 \rightarrow C_6H_5OCH_2CH_3^{+\cdot} \text{-*}\rightarrow C_6H_5OH^{+\cdot} + CH_2{=}CH_2$

ΔH_f $\quad -102^2 \qquad\qquad\qquad\qquad 722^2 \qquad 52^2$

Calculated AE = 722 + 52 - (-102) = 876 $kJmol^{-1}$
= 9.08 eV
Measured AE (monoenergetic electron appearance energy)
= 10.30 ± 0.05 eV

Therefore, we may assume that the fast CO produced from the metastable dissociation of $C_6H_5OH^{+\cdot}$ probably has significantly more internal energy than the fast CO produced from the metastable dissociation of CH_3CO^+ and that the fast CH_2=CH_2 produced from the metastable dissociation of $C_6H_5OCH_2CH_3^{+\cdot}$ has significantly more internal energy than the fast CH_2=CH_2 produced from the metastable dissociation of $CH_3C(O)CH_2CH_2CH_3^{+\cdot}$. This is shown by comparing the CIDI mass spectra of CH_2=CH_2 produced from $CH_3C(O)CH_2CH_2CH_3^{+\cdot}$ and $C_6H_5OCH_2CH_3^{+\cdot}$, the latter exhibiting more fragmentation. The ratios of m/z 28:m/z 27:m/z 26:m/z 25 in the two CIDI mass spectra are 100:24:16:<1 and 100:27:19:2 for $CH_3C(O)CH_2CH_2CH_3^{+\cdot}$ and $C_6H_5OCH_2CH_3^{+\cdot}$ respectively. An increase in internal energy of the neutral increases the extent of fragmentation. This has been shown in the NO/O_2 and Xe/O_2 neutralization reionization mass spectra of $H_2O^{+\cdot}$ as well as for the NO/O_2, Xe/O_2, SF_6/O_2 and He/O_2 neutralization reionization mass spectra of CH_3^+.[55]

The translational energy, E_{trans}, of the fast neutrals depends on the accelerating voltage, V_{acc}, the mass of the metastable ion, m_1, and the mass of the neutral, m_3, according to Equation 5.2.

(5.2) $$E_{trans} = (m_3/m_1)V_{acc}$$

The accelerating voltage was adjusted for each ion so that the metastably generated neutrals would all be generated with the same translational energy. The results of ionization efficiency measurements are shown in Table 18.

Table 18 Collision Induced Ionization Efficiencies of CO & $CH_2=CH_2$[a]

Metastable Ion	Precursor Molecule	Neutral Lost	E_{trans} (Volts) 5209	3907	2605	2000
CH_3CO^+	$CH_3C(O)CH_3$	CO	7.58×10^{-3}	3.42×10^{-3}	1.09×10^{-3}	2.83×10^{-4}
CH_3CO^+	$CH_3C(O)CH_2CH_3$	CO	5.46×10^{-3}	3.40×10^{-3}	1.07×10^{-3}	
CH_3CO^+	$CH_3C(O)CH=CH_2$	CO	6.62×10^{-3}	2.98×10^{-3}	1.01×10^{-3}	
CH_3CO^+	$CH_3C(O)C(O)CH_3$	CO	8.00×10^{-3}	3.40×10^{-3}	1.34×10^{-3}	
CH_3CO^+	$CH_3C(O)OCH_2CH_3$	CO	4.67×10^{-3}			
$CH_2=CHCO^+$	$CH_2=CHC(O)CH_3$	CO		1.57×10^{-3}	5.83×10^{-4}	1.89×10^{-4}
$CH_2=CHCO^+$	$CH_2=CHC(O)CH_2CH_3$	CO		1.99×10^{-3}	5.84×10^{-4}	
$CH_2=CHCO^+$	$CH_2=CHCO_2H$	CO		1.61×10^{-3}	5.73×10^{-4}	1.35×10^{-4}
$CH_2=CHCO^+$	$CH_2=CHC(O)OCH_2CH_3$	CO		1.75×10^{-3}	5.69×10^{-4}	1.48×10^{-4}
$C_6H_5OH^{+\cdot}$	C_6H_5OH	CO			1.50×10^{-3}	4.40×10^{-4}
$C_6H_5OH^{+\cdot}$	$C_6H_5OCH_2CH_3$	CO			2.30×10^{-3}	3.10×10^{-4}
$CH_3(CO)CH_2CH_2CH_3^{+\cdot}$	$CH_3C(O)CH_2CH_2CH_3$	$CH_2=CH_2$			4.39×10^{-4}	2.15×10^{-4}
$C_6H_5OCH_2CH_3^{+\cdot}$	$C_6H_5OCH_2CH_3$	$CH_2=CH_2$				8.10×10^{-5}

a. Values good to within ± 5%

Before discussing the results shown in Table 18 one must consider what factors may prevent the measured ionization efficiencies from equalling the true ionization efficiencies. Three factors were examined: scattering, the relationship between relative peak heights and relative ion abundances and multiplier discrimination.

Section 5.2.1 Scattering

In order to determine whether a significant amount of ionized neutrals were deflected out of the beam path upon collision with the target gas the Y_3 slit (which immediately follows the collision cell, Figure 1.3) was narrowed. In no case did the CIDI peak decrease in intensity when the Y_3 slit was only slightly narrowed. Only after the slit width had been decreased by a significant amount did the CIDI peak intensities start to decrease. Therefore, Y_3 when fully open is more than wide enough for the entire beam to pass through it (no large amount of scattering).

Section 5.2.2 Relative Peak Heights and Relative Ion Abundances: The validity of assuming that peak heights are proportional to ion flux.

In the absence of an energy resolving slit, the metastable peak height in a MIKE spectrum will be closely proportional to the ion flux. However, in the presence of an energy resolving slit which is narrower than the metastable ion peak width, the entire ion flux cannot pass through the slit at any one point during the scan of the electrostatic sector. Hence the height of the metastable peak will be reduced relative to the height in the absence of an energy resolving slit. Therefore, the height of broad metastable peaks will decrease relative to narrow metastable peaks with increasing resolution and the peak heights are not proportional to the ion flux. The same logic applies to peaks in a CIDI mass spectrum.

The widths at the base of the mainbeams with all the slits fully open were approximately 55-60 V indicating the approximate width of the energy resolving slits. The widths at the bases of the metastable peaks under conditions of high energy resolution were 30, 35, 200, 50 and 70 V for

$CH_3CO^+ \rightarrow {}^+CH_3 + CO$
$CH_2{=}CHCO^+ \rightarrow {}^+CH{=}CH_2 + CO$
$C_6H_5OH^{+\cdot} \rightarrow C_5H_6^{+\cdot} + CO$
$CH_3C(O)CH_2CH_2CH_3^{+\cdot} \rightarrow CH_2{=}C(OH)CH_3^{+\cdot} + CH_2{=}CH_2$
$C_6H_5OCH_2CH_3^{+\cdot} \rightarrow C_6H_5OH^{+\cdot} + CH_2{=}CH_2$

respectively. Note cnly for CO loss from $C_6H_5OH^{+\cdot}$ was the metastable peak width wider than the slit width.

The effect of narrowing the energy resolving slit, Y_5 (located after the electrostatic sector), on the observed metastable and CIDI peaks was studied. When the width of Y_5 was decreased slightly the height of the metastable peaks and the peaks in the CIDI mass spectra, with the exception of CO loss from ionized phenol, did not decrease. Only after the width had been significantly decreased did the heights start to diminish. For CO loss from $C_6H_5OH^{+\cdot}$ both the height of the metastable peak, m/z 66, and the CIDI peak, m/z 28, were diminished when the width of the slit was first decreased indicating that these peaks were broader than the width of the Y_5 slit when fully open. Therefore, for this case the peak heights may not accurately reflect the ion abundances.

To double-check these findings, the relative abundances of the main beam (no charge on the deflector electrode) to the abundance of all of the peaks in the CIDI mass spectrum were recorded at the

first multiplier (no energy resolving slit) and at the second multiplier (following Y_5). There is no separation of the ionized neutrals in a CIDI mass spectrum prior to the first multiplier. Therefore, all the ions arrive at the first multiplier and are detected together. What is observed is a single point at a height above the baseline which corresponds to the abundance of all the ions formed upon collisional ionization. The ratio of the mainbeam:CIDI peaks will be equal at multiplier one and multiplier two if there is no energy resolution prior to multiplier two (Y_5 width > CIDI peak widths).

For CO loss from CH_3CO^+ (from acetone), CO loss from $CH_2{=}CHCO^+$ (from ethyl acrylate) and $CH_2{=}CH_2$ loss from $C_6H_5OCH_2CH_3^{+\cdot}$ the ratio of the height of the main beam to the sum of the heights of the CIDI peaks were equal, within experimental error, at the first and second multipliers indicating no effect due to energy resolution. Unfortunately, there was not enough sensitivity at the first multiplier to observe a signal following CIDI of CO generated from $C_6H_5OH^{+\cdot}$.

The half-height widths of the metastable peak, m/z 66, and the CIDI peak, m/z 28, for CO loss from ionized phenol are nearly equal. Therefore, it is safe to assume that when measuring the ionization efficiency of CO, the ratio of the peak heights would be almost the same in the presence or absence of the energy resolving slits, Y_4 and Y_5.

Section 5.2.3 Multiplier Discrimination

The performance of the electron multiplier was compared with that of the Faraday cup (which measures absolute ion abundances) in order to determine the degree of multiplier discrimination. Previously it was shown that for a given mass and a constant multiplier voltage, the sensitivity was independent of the conversion dynode voltage from -3 to -5 kV and that changing the ion kinetic energy by a factor of four (from 8 kV to 2 kV) produces only a 35% change in sensitivity.[137]

In this study, the effects on multiplier performance of varying the mass and translational energy were determined by comparing the intensities of the peaks in the CA mass spectrum of $CH_3C(O)CH_2CH_2CH_2CH_3^{+\cdot}$ recorded with the electron multiplier to the intensities of the peaks recorded with the Faraday cup. These effects were also studied at various accelerating voltages. The results are shown in Tables 19-22 and plotted in Figures 5.2-5.5. All peak intensities are given relative to the peak at m/z 85 = 1000.

It was not possible to measure the ionization efficiencies using the Faraday cup due to the very low response of the Faraday cup relative to the electron multiplier.

Therefore, in order to get a more accurate comparison of the ionization efficiencies, the measured values must be corrected for changes in sensitivity due to ion kinetic energy and mass discrimination.

Table 19 CA Mass Spectrum (He) of $CH_3C(O)CH_2CH_2CH_2CH_3^{+\cdot}$
Accelerating Voltage = 8000 V.

m/z	Peak Intensity Faraday Cup	Peak Intensity Electron Multiplier	Multiplier Discrimination[a]
15	3.3	1.1	0.33 ± 0.05
27	17	8.9	0.52 ± 0.05
29	16	9.2	0.57 ± 0.05
31	4.7	2.6	0.55 ± 0.05
39	24	17	0.71 ± 0.05
41	37	27	0.73 ± 0.05
43	140	93	0.66 ± 0.05
45	6.1	4.6	0.75 ± 0.05
51	3.1	2.3	0.74 ± 0.05
53	10	8.3	0.83 ± 0.05
55	17	14	0.82 ± 0.05
57	12	9.8	0.82 ± 0.05
58	310	270	0.87 ± 0.05
59	16	14	0.88 ± 0.05
65	3.9	3.5	0.90 ± 0.05
67	24	22	0.91 ± 0.05
69	16	14	0.88 ± 0.05
71	170	160	0.94 ± 0.05
72	50	49	0.98 ± 0.05
81	7.5	7.7	1.02 ± 0.05
85	1000	1000	1.00 ± 0.05
99	1.9	1.8	0.95 ± 0.05

a. Multiplier Discrimination = Peak Intensity (Multiplier)/Peak Intensity (Faraday Cup)

Table 20 CA Mass Spectrum (He) $CH_3C(O)CH_2CH_2CH_2CH_3^{+\cdot}$
Accelerating Voltage = 6000 V.

m/z	Peak Intensity Faraday Cup	Peak Intensity Electron Multiplier	Multiplier Discrimination[a]
15	1.6	0.47	0.29 ± 0.05
27	9.0	5.2	0.58 ± 0.05
29	10	5.8	0.58 ± 0.05
31	2.8	1.9	0.68 ± 0.05
39	14	9.7	0.69 ± 0.05
41	26	19	0.73 ± 0.05
43	97	65	0.67 ± 0.05
45	4.1	3.2	0.78 ± 0.05
53	7.2	5.5	0.76 ± 0.05
55	12	10	0.83 ± 0.05
57	9.3	8.4	0.90 ± 0.05
58	290	250	0.86 ± 0.05
59	16	14	0.88 ± 0.05
65	3.4	2.6	0.76 ± 0.05
67	19	17	0.89 ± 0.05
69	12	12	1.00 ± 0.05
71	160	150	0.94 ± 0.05
72	49	49	1.00 ± 0.05
81	6.2	6.1	0.98 ± 0.05
85	1000	1000	1.00 ± 0.05
99	1.5	1.5	1.00 ± 0.05

a. Multiplier Discrimination = Peak Intensity (Multiplier)/Peak Intensity (Faraday Cup)

Table 21 CA Mass Spectrum (He) $CH_3C(O)CH_2CH_2CH_2CH_3^{+\cdot}$
Accelerating Voltage = 4000 V.

m/z	Peak Intensity Faraday Cup	Peak Intensity Electron Multiplier	Multiplier Discrimination[a]
15	1.4	0.45	0.27 ± 0.05
27	6.3	3.2	0.51 ± 0.05
29	7.2	4.2	0.58 ± 0.05
39	9.0	5.5	0.61 ± 0.05
41	23	14	0.61 ± 0.05
43	81	45	0.56 ± 0.05
53	5.8	4.2	0.72 ± 0.05
55	10	7.6	0.76 ± 0.05
58	330	240	0.73 ± 0.05
67	17	14	0.83 ± 0.05
69	11	9.3	0.85 ± 0.05
71	190	160	0.84 ± 0.05
72	57	49	0.86 ± 0.05
85	1000	1000	1.00 ± 0.05
99	1.2	1.2	1.00 ± 0.05

a. Multiplier Discrimination = Peak Intensity (Multiplier)/Peak Intensity (Faraday Cup)

Table 22 CA Mass Spectrum (He) $CH_3C(O)CH_2CH_2CH_2CH_3^{+\cdot}$
Accelerating Voltage = 2000 V.

m/z	Peak Intensity Faraday Cup	Peak Intensity Electron Multiplier	Multiplier Discrimination[a]
43	36	22	0.61 ± 0.05
58	240	180	0.75 ± 0.05
71	160	130	0.81 ± 0.05
72	64	56	0.88 ± 0.05
85	1000	1000	1.00 ± 0.05

a. Multiplier Discrimination = Peak Intensity (Multiplier)/Peak Intensity (Faraday Cup)

Figure 5.2 Multiplier Discrimination at an Accelerating Voltage = 8000 V

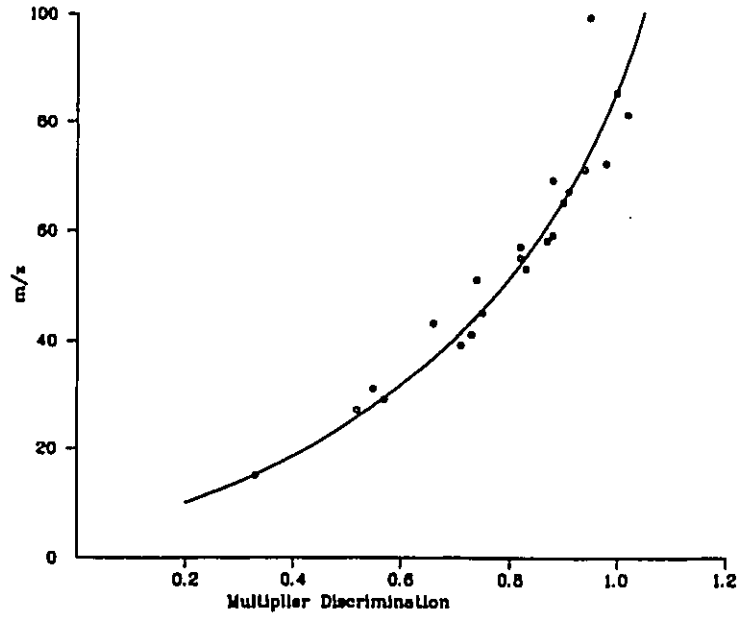

Figure 5.3 Multiplier Discrimination at an Accelerating Voltage = 6000 V

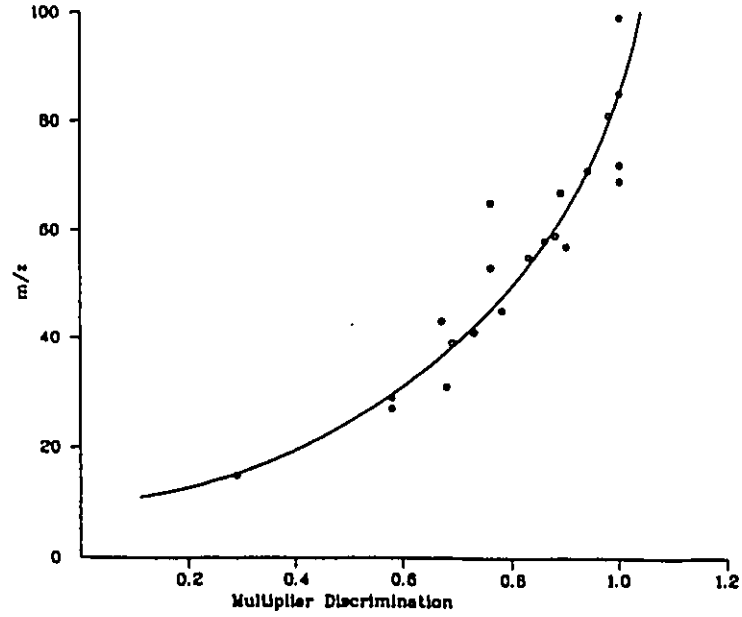

Figure 5.4 Multiplier Discrimination at an Accelerating Voltage = 4000 V

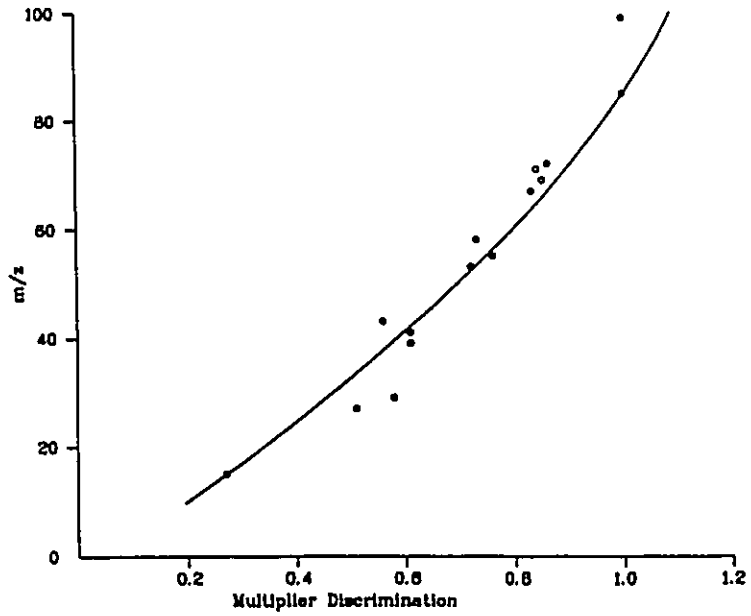

Figure 5.5 Multiplier Discrimination at an Accelerating Voltage = 2000 V

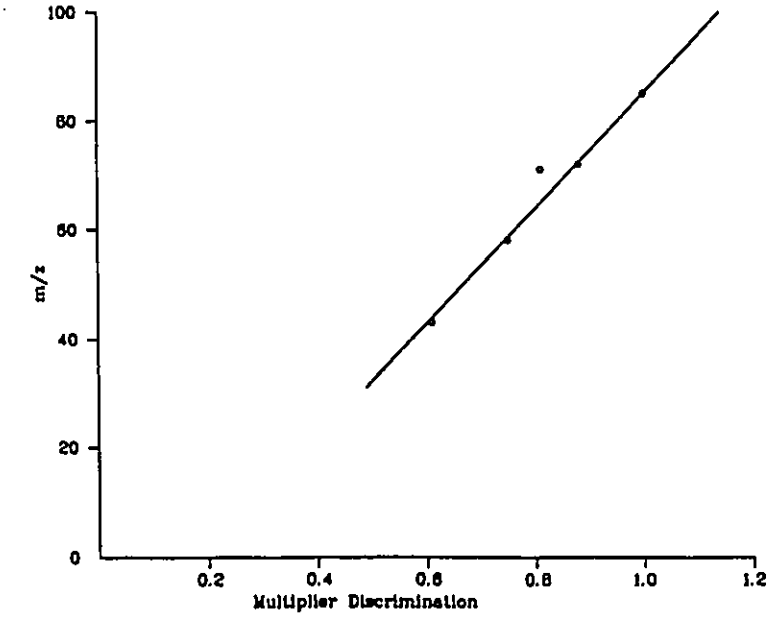

For example we will show how the correction is made for the measured value of the ionization efficiency of CO, E_{trans} = 5209 V, generated by the metastable dissociation of CH_3CO^+ with acetone as the precursor molecule.

V_{acc} = 8000 V.
$E_{trans}(CO)$ = (28/43)8000 = 5209 V
$E_{trans}(CH_3^+)$ = (15/43)8000 = 2791 V

Measured Ionization Efficiency = Intensity (CO)/Intensity (CH_3^+)
= 7.58×10^{-3}

Correction for mass discrimination, m/z 28, V_{acc}=8000 V (Figure 5.2)
= (1/0.53)
Correction for mass discrimination, m/z 15, V_{acc}=8000 V (Figure 5.2)
= (1/0.33)

Corrected value of ionization efficiency
= 7.58×10^{-3}(1/0.53)/(1/0.33)
= 4.72×10^{-3}

The corrected values of the ionization efficiencies are given in Table 23.

Table 23 Corrected Values of the Collision Induced Ionization Efficiencies of CO & $CH_2=CH_2$[a]

Metastable Ion	Precursor Molecule	Neutral Lost	E_{trans} (Volts) 5209	3907	2605	2000
CH_3CO^+	$CH_3C(O)CH_3$	CO	4.72×10^{-3}	1.77×10^{-3}	5.66×10^{-4}	1.47×10^{-4}
CH_3CO^+	$CH_3C(O)CH_2CH_3$	CO	3.40×10^{-3}	1.76×10^{-3}	5.56×10^{-4}	
CH_3CO^+	$CH_3C(O)CH=CH_2$	CO	4.12×10^{-3}	1.54×10^{-3}	5.24×10^{-4}	
CH_3CO^+	$CH_3C(O)C(O)CH_3$	CO	4.98×10^{-3}	1.76×10^{-3}	6.96×10^{-4}	
CH_3CO^+	$CH_3C(O)OCH_2CH_3$	CO	2.91×10^{-3}			
$CH_2=CHCO^+$	$CH_2=CHC(O)CH_3$	CO		1.54×10^{-3}	5.72×10^{-4}	1.85×10^{-4}
$CH_2=CHCO^+$	$CH_2=CHC(O)CH_2CH_3$	CO		1.95×10^{-3}	5.73×10^{-4}	
$CH_2=CHCO^+$	$CH_2=CHCO_2H$	CO		1.58×10^{-3}	5.62×10^{-4}	1.32×10^{-4}
$CH_2=CHCO^+$	$CH_2=CHC(O)OCH_2CH_3$	CO		1.72×10^{-3}	5.58×10^{-4}	1.45×10^{-4}
$C_6H_5OH^{+\cdot}$	C_6H_5OH	CO			2.60×10^{-5}	7.58×10^{-6}
$C_6H_5OH^{+\cdot}$	$C_6H_5OCH_2CH_3$	CO			3.99×10^{-5}	5.34×10^{-6}
$CH_3(CO)CH_2CH_2CH_3^{+\cdot}$	$CH_3C(O)CH_2CH_2CH_3$	$CH_2=CH_2$			7.12×10^{-4}	3.30×10^{-4}
$C_6H_5OCH_2CH_3^{+\cdot}$	$C_6H_5OCH_2CH_3$	$CH_2=CH_2$				1.53×10^{-4}

a. Values good to within ± 5%

Section 5.2.4 Translational Energy

In all cases the ionization efficiencies of CO and $CH_2=CH_2$ increase with the translational energy from 2000-5209 V. The increase in ionization efficiency with translational energy has been shown to apply to the electron detachment mechanism but not to the electron transfer mechanism.[123,124] The electron detachment mechanism has been shown to have maximum ionization efficiency at energies between 150 and 1500 V.[123,124] Therefore, we may conclude that ionization of CO and $CH_2=CH_2$ occur by the electron transfer mechanism as is expected for neutrals with ionization energies greater than 7 eV.[55,122] (EI_{CO} = 14.01 eV^2, $IE_{Ethylene}$ = 12.07 eV^2)

Section 5.2.5 Internal Energy

Analysis of the results shown in Table 23 revealed that the ionization efficiencies of CO and $CH_2=CH_2$ decreased with increasing internal energy of the neutral. The ionization efficiency of CO generated from ionized phenol is ~ 20x less than the ionization efficiency of CO generated from CH_3CO^+ or $CH_2=CHCO^+$. The ionization efficiency of $CH_2=CH_2$ generated from ionized 2-pentanone is ~ 2x less than the ionization efficiency of $CH_2=CH_2$ generated from $C_6H_5OCH_2CH_3^{+\cdot}$. These results are opposite to the result for $Br^{\cdot}$. The ionization efficiency of $Br^{\cdot}$ increased with increasing internal energy and this was attributed to electronic excitation.[55]

The lowest lying excited states of CO, $a^3\Pi_r$ and $a'^3\Sigma^+$, lie 6.0 and 6.9 eV above the ground state $X^1\Sigma^+$.[126] The lowest lying excited state of ethylene has a twisted geometry such that the planes of

the two CH_2 groups are perpendicular and lies 2.8 eV above the planar ground state $X^1\Sigma_g^+$.[138] Therefore, the internal energy of the CO produced by the dissociation of ionized phenol (E_{rev} = 1.0 eV) and of the ethylene produced by the dissociation of ethyl phenyl ether (E_{rev} = 1.2 eV) must be rotational/vibrational energy.

It seems reasonable to suggest that if there is a lot of energy in the CO stretching mode then collision with the target will more likely lead to simple bond dissociation than if the CO is in its ground state. The ground states of CO and CO^+ have closely similar geometries.[126] Therefore, according to the Franck-Condon principle the most probable ionizing transition will occur between states in which the positions of the nuclei are unchanged (ie. $CO(v=0) \rightarrow CO^+(v=0)$, $CO(v=1) \rightarrow CO^+(v=1)$ ...). However, another result of the Franck-Condon principle is that vibrationally excited CO may more likely produce a vertical transition to a dissociative electronic state than CO(v=0). Thus, at high internal energies, ionization (which requires 1353 $kJmol^{-1}$, $\Delta H_f[CO]$ = -111 $kJmol^{-1}$ [2], $\Delta H_f[CO^{+\cdot}]$ = 1242 $kJmol^{-1}$ [2]) may be less favourable than bond dissociation (which requires 1076 $kJmol^{-1}$, $\Delta H_f[CO]$ = -111 $kJmol^{-1}$ [2], $\Delta H_f[C]$ = 716 $kJmol^{-1}$ [2], $\Delta H_f[O]$ = 249 $kJmol^{-1}$ [2]).

It is also possible that the contribution from ionization of the target may increase with increasing internal energy. This will also decrease the ionization efficiency of CO. Note that when the ionization energy of the neutral is greater than the ionization energy of the target, ionization of the target is a major process.[55] IE_{CO} = 14.01 eV^2 > IE_{Oxygen} = 12.07 eV^2.

The He collision induced ionization efficiencies of CO (E_{trans} = 2605 V) generated from CH_3CO^+ (from acetone) and $C_6H_5OH^{+\cdot}$ (from phenol) were measured and are equal to (after correction for multiplier discrimination and internal energy) 8.78×10^{-4} and 6.30×10^{-5} respectively.

The IE_{CO} = 14.01 eV^2 < IE_{He} = 24.58 eV^2 and so ionization of the target will not be of importance. If the observed decrease in ionization efficiency with increasing internal energy is due to ionization of the target then this result should be observed when O_2 is used as target gas and not when He is used as target gas. However, the He ionization efficiency of CO generated from $C_6H_5OH^+$ is 14x less than the He ionization efficiency of CO generated from CH_3CO^+. Therefore, the decrease in the ionization efficiency of the CO with an increase in internal energy cannot be explained by increased ionization of the target.

Even though the effect of increasing the internal energy is much less, the same reasoning may be applied to ethylene. Collision of vibrationally excited ethylene with oxygen may promote simple bond dissociation reactions (6) and (7) over electron detachment (8) reducing the ionization efficiency with respect to ethylene at or near its ground state. Ground state $[CH_2=CH_2]^{+\cdot}$ has a twisted geometry such that the plane of the two CH_2 groups are at an angle of 30°.[138] Therefore, a vertical transition from ground state (planar) $CH_2=CH_2$ will produce vibrationally (torsion) excited $[CH_2=CH_2]^{+\cdot}$. Transitions of vibrationally excited $CH_2=CH_2$ increased the probability of dissociative ionization (as already noted in

Section 5.2) and may have increased the probability of transitions to dissociative electronic states of $CH_2=CH_2$.

The energy requirements for reactions (6), (7) and (8) are 431, 176 and 1014 $kJmol^{-1}$ respectively.

(6) C_2H_4 (ΔH_f = 52 $kJmol^{-1}$ [2]) $\rightarrow$ C_2H_3 (ΔH_f = 265 $kJmol^{-1}$ [2]) + $H\cdot$ (ΔH_f = 218 $kJmol^{-1}$ [2])
(7) C_2H_4 (ΔH_f = 52 $kJmol^{-1}$ [2]) $\rightarrow$ C_2H_2 (ΔH_f = 228 $kJmol^{-1}$ [2]) + H_2 (ΔH_f = 0)
(8) C_2H_4 (ΔH_f = 52 $kJmol^{-1}$ [2]) $\rightarrow$ $C_2H_4^{+\cdot}$ (ΔH_f = 1066 $kJmol^{-1}$ [2]) + e

Note that ionization of the target (O_2) is not very likely since $IE_{Ethylene}$ = 10.51 eV^2 < IE_{Oxygen} = 12.07 eV^2.

Section 5.3 Conclusions

The ionization efficiencies of CO and $CH_2=CH_2$ with oxygen as target increase with increasing translational energy, as is expected for ionization by the electron detachment mechanism. However, their ionization efficiencies decrease with increasing internal energy. The reason for this observation is unknown. However, it may be due to an increased probability of bond dissociation. It cannot be explained by increased ionization of the target.

The importance of making corrections for multiplier discrimination should be emphasized. If possible, systems should be used whose metastably generated ions and neutrals are of approximately equal mass and thus have closely similar translational energy.

Section 5.4 Experimental

Monoenergetic electron appearance energies were measured using the energy selected electron impact ion source and quadrupole mass filter described in Chapter 1. Metastable peak appearance energies were measured on the Kratos AEI MS-902S mass spectrometer described in Chapter 1. The reference AE was the metastable loss of $CH_3^{\cdot}$ from diethyl ether (AE = 10.26 eV[30]).

The MIKE, CA and CIDI mass spectra were recorded on the VG Analytical ZAB 2F mass spectrometer described in Chapter 1. Unless otherwise stated the ionizing electron energy was 70 eV and all of the slits were fully open. Kinetic energy release ($T_{0.5}$) values were recorded under conditions of good energy resolution such that the width at half-height of the main beam was less than 3V. Helium was used as collision gas in the CA mass spectra at a pressure corresponding to 10% beam reduction. O_2 was used as collision gas in the CIDI mass spectra. The pressure of O_2 used in all cases corresponded to 10% beam reduction of CH_3CO^+, m/z 43, from acetone (measured pressure of O_2 ~ $4X10^{-7}$ torr). This pressure corresponded to 90 ± 5% beam reduction for all ions studied. A constant pressure for all of the CIDI mass spectra was necessary due to the large variation in ionization efficiency with target gas pressure.

All compounds were purchased from Aldrich Chemical Co., Inc. and were of research grade purity.

I do not know what I may appear to the world, but to myself I seem to have been only like a boy playing on the seashore and diverting myself in now and then finding a smoother pebble or a prettier shell than ordinary, whilst the great ocean of truth lay all undiscovered before me.

ISAAC NEWTON

ARE BH_3 AND $BH_4^{\cdot}$ STABLE SPECIES IN THE GAS PHASE? A NEUTRALIZATION REIONIZATION MASS SPECTROMETRY STUDY

Section 6.1 Introduction

Borane, BH_3, has six valence electrons and is expected to have a planar structure (D_{3h} symmetry) in a singlet ground state ($^1A_1$).[139] The empty p orbital accounts for its reactivity as a Lewis acid. Borane rapidly dimerizes to the more stable B_2H_6. The transient existence of BH_3 has been used to explain many reactions of borohydrides.

The existence of BH_3 in the gas phase has been investigated by mass spectrometry. It has been concluded that pyrolysis of B_2H_6 and BH_3CO both lead to BH_3 based on either the intensity of the m/z 14, $^{11}BH_3^+$, peak as a function of furnace temperature[140-144] or a reduction in $AE(^{11}BH_3^+)$ when the furnace temperature was increased.[140,145-147] This reduced appearance energy was assumed to be due to ionization of $^{11}BH_3$ produced following pyrolysis rather than formation of $^{11}BH_3^+$ directly from diborane. The measured values for the ionization energy were 11.4 eV[140], 12.32 eV[145], 12.24 eV[146] and 12.03 eV.[147]

It was observed that m/z 13 ($^{11}BH_2^+$) in the mass spectrum of diborane was produced from ionization of B_2H_6 and from a lighter weight neutral ($^{11}BH_3$).[148] This conclusion was based on molecular beam velocity analysis spectrometry in which the neutrals produced following pyrolysis of diborane were separated based on their velocity prior to entering the source of a quadrupole mass spectrometer.

The hydride affinity of BH_3 was determined in a flowing afterglow triple quadrupole mass spectrometer by measuring the threshold for the reaction $BH_4^- + CO_2 \rightarrow BH_3 + HCO_2^-$.[149] A value of 310 ± 10 $kJmol^{-1}$ was obtained.

It was not until quite recently that BH_3 has been detected spectroscopically. The emission spectrum of BH_3 was observed following ArF 193 nm laser photolysis of B_2H_6.[150] The gas phase IR spectrum of BH_3 (trapped in an Ar matrix) was measured following pyrolysis of BH_3CO.[151]

Ab initio calculations at the 4-31 G*, 6-311 G**, and Moller-Plesset 6-311 G** levels show a genuine minimum for the hypervalent radical $BH_4\cdot$ for both C_{2v} and D_{2d} geometries with the former geometry slightly lower in energy.[152]

$BH_4\cdot$ and $BD_4\cdot$ radicals have been observed in the powder e.s.r. spectrum of $NaBH_4/NaBD_4$ following radiolysis (^{60}Co γ-rays) at 77 K.[153] Interpretation of the spectra indicated a C_{2v} geometry for the hypervalent radicals. However, $BH_4\cdot$ and $BD_4\cdot$ hypervalent radicals have never been observed by mass spectrometry.

The purpose of this study was to determine whether or not BH_3/BD_3 and $BH_4\cdot/BD_4\cdot$ could be observed by neutralization reionization mass spectrometry.

Section 6.2 BH_3

BH_3 is a very weak peak in the normal mass spectrum of B_2H_6 (< 1% of the base peak, m/z 27). Under conditions of high mass resolution (the width of the Y_1, Y_2 and Y_3 slits decreased) it was evident that there were three ions present at the nominal mass to charge ratio m/z 14: 9% $^{11}BH_3^+$ (m/z 14.03278), 29% CH_2^+ (14.01565) and 62% N^+ (14.00307). See Figure 6.1. The presence of the two lower mass ions certainly complicates the spectra of $^{11}BH_3$ as will be seen below.

Figure 6.1 High Mass Resolution of m/z 14 in the Normal Mass Spectrum of B_2H_6

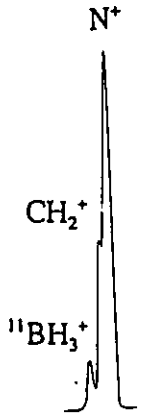

By appropriately tuning the magnet under conditions of high mass resolution it was possible to sit on top of the $^{11}BH_3^+$ peak. In this way $^{11}BH_3^+$ could be mass selected with a minimum of interference from CH_2^+ and N^+ (it was not possible to completely remove these interferences since the three peaks were not fully resolved). The MIKE, CA and NR mass spectra were recorded under the above conditions of mass resolution.

There were no metastable peaks observable in the MIKE spectrum of $^{11}BH_3^+$. The relative abundances of the peaks in the O_2 CA and Xe/O_2 NR mass spectra of $^{11}BH_3^+$ are shown in Table 24 as well as the Xe/O_2 NR mass spectrum (recorded while the magnet was tuned to sit atop the N^+ peak) of the interfering ions, CH_2^+ and N^+.

Table 24 Various Mass Spectra of m/z 14 from B_2H_6

Ion	Spectrum	m/z 11	m/z 12	m/z 13	m/z 14
$^{11}BH_3^+$	O_2 CA	14	47	100	
	Xe/O_2 NRMS	11	47	100	33
N^+	Xe/O_2 NRMS		1	3	100
$^{11}BH_3^-$	O_2 CR	32	100	99	6

There is a recovery at m/z 14 in the Xe/O_2 NRMS of $^{11}BH_3^+$. It was possible to tune the magnet to the high mass side of the $^{11}BH_3^+$ peak (resulting in a 50% loss of signal intensity) without altering the ratio of the peaks in the NRMS spectrum. If the recovery was due to interference from CH_2^+ or N^+ then retuning the magnet should have changed the relative abundances of $^{11}BH_3^+$ and the two interfering ions and thus the ratio of the peaks in the NR mass spectrum. Since there was no change observed it may be tentatively concluded that BH_3 exists as a stable neutral species for the time required to travel between collision cell I and collision cell II (ca 5×10^{-7} seconds).

Negative-ion chemical ionization (H_2O) of B_2H_6 produced BH_3^- anions. CIDI of these ions produced no recovered BH_3^+ indicating that spontaneous electron loss in the metastable time frame could not be observed. The relative abundances of the peaks in the O_2

charge reversal (CR) mass spectrum are shown in Table 24. Note that the peak heights of m/z 12 and m/z 13 are nearly identical unlike the peak heights of m/z 12 and m/z 13 in the CA or NR mass spectra. Unfortunately there was insufficient intensity to record the $^{-}NR^{-}$ or $^{-}NR^{+}$ mass spectra.

Section 6.3 BD_3

$^{11}BD_3^+$ and $^{10}BD_3^+$ are both very weak peaks in the normal mass spectrum of B_2D_6 (< 1% of the base peak, m/z 32). Under conditions of high mass resolution it was found that there were three peaks present at the nominal mass to charge ratio m/z 17: 65% $^{11}BD_3^+$ (m/z 17.05161), 20% CH_5^+ (m/z 17.03912) and 15% OH^+ (m/z 17.00274). The peak at m/z 16 could also be resolved into three component ions: 8% $^{10}BD_3^+$ (m/z 16.05524), 11% CH_4^+ (16.03130) and 81% O^+ (15.99492). See Figure 6.2

Figure 6.2 High Mass Resolution of m/z 17 and m/z 16 in the Normal Mass Spectrum of B_2D_6

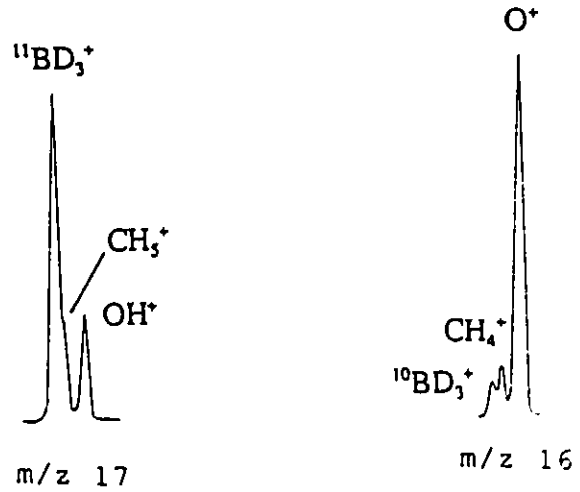

The only peak in the MIKE spectrum of $^{11}BD_3^+$ was $^{11}BD_2^+$ at m/z 15. The O_2 CA mass spectrum had peaks at m/z 11, m/z 13, m/z 14, m/z 15 and m/z 16 in the ratio 5:34:2:100:12. There was interference due to CH_5^+ or CH_5^+ and OH^+ as shown by the peaks at m/z 14 and m/z 16. By tuning the magnet to the high mass side of the $^{11}BD_3^+$ peak such that the intensity was reduced by 50% the peaks at m/z 14 and m/z 16 could be completely eliminated with only a slight change in the ratio of m/z 11, m/z 13 and m/z 15.

The relative heights of the peaks in the Xe/O_2 NRMS of m/z 17 recorded while sitting atop the OH^+ and $^{11}BD_3^+$ peaks and while sitting on the high mass side of the $^{11}BD_3^+$ peak are shown in Table 25.

Table 25 The Xe/O_2 NRMS of m/z 17 from B_2D_6

Ion	m/z 11	m/z 13	m/z 14	m/z 15	m/z 16	m/z 17
OH^+	1	4	1	4	9	100
$^{11}BD_3^+$	10	46	3	100	4	8
High Mass Side $^{11}BD_3^+$	11	49	<1	100	<1	9

The NRMS of $^{11}BD_3^+$ had peaks at m/z 14 and m/z 16. However, these peaks were not completely removed by tuning the magnet to the high mass side of the $^{11}BD_3^+$ peak. Therefore, the observed recovery at m/z 17 may be due to interference from CH_5^+ and or OH^+.

The Xe/O_2 NRMS of CH_5^+ is known to have no recovery at m/z 17[154] and so the observed recovery must be due to either $^{11}BD_3^+$ or OH^+. Based on the m/z 14:m/z 16:m/z 17 ratio it can be seen that on going from the OH^+ peak to the $^{11}BD_3^+$ peak the amount of CH_5^+

increases relative to the amount of $OH^{\cdot}$. On going from the top of the $^{11}BD_3^+$ peak to the high mass side of the $^{11}BD_3^{\cdot}$ peak the amount of CH_5^+ and $OH^{\cdot}$ decrease relative to $^{11}BD_3^+$; however, the recovery signal does not decrease relative to the $^{11}B^{\cdot}$, $^{11}BD^{\cdot}$ and $^{11}BD_2^{\cdot}$ peaks indicating that the recovery is $^{11}BD_3^+$.

The Xe/O_2 NRMS of m/z 16 had peaks at m/z 10, m/z 12, m/z 13, m/z 14, m/z 15 and m/z 16 in the ratio 9:50:9:100:6:44. Note that the ratio of m/z 10:m/z 12:m/z 14 from $^{10}BD_3^+$ is close to the ratio of m/z 11:m/z 13:m/z 15 for $^{11}BD_3^+$ while the recovery at m/z 16 is much more abundant than the recovery at m/z 17. Unfortunately, it would be next to impossible to tell if the recovery was $^{10}BD_3^{\cdot}$, $O^{\cdot}$ and/or CH_4^+.

The $^{10}BD_3^-$ and $^{11}BD_3^-$ ions were not studied because there would have been far too much interference from O^- and OH^- produced in the negative-ion chemical ionization (H_2O) of B_2D_6.

Section 6.4 $BH_4^{\cdot}$

BH_4^+ is an extremely weak peak in the normal mass spectrum of B_2H_6 (< 0.01% of the main beam). It was observed under high mass resolution conditions that the peak at m/z 15 corresponded to only 1% $^{11}BH_4^+$ (m/z 15.04060) and 99% CH_3^+ (m/z 15.02348). Therefore there was too much interference to obtain any useful information concerning the stability of $BH_4^{\cdot}$ from the NRMS of m/z 15.

BH_4^- generated by negative-ion chemical ionization (H_2O) of B_2H_6 was studied. BH_4^- (ΔH_f = -85 $kJmol^{-1}$ [2]) is much more stable than CH_3^- (ΔH_f = 185 $kJmol^{-1}$ [2]) and therefore CH_3^- should not cause any major interference.

There were no peaks observed in the MIKE spectrum of m/z -15. The CIDI mass spectrum of m/z -15 was very weak, however there were two peaks observable at m/z 12 and m/z 13 in the ratio 40:100 (see Table 26). This result is unlike the CIDI spectrum of CH_3^- where peaks are observed at m/z 12, m/z 13, m/z 14 and m/z 15 in the ratio 12:24:47:100.[78] Hence the observed peaks may be assigned to $^{11}BH^+$ and $^{11}BH_2^+$ produced by the dissociative ionization of $BH_4^\cdot$ following the metastable loss of an electron from BH_4^-.

The relative abundances of the peaks in the O_2 CR and Xe/O_2 $^-NR^+$ mass spectra are shown in Table 26.

Table 26 Various Spectra of m/z -15 from B_2H_6

Spectrum	m/z 11	m/z 12	m/z 13	m/z 14	m/z 15
O_2 CIDI		40	100		
O_2 CR	10	40	100	22	2
Xe/O_2 $^-NR^+MS$	10	45	100	10	

Note that the ratio of m/z 12 to m/z 13 are the same in all three spectra indicating that it is the same ion being observed in all cases. Unfortunately, there was no observable recovery in the $^-NR^+MS$, possibly due to the lack of intensity.

Section 6.5 $BD_4^\cdot$

Under conditions of high mass resolution it was found that the peak at m/z 19 consisted of 40% $^{11}BD_4^+$ (m/z 19.06571) and 60% H_3O^+. (m/z 19.01839). See Figure 6.3.

Figure 6.3 High Mass Resolution of m/z 19 in the Normal Mass Spectrum of B_2D_6

The O_2 CA mass spectrum of $^{11}BD_4^+$ consisted of peaks at m/z 11, m/z 13, m/z 15 and m/z 17 in the ratio 2:14:100:1.5. As the magnet was tuned to a slightly lower masses a peak at m/z 18 (from H_3O^+) appeared and grew rapidly as the magnet was tuned to increasingly lower masses.

The relative abundances of the peaks in the Xe/O_2 NRMS of $^{11}BD_4^+$ and H_3O^+ are shown in Table 27.

Table 27 The Xe/O_2 NRMS of m/z 19 from B_2D_6

Ion	m/z 11	m/z 13	m/z 15	m/z 16	m/z 17	m/z 18	m/z 19
H_3O^+				1	3.5	8	100
$^{11}BD_4^+$	16	73	94	1	13	8	100
High mass side $^{11}BD_4^+$	18	75	100	<1	14	5	61

The relative intensity of the peaks due solely to H_3O^+ (m/z 16 and m/z 18) to the intensity of the recovery peak at m/z 19 does not change as the relative amounts of $^{11}BD_4^+$ and H_3O^+ are changed by tuning the magnet to sit successively on top of the H_3O^+ peak, on

top of the $^{11}BD_4^+$ peak and on the high mass side of the $^{11}BD_4^+$ peak. Therefore, it may be concluded that the recovery signal is due solely to H_3O^+.

The negative-ion CI (H_2O) of B_2D_6 produced relatively intense peaks at m/z -18 and m/z -19 in the ratio 100:60. Based on the natural abundance of ^{18}O these peaks are <5% ^{18}O and ^{18}OH. The O_2 CR mass spectrum of m/z -18 had peaks at m/z 10-18 in the ratio 1:5:15:57:100:82:42:15:9. The presence of peaks at both m/z 10 and m/z 11 indicates the presence of both $^{10}BD_4^-$ and $^{11}BD_3H^-$ (produced by H/D exchange between B_2D_6 and H_2O in the ion source). H/D exchange was observed between B_2H_6 and D_2 following excitation by an ArF 193 nm laser.[155] No signals were observable in the CIDI mass spectrum of m/z -18 indicating that spontaneous electron loss in the metastable time frame cannot be observed.

The $O_2/O_2^-NR^+$ mass spectrum of m/z -18 had peaks at m/z 10-16 and m/z 18 in the ratio 6:21:40:52:98:100:<1:79. The total absence of a peak at m/z 17 and the very small ratio of m/z 16:m/z 18 makes it extremely unlikely that the observed recovery is due to H_2O^+ or OD^+. The recovery was corrected for the natural isotopic abundance of ^{18}O. It was found that ca 40% of the recovery was due to $^{18}O^+$. Therefore, it may be concluded that there was recovery of $^{10}BD_4^+/^{11}BD_3H^+$.

The peak at m/z -19 in the normal mass spectrum will contain $^{11}BD_4^-$ and may contain $^{18}OH^-$, HDO^- and/or H_3O^-. The O_2 CR mass spectrum of m/z -19 was very weak and only three peaks could be observed: a recovery at m/z 19 and two weaker peaks of approximately equal intensity at m/z 13 and m/z 15.

The O_2/O_2 $^{-}NR^{+}$ mass spectrum of m/z -19 was also extremely weak. Only two peaks were observable, one at m/z 15 and a recovery at m/z 19. The B_2D_6 (which had been introduced via the unheated glassline) was removed from the source by closing the valve between the glassline and the source without changing the pressure of H_2O in the source or the target gas pressures. The removal of the B_2D_6 was monitored by observing the dissapearance of the peak at m/z -27 while the deflector electrode was grounded. Following the removal of the B_2D_6 it was observed that the recovery signal had completely disappeared. The recovery signal returned when B_2D_6 was reintroduced into the source indicating that the recovery was due to $^{11}BD_4^{+}$ and not $^{18}OH^{+}$, HDO^{+} and/or H_3O^{+}.

Section 6.6 Conclusions

Experimental evidence for the stability of BH_3, BD_3 and the hypervalent radicals $BH_4\cdot$ and $BD_4\cdot$ has been provided. The recovery in the Xe/O_2 NRMS of m/z 14 from B_2H_6 and m/z 17 from B_2D_6 were shown to be $^{11}BH_3^{+}$ and $^{11}BD_3^{+}$ respectively. It was concluded that the peaks at m/z 12 and m/z 13 in the CIDI mass spectrum of m/z -15 from negative-ion chemical ionization (H_2O) of B_2H_6 were due to dissociative ionization of $^{11}BH_4\cdot$ hypervalent radicals produced by spontaneous electron loss from $^{11}BH_4^{-}$. The recovery in the O_2/O_2 $^{-}NR^{+}$ mass spectrum of m/z -18 from negative-ion chemical ionization (H_2O) of B_2D_6 was shown to be due to $^{10}BD_4^{+}/^{11}BD_3H^{+}$ as well as $^{18}O^{-}$.

Section 6.7 Experimental

All experiments were performed on the ZAB 2f mass spectrometer described in Chapter 1 at an ionizing electron energy of 70 eV. O_2 Collisional Activation and O_2 Charge Reversal mass spectra were recorded at a target gas pressure corresponding to 90% transmission of the main beam. Neutralization Reionization mass spectra were recorded at pressures such that the transmission of the main beam was reduced by 10% by the neutralization target in Cell I and by a further 30% by the reionization target in Cell II. 30% beam reduction due to the reionization target tended to give the maximum intensity of any recovery signals observed.

B_2H_6 and B_2D_6 were synthesized[156] by the oxidation of $NaBH_4/NaBD_4$ with I_2:

$$2NaBH_4 + I_2 \rightarrow 2NaI + B_2H_6 + H_2$$

$$2NaBD_4 + I_2 \rightarrow 2NaI + B_2D_6 + H_2.$$

REFERENCES

1. M.E. Rose and R.A.W. Johnstone, Mass Spectrometry For Chemists and Biochemists, Cambridge University Press, Cambridge (1987).

2. S.G. Lias, J.E. Bartmess, J.F. Liebman, J.L. Holmes, R.D. Levin and W.G. Mallard, *J. Phys. Chem. Ref. Data* 17 (1988).

3. F.M. Harris, G.W. Trott, T.G. Morgan, A.G. Brenton, E.E. Kingston and J.H. Beynon, *Mass Spectrom. Rev.* 3, 209 (1984).

4. J. Roboz, Introduction to Mass Spectrometry: Instrumentation and Techniques, John Wiley and Sons, Inc., New York (1968).

5. J.A. Hipple, R.E. Fox and E.U. Condon, *Phys. Rev.* 69, 347 (1946).

6. R.E. Fox, W.M. Hickan, T.K. Jeldaas and D.J. Grove, *Phys. Rev.* 84, 859 (1951).

7. K. Maeda, G.P. Semeluk and F.P. Lossing, *Int. J. Mass Spectrom. Ion Phys.* 1, 395 (1968).

8. H.M. Rosenstock, M.O. Wallenstein, A.L. Wahrhaftig and H. Eyring, *Natl. Acad. Sci. (US)* 38, 667 (1952).

9. H.M. Rosenstock and M. Krauss (F.W. McLafferty editor), Mass Spectra of Organic Ions, Academic Press, New York (1963).

10. F.H. Field and J.L. Franklin, Electron Impact Phenomena, Academic Press, New York (1957).

11. D.P. Stevenson and J.A. Hipple, *J. Am. Chem. Soc.* 64, 1588 (1942).

12. T.A. Molenaar-Langeveld, N.M.M. Nibbering, R.P. Morgan and J.H. Beynon, *Org. Mass Spectrom.* 13, 172 (1978).

13. F.W. McLafferty, *Anal. Chem.* 34, 2, 16, 26 (1962).

14. J.L. Holmes and J.K. Terlouw, *Org. Mass Spectrom.* 15, 383 (1980).

15. J.L. Holmes, *Org. Mass Spectrom.* 20, 169 (1985).

16a. J. Franck, *Trans. Faraday Soc.* 21, 536 (1926).

b. E.U. Condon, *Phys. Rev.* 32, 858, (1928).

17. K.S. Haber, J.W. Zwanziger, F.X. Campos, R.T. Wiedmann and E.R. Grant, *Chem. Phys. Lett.* 144, 58 (1988).

18. C.R. Brundle, D. Neumann, W.C. Price, D. Evans, A.W. Potts and D.G. Streets, *J. Chem. Phys.* 53, 705 (1970).

19. S.W. Benson, Thermochemical Kinetics, second edition, Wiley-Interscience, New York (1976).

20. K.C. Kim, J.H. Beynon and R.G. Cooks, *J. Chem. Phys.* 61, 1305 (1974).

21. J.L. Holmes and F.P. Lossing, *Can. J. Chem.* 57, 249 (1979).

22. P.C. Burgers and J.L. Holmes, *Int. J. Mass Spectrom. Ion Proc.* 58, 15 (1984).

23. W.A. Chupka, *J. Chem. Phys.* 30, 191 (1959).

24a. E.P. Wigner, *Phys. Rev.* 73, 1002 (1948).

b. S. Geltman, *Phys. Rev.* 102, 171 (1956).

25. H.M. Rosenstock, *Int. J. Mass Spectrom. Ion Phys.* 20, 139 (1976).

26. R.W. Kiser, Introduction to Mass Spectrometry and Its Applications, Prentice-Hall Inc., Inglewood Cliffs N.J. (1965).

27a. J.W. Warren and C.A. McDowell, *Discussions Faraday Soc.* 10, 53 (1951).

b. J.W. Warren, *Nature* 165, 810 (1950).

28. H.M. Rosenstock, K. Draxl, B.W. Steiner and J.T. Herron, *J. Phys. Chem. Ref. Data* 6 (1977).

29. J.D. Morrison, *International Review of Science: Physical Chemistry; Series One* 5, Page 25-54, Butterworth & Co. Ltd., London, U.K. (1975).

30. F.P. Lossing, *J. Am. Chem. Soc.* 99, 7526 (1977).

31. J.L. Beauchamp and R.C. Dunbar, *J. Am. Chem. Soc.* 92, 1477 (1970).

32. EPA/NIH Mass Spectral Data Base (US Government Printing Office).

33. R.G. Cooks, J.H. Beynon, R.M. Caprioli and G.R. Lester, Metastable Ions, Elsivier Scientific Publishing Company, Amsterdam (1973).

34. C. Ottinger, *Phys. Lett.* 17, 269 (1965).

35. J.L. Holmes and F.P. Lossing, *J. Am. Chem. Soc.* 102, 3732 (1980).

36. J.L. Holmes and A.D. Osborne, *Int. J. Mass Spectrom. Ion Phys.* 23, 189 (1977).

37. J.L. Holmes and A.D. Osborne, *Org. Mass Spectrom.* 13, 133 (1978).

38. J.K. Terlouw and J.L. Holmes, *Org. Mass Spectrom.* 15, 383 (1980).

39. T.W. Shannon and F.W. McLafferty, *J. Am. Chem. Soc.* 88, 5021 (1966).

40. H.M. Rosenstock, V.H. Dibeler and F.N. Harllee, *J. Chem. Phys.* 40, 591 (1964).

41. E.G. Jones, L.E. Bauman, J.H. Beynon and R.G. Cooks, *Org. Mass Spectrom.* 7, 185 (1973).

42. J.L. Holmes and J.K. Terlouw, *Can. J. Chem.* 53, 2076 (1975).

43. J.K. Terlouw, J. Wezenberg, P.C. Burgers and J.L. Holmes, *J. Chem. Soc. Chem. Commun.*, 1121 (1983).

44. R.P. Morgan, J.H. Beynon, R.H. Bateman and B.N. Green, *Int. J. Mass Spectrom. Ion Phys.* 28, 171 (1978).

45. A.A. Mommers, PhD Thesis, University of Utrecht, Utrecht, The Netherlands (1985).

46. F.W. McLafferty, P.F. Bente III, R. Kornfeld, S. Tsai and I. Howe, *J. Am. Chem. Soc.* 95, 2120 (1973).

47. K. Levsen and H.D. Beckey, *Org. Mass Spectrom.* 9, 570 (1974).

48. H.S.W. Massey, *Rep. Prog. Phys.* XII, 248 (1949).

49. K. Levsen and F.W. McLafferty, *J. Am. Chem. Soc.* 96, 139 (1974).

50. K.L. Busch, G.L. Glish and S.A. McLuckey, Mass Spectrometry/Mass Spectrometry - Techniques and Applications of Tandem Mass Spectrometry, VCH Publishers, Inc., New York (1988).

51. B. Van De Graaf, P.P. Dymerski and F.W. McLafferty, *J. Chem. Soc. Chem. Commun.*, 978 (1975).

52. P.C. Burgers, J.K. Terlouw and J.L. Holmes, *Org. Mass Spectrom.* 17, 369 (1982).

53. J.L. Holmes, *Mass Spectrom. Rev.* 8, 513 (1989).

54. J. Main-Bobo, S. Olesik, W. Gase, T. Baer, A.A. Mommers and J.L. Holmes, *J. Am. Chem. Soc.* 108, 677 (1986).

55. C.E.C.A. Hop, PhD Thesis, University of Utrecht, Utrecht, The Netherlands (1989).

56. J.H.O.J. Wijenberg, J.H. Van Lenthe, P.J.A. Ruttink, J.L. Holmes and P.C. Burgers, *Int. J. Mass Spectrom. Ion Phys.* 77, 141 (1987).

57. J.L. Holmes, C.E.C.A. Hop and J.K. Terlouw, *Org. Mass Spectrom.* 21, 776 (1986).

58. P.C. Burgers, J.L. Holmes, A.A. Mommers, J.E. Szulejko and J.K. Terlouw, *Org. Mass Spectrom.* 19, 442 (1984).

59a. P.C. Burgers and J.L. Holmes, *Org. Mass Spectrom.* 19, 452 (1984).

b. W.J. Bouma, R.H. Nobes and L. Radom, *Org. Mass Spectrom.* 17, 315 (1982).

60. P.O. Danis, R. Feng and F.W. McLafferty, *Anal. Chem.* 58, 348 (1986).

61. G.I. Gellene and R.F. Porter, *Int. J. Mass Spectrom. Ion Phys.* 64, 55 (1985).

62. C. Wesdemiotis, R. Feng, P.O. Danis, E.R. Williams and F.W. McLafferty, *J. Am. Chem. Soc.* 108, 5847 (1986).

63a. B.F. Yates, W.J. Bouma and L. Radom, *J. Am. Chem. Soc.* 109, 2250 (1987).

b. P. Von R. Schleyer, *J. Am. Chem. Soc.* 105, 6389 (1983).

64. C.E.C.A. Hop, J. Bordas-Nagy, J.L. Holmes and J.K. Terlouw, *Org. Mass Spectrom.* 23, 155 (1988).

65. J.H. Bowie, *Mass Spectrom. Rev.* 3, 161 (1984).

66. J.H. Bowie, *Acc. Chem. Res.* 13, 76 (1980).

67. M. Bowers, Gas Phase Ion Chemistry, Volume 2, Academic Press, New York (1979).

68. L.G. Christophorou, *Advances in Electronics and Electron Physics* 46, 55 (1978).

69a. J.P. Johnson, D.L. McCorkle, L.G. Christophorou and J.G. Carter, *J. Chem. Soc., Faraday Trans. 2* 71, 1742 (1975).

b. P.W. Harland and J.C.J. Thynne, *Int. J. Mass Spectrom. Ion Phys.* 10, 11 (1972).

70. J.H. Bowie, *J. Am. Chem. Soc.* 95, 5795 (1973).

71a. J.H. Bowie and T. Blumenthal, *J. Am. Chem. Soc.* 97, 2959 (1975).

b. J.H. Bowie and T. Blumenthal, *Aust. J. Chem.* 29, 115 (1976).

72. I. Howe, J.H. Bowie, J.E. Szulejko and J.H. Beynon, *J. Chem. Soc. Chem. Commun.*, 983 (1979).

73a. P.G. Fournier, J. Appell, F.C. Fehsenfeld and J. Durup, *J. Phys. B* 5, L59 (1972).

b. F.C. Fehsenfeld, J. Appell, P.G. Fournier and J. Durup, *J. Phys. B* 6, L268 (1973).

74a. J.H. Bowie and J.A. Benbow, *Org. Mass Spectrom.* 13, 103 (1978).

b. J.H. Bowie and P.Y. White, *Aust. J. Chem.* 31, 1511 (1978).

75. P.C. Burgers, J.L. Holmes, A.A. Mommers and J.E. Szulejko, *J. Am. Chem. Soc.* 106, 521 (1984).

76. M.M. Bursey, J.R. Hass, D.J. Harvan and C.E. Parker, *J. Am. Chem. Soc.* 101, 5485 (1979).

77. J.A. Benbow, J.H. Bowie and G. Klass, *Org. Mass Spectrom.* 12, 432 (1977).

78. R. Clair, J.L. Holmes, A.A. Mommers and P.C. Burgers, *Org. Mass Spectrom.* 20, 207 (1985).

79. R.S. Mercer and A.G. Harrison, *Org. Mass Spectrom.* 22, 710 (1987).

80. C. Wesdemiotis and R. Feng, *Org. Mass Spectrom.* 23, 416 (1988).

81. R. Feng, C. Wesdemiotis and F.W. McLafferty, *J. Am. Chem. Soc.* 109, 6521 (1987).

82. P.C. Burgers and J.L. Holmes, *Org. Mass Spectrom.* 17, 123 (1982).

83. P.C. Burgers and J.L. Holmes, *Int. J. Mass Spectrom. Ion Proc.* 58, 15 (1984).

84. J.K. McLeod and C. Djerassi, *J. Am. Chem. Soc.* 88, 1840 (1966).

85. A.N.H. Yeo and C. Djerassi, *J. Am. Chem. Soc.* 94, 482 (1972).

86. F.M. Benoit and A.G. Harrison, *Org. Mass Spectrom.* 11, 599 (1976).

87. E.L. Chronister and T.H. Morton, *J. Am. Chem. Soc.* 112, 133 (1990).

88. F. Borchers, K. Levsen and H.D. Beckey, *Int. J. Mass Spectrom. Ion Phys.* 21, 125 (1976).

89a. F. Borchers, K. Levsen, C.B. Theissling and N.M.M. Nibbering, *Org. Mass Spectrom.* 12, 746 (1977).

b. A. Maquestiau, Y. Van Haverbeke, R. Flammang, C. De Meyer, K.G. Das and G.S. Reddy, *Org. Mass Spectrom.* 12, 631 (1977).

90. G. Sozzi, H.E. Audier, P. Morgues and A. Millet, *Org. Mass Spectrom.* 22, 746 (1987).

91. T.H. Morton, *J. Am. Chem. Soc.* 102, 1596 (1980).

92. F.B. Burns and T.H. Morton, *J. Am. Chem. Soc.* 98, 7308 (1976).

93a. W.J. Marinelli and T.H. Morton, *J. Am. Chem. Soc.* 100, 3536 (1978).

b. W.J. Marinelli and T.H. Morton, *J. Am. Chem. Soc.* 101, 1908 (1979).

94. R.W. Kondrat and T.H. Morton, *Org. Mass Spectrom.* 23, 555 (1988).

95. M.C. Blanchette, J.L. Holmes and F.P. Lossing, *Org. Mass Spectrom.* 24, 673 (1989).

96. K. Raghavachari, R.A. Whiteside, J.A. Pople and P. Von R. Schleyer, *J. Am. Chem. Soc.* 103, 5649 (1981).

97. J. Riley and T. Baer, *J. Am. Soc. Mass Spectrom.* 2, 464 (1991).

98. E. Uggerud, T. Drewello, H. Schwarz, E.B. Vadler, S.E. Biali and Z. Rappaport, *Int. J. Mass Spectrom. Ion Proc.* 71, 287 (1986).

99. W. Koch, B. Liu and P. Von R. Schleyer, *J. Am. Chem. Soc.* 111, 3479 (1989).

100. D.F. McMillen and D.M. Golden, *Ann. Rev. Phys. Chem.* 33, 493 (1982).

101. J.L. Holmes and F.P. Lossing, *Int. J. Mass Spectrom. Ion Proc.* 92, 111 (1989).

102. R.F.W. Bader, *Can. J. Chem.* 64, 1036 (1986).

103. C.L. Perrin, *J. Am. Chem. Soc.* 113, 2865 (1991).

104. J.L. Holmes and F.P. Lossing, *Org. Mass Spectrom.* 26, 537 (1991).

105. S. Hammerum and H.E. Audier, *J. Chem. Soc. Chem. Commun.*, 860 (1988).

106a. M.C. Bissonnette, M. George and J.L. Holmes, *Int. J. Mass Spectrom. Ion Proc.* 101, 309 (1990).

b. M.C. Bissonnette, M. George and J.L. Holmes, *Org. Mass Spectrom.* 90, 689 (1990).

107. F. Camps, J. Coll and J.M. Moretó, *Synthesis*, 186 (1982).

108. B.B. Dandrée and J. Seyden-Penne, *Bull. Soc. Chim. Fr.*, 415 (1967).

109a. W.H. McFadden, M. Lounsbury and A.L. Wahrhaftig, *Can. J. Chem.* 36, 990 (1958).

b. W.H. McFadden, D.R. Black and J.W. Corse, *J. Phys. Chem.* 67, 1517 (1963).

c. C.G. MacDonald, J.S. Shannon and G. Sugowdz, *Tetrahedron Letters*, 807 (1963).

110a. W. Benz and K. Biemann, *J. Am. Chem. Soc.* 86, 2375 (1964).

b. S. Meyerson and L.C. Leitch, *J. Am. Chem. Soc.* 86, 2555 (1964).

111. G.J. Bukovits and H. Budzikiewicz, *Org. Mass Spectrom.* 18, 219 (1983).

112. A.M. Duffield, S.D. Sample and C. Djerassi, *Chem. Commun.*, 193 (1966).

113. J.L. Holmes and F.P. Lossing, *Can. J. Chem.* 60, 2365 (1982).

114. J.B. Pedley, R.D. Naylor and S.P. Kirby, Thermochemical Data of Organic Compounds, Chapman and Hall, London (1986).

115. J.L. Holmes, M. Fingas and F.P. Lossing, *Can. J. Chem.* 59, 80 (1981).

116. Y.H. Li, J.A. Herman and A.G. Harrison, *Can. J. Chem.* 59, 1753 (1981).

117. D.L. Miller and M.L. Gross, *Org. Mass Spectrom.* 18, 239 (1983).

118. R.D. Bowen, M.P. Barbalas, F.P. Pagano, P.J. Todd and F.W. McLafferty, *Org. Mass Spectrom.* 15, 51 (1980).

119. J.L. Holmes, J.K. Terlouw, P.C. Burgers and R.T.B. Rye, *Org. Mass Spectrom.* 15, 149 (1980).

120a. M.P. Barbalas, F. Turecek and F.W. McLafferty, *Org. Mass Spectrom.* 17, 595 (1982).

b. F.W. McLafferty, M.P. Barbalas and F. Turecek, *J. Am. Chem. Soc.* 105, 1 (1983).

121. G. Sozzi, H.E. Audier and A. Millet, *Bull. Soc. Chim. Fr.*, 292 (1984).

122. G.I. Gellene and R.F. Porter, *Int. J. Mass Spectrom. Ion Proc.* 74, 13 (1986).

123. Y.F. Bydin and A.M. Bukhteev, *Sov. Phys. Tech. Phys.* 5, 512 (1960).

124. A.M. Bukhteev, Y.F. Bydin and V.M. Dukelskiv, *Sov. Phys. Tech. Phys.* 6, 496 (1961).

125. P.C. Burgers, J.L. Holmes, A.A. Mommers and J.E. Szulejko, *Org. Mass Spectrom.* 18, 596 (1983).

126. A.A. Radzig and B.M. Smirnov, Reference Data on Atoms, Molecules and Ions, Springer-Verlag, Berlin (1985).

127. P.C. Burgers, J.L. Holmes, J.E. Szulejko, A.A. Mommers and J.K. Terlouw, *Org. Mass Spectrom.* 18, 254 (1983).

128. J.K. Terlouw, W. Heerma and J.L. Holmes, *Org. Mass Spectrom.* 16, 306 (1981).

129. J.L. Holmes, J.K. Terlouw and P.C. Burgers, *Org. Mass Spectrom.* 15, 140 (1980).

130. Z.V.I. Zaretskii and P. Dan, *Org. Mass Spectrom.* 16, 372 (1981).

131. C.J. Porter, A.G. Brenton and J.H. Beynon, *Int. J. Mass Spectrom. Ion Phys.* 36, 69 (1980).

132. M.K. Hoffman, M.D. Friesen and G. Richmond, *Org. Mass Spectrom.* 12, 150 (1977).

133. M.D. Migahed and F.H. Abd El-Kader, *Int. J. Mass Spectrom. Ion Phys.* 31, 373 (1979).

134. J.F. Elder Jr., J.H. Beynon and R.G. Cooks, *Org. Mass Spectrom.* 10, 273 (1975).

135. J.J. Zwinselman, N.M.M. Nibbering, N.E. Middlemiss, J.H. Vajda and A.G. Harrison, *Int. J. Mass Spectrom. Ion Phys.* 38, 163 (1981).

136. D.H. Russel, D.H. Smith, R.J. Warmack and L.K. Bertram, *Org. Mass Spectrom.* 14, 474 (1979).

137. J.L. Holmes and J.E. Szulejko, *Org. Mass Spectrom.* 18, 273 (1983).

138. A.J. Merer and R.S. Mulliken, *Chem. Rev.* 69, 639 (1969).

139. A.D. Walsh, *J. Chem. Soc.*, 2296 (1953).

140. T.P. Fehlner and W.S. Koski, *J. Am. Chem. Soc.* 86, 2734 (1964).

141. T.P. Fehlner and W.S. Koski, *J. Am. Chem. Soc.* 87, 409 (1965).

142. T.P. Fehlner and G.W. Mappes, *J. Phys. Chem.* 73, 873 (1969).

143. O. Herstad, G.A. Pressley Jr. and F.E. Stafford, *J. Phys. Chem.* 74, 874 (1970).

144. G.W. Mappes and T.P. Fehlner, *J. Am. Chem. Soc.* 92, 1562 (1970).

145. J.H. Wilson and H.A. McGee Jr., *J. Chem. Phys.* 46, 1444 (1967).

146. P.S. Ganguli and H.A. McGee Jr., *J. Chem. Phys.* 50, 4658 (1969).

147. B. Ruščić, C.A. Mayhew and J. Berkowitz, *J. Chem. Phys.* 88, 5580 (1988).

148. B.S. Askins and C. Riley, *Inorg. Chem.* 16, 481 (1977).

149. D.B. Workman and R.R. Squires, *Inorg. Chem.* 27, 1848 (1988).

150. J.A. Harrison, R.F. Meads and L.F. Phillips, *Chem. Phys. Lett.* 148, 125 (1988).

151. K. Kawaguchi, J.E. Butler, C. Yamada, S.H. Bauer, T. Minowa, H. Kanamori and E. Hirota, *J. Chem. Phys.* 87, 2438 (1987).

152. T.A. Claxton, T. Chen and M.C.R. Symons, *Faraday Discuss. Chem. Soc.* 78, 121 (1984).

153. M.C.R. Symons, T. Chen and C. Glidewell, *J. Chem. Soc. Chem. Commun.*, 326 (1983).

154. J. Bordas-Nagy, J.L. Holmes and C.E.C.A. Hop, *Int. J. Mass Spectrom. Ion Proc.* 85, 241 (1988).

155. M.P. Irion and L. Kompa, *J. Chem. Phys.* 76, 2338 (1982).

156. G.F. Freeguard and L.H. Long, *Chem. Ind.*, 471 (1965).